

## ABSTRACT

Title of Dissertation: Quantitative Motion Analysis of the Upper Limb: Establishment of Normative Kinematic Datasets and Systematic Comparison of Motion Analysis Systems

Sophie L. Wang, Doctor of Philosophy, 2022

Dissertation directed by: Dr. Kimberly L. Kontson, Food and Drug Administration  
Dr. Ian White, Department of Bioengineering

Upper limb prosthetic devices with advanced capabilities are currently in development. With these advancements brings to light the importance of objectively and quantitatively measuring effectiveness and benefit of these devices. Recently, the application of motion capture (i.e., digital tracking of upper body movements in space) to performance-based outcome measures has gained traction as a possible tool for human movement assessment that could facilitate optimal device selection, track rehabilitative progress, and inform device regulation and review.

While motion capture shows promise, the clinical, regulatory, and industry communities would benefit from access to large clinical and normative datasets from different motion capture systems and a better understanding of advantages and limitations of different motion capture approaches. The first objective of this dissertation is to establish kinematic datasets of normative and upper-limb prosthesis user motion. The normative kinematic distributions of many performance-based outcome measures are not established, and it is difficult to determine

departures from normative patterns without relevant clinical expertise. In Specific Aim 1, normative and clinically relevant datasets were created using a gold standard motion capture system to record participants performing standardized tasks from outcome measures.

Without kinematic data, it is also difficult to identify informative kinematic features and tasks that exhibit characteristic differences from normative motion. The second objective is to identify salient kinematic characteristics associated with departures from normative motion. In Specific Aim 2, an unsupervised K-means machine learning algorithm was applied to the previously collected data to determine motions and tasks that distinguish between normative and prosthesis user movement.

The third objective is to compare three commonly used motion capture systems that vary in motion tracking mechanisms. The most informative tasks and kinematic characteristics previously identified will be used to evaluate the detection of these differences for several motion capture systems with varying tracking methods in Specific Aim 3.

QUANTITATIVE MOTION ANALYSIS OF THE UPPER LIMB:  
ESTABLISHMENT OF NORMATIVE KINEMATIC DATASETS AND  
SYSTEMATIC COMPARISON OF MOTION ANALYSIS SYSTEMS

by

Sophie L. Wang

Dissertation submitted to the Faculty of the Graduate School of the  
University of Maryland, College Park, in partial fulfillment  
of the requirements for the degree of  
Doctor of Philosophy  
2022

Advisory Committee:

Dr. Kimberly L. Kontson, Co-Chair

Professor Ian White, Co-Chair

Dr. Gene Civillico

Associate Professor Yu Chen

Professor Rodolphe Gentili (Dean's Representative)

© Copyright by  
Sophie L Wang  
2022

# Dedication

*To my family and friends*

For their patience, support, participation, and encouragement throughout this  
experience

## Acknowledgements

I thank my co-advisor Dr. Kim Kontson for all of her work and mentorship, my co-advisor Dr. Ian White for his support and encouragement, and Dr. Gene Civillico for his creativity and enthusiasm.

I would like to acknowledge the past and present members of the Functional Performance and Device Use lab (Janelle Joyner, David Nahmias, Wesley Niswander, Ellenor Brown, Peter Gaskins, Heather Benz, Conor Bloomer, Tyler Oliver, Alec Boyle, Mahsa Alborz, Jake Horder, Ryan Jobson, Michael Reilly, Barbara Myklebust, Sydney Barovsky...) for their aid and collaboration. It was always a joy and a pleasure to work together in the lab and to spend time together away from the lab.

...the members of the OSEL and DBP for feedback and all manner of support (James Coburn, Dan Hammer, Kyoko Fujimoto, Trent Robertson, Jorge Hernandez, Srikanth Vasudevan, Sundar Rajan, Zhuolin Liu, Ricardo Villanueva, Tayeb Zaidi, Andrea Kim, Zane Arp, among others).

...my dissertation committee (Dr. Kim Kontson, Dr. Ian White, Dr. Gene Civillico, Dr. Rodolphe Gentili, Dr. Yu Chen) for their care in this process.

...the many participants who volunteered their time and effort to bring this project to fruition.

Thank you to my parents, Dr. Yang Luo and Dr. Mingyu Wang, for being my example and for the unending motivation. Thank you to my sister, the soon to be Dr. Caroline Wang, for the sympathy, company, and cute cat pictures.

# Table of Contents

Dedication.....	ii
Acknowledgements.....	iii
Table of Contents.....	iv
List of Tables.....	vi
List of Figures.....	vii
List of Abbreviations.....	ix
Chapter 2: Introduction.....	1
2.1 Specific Aim 1: Development of Kinematic Databases.....	4
2.2 Specific Aim 2: Application of Machine Learning to Identify Salient Kinematic Characteristics.....	5
2.3 Specific Aim 3: Comparison of Motion Capture Systems.....	7
Chapter 3: Establishment of Kinematic Databases.....	10
3.1 Introduction.....	10
3.2 Methods.....	12
3.2.1 Functional Tasks.....	12
3.2.2 General Participant Information.....	14
3.2.3 Bypass Training and Condition Descriptions.....	17
3.2.4 Motion Analysis.....	21
3.2.5 Data Cleaning and Processing.....	23
3.3 Results.....	24
3.4 Discussion.....	25
Chapter 4: Application of Machine Learning to Identify Salient Kinematic Characteristics.....	29
4.1 Introduction.....	29
4.2 Methods.....	31
4.2.1 Participants Selected.....	31
4.2.2 Functional Tasks.....	34
4.2.3 Data Analysis.....	35
4.2.4 Evaluation of algorithm performance – Deviation from Chance (DfC) metric.....	39
4.2.5 Statistical Analysis.....	40
4.3 Results.....	40
4.4 Discussion.....	45
Chapter 5: Comparisons of Motion Capture Systems.....	51
5.1 Introduction.....	51
5.2 Methods.....	53
5.2.1 Participants Selected.....	54
5.2.2 Functional Tasks.....	56
5.2.3 Motion Analysis Systems.....	57
5.2.4 Data Analysis.....	61
5.3 Results.....	68
5.4 Discussion.....	80
Chapter 6: Conclusions and Future Work.....	86

6.1 Conclusions.....	86
6.2 Future Work.....	88
Appendices.....	91
Bibliography .....	109

## List of Tables

Table 2.1: Description of tBBT and tasks from the JHFT, AMULA, and CAPPFUL13	
Table 3.1 Percentage of times a (A) task and (B) DOF were associated with deviations from chance distributions significantly greater than the threshold. (Table modified from Table 1. of Wang et al., 2021[93]).....	43
Table 4.1 Description of tBBT and subtasks from the JHFT, AMULA, and CAPPFUL performed in the current chapter (Table modified from Table 1 of Wang et al., 2022[95]).....	57
Table 4.2. Definitions of Parent and Child Segments for each joint of Interest. (Modified from Table A1. Of Wang et al., 2022[95]) .....	63
Table 4.3 ICC values with 95% confidence intervals for each DoF, task, and motion system comparison. Red cells indicate a weak correlation ( $ICC < 0.4$ ). Yellow cells indicate a moderate correlation ( $0.4 \leq ICC < 0.75$ ). Green cells indicate a strong correlation ( $ICC \geq 0.75$ ) (Table modified from Table 2 of Wang et al., 2022{Wang, 2022 #1933}) .....	76

## List of Figures

Figure 2.1. Brace Condition. Induces limitations on wrist and hand DOFs through a cock-up splint, Coban wrap, and paper tape. ....	15
Figure 2.2. Upper limb prosthesis bypass devices. A) Body Powered Bypass device, right side configuration with body-powered voluntary open Hosmer 5x split hook terminal device (Arm Dynamics, Dallas, TX). B) DEKA Bypass device, right-hand radial configuration with powered wrist (Next Step Bionics, Manchester, NH). C) Myoelectric Bypass device, right-hand radial configuration TouchBionic i-limb Ultra with manual wrist (OSSUR, NJ, USA). (Figure modified from Figure 1 of Wang et al., 2021[93]).....	16
Figure 2.3 My i-limb grip selection screenshot (Touch Bionics, Apple App Store, 2020) (Figure modified from Figure 1 of Wang et al., 2022[95]) .....	21
Figure 2.4 A) Vicon Nexus Upper Body Plug-In-Gait locations of the 27 markers. B) Object interaction segmentation: an example of the object approach and completion of object interaction points in JHFT Task 4 – Simulated Feeding. ....	24
Figure 3.1 Upper limb prosthesis bypass devices. A) Body Powered Bypass device, right side configuration with body-powered voluntary open Hosmer 5x split hook terminal device. B) DEKA Bypass device, right-hand radial configuration with powered wrist. (Figure 1 of Wang et al., 2021[93]) .....	32
Figure 3.2 Flowchart of data collection and processing and the calculation of deviation from chance (DfC) metric. (Figure 2 of Wang et al., 2021[93]).....	38
Figure 3.3 Average and standard deviation from chance (DfC) for all tasks, DOFs, and bypass condition comparisons: A-F) Body Powered Bypass v. Norm Joint results, G-L) DK Bypass v. Norm Joint Results. Tasks JHFT1 - Writing, JHFT2 - Page Turning, JHFT3 - Picking Up Small Objects, JHFT4 - Simulated Feeding, JHFT5 - Stacking Checkers, JHFT6 - Moving Large Light Objects and JHFT7 - Moving Large Heavy Objects Distributions significantly greater than the threshold at DfC = 25 (red dotted line) denoted by a * ( $p < 0.05$ ). (Figure 3 of Wang et al., 2021[93]) .....	43
Figure 4.1 A) Right-hand Ossur (TouchBionics) i-limb Ultra myoelectric terminal device. Medial offset = 15°; B) my i-limb grip selection screenshot (Touch Bionics, Apple App Store, 2020). (Figure 1 of Wang et al., 2022[95]).....	55
Figure 4.2 Illustration of sensor locations with the anterior view on the left and posterior view on the right. Orange boxes represent IMU sensors. Blue dots represent retroreflective markers. The black box represents the bypass device and the location relative to the forearm of the participant. The grey boxes represent the myoelectric terminal device. (Figure A1. of Wang et al., 2022[95]) .....	58
Figure 4.3 Distributions of (a) right elbow flexion RMSE and (b) right elbow flexion bias across subjects for the IMU system (Xsens) and markerless system (Kinect) compared to the Vicon reference system. X-axis identifies the task and associated joint angle. F/E = flexion/extension, Ab/Ad = abduction/adduction, LaF = lateral flexion, Rot = rotation. Black dots indicate medians, empty circles indicate outliers, bold line indicates quartiles, and whiskers indicate non-outlier maximums and minimums. (Figure 2 of Wang et al., 2022[95]).....	72
Figure 4.4 Distributions of (a) right shoulder joint angle RMSE and (b) right shoulder joint angle bias across subjects for the IMU system (Xsens) and markerless system (Kinect) compared to the Vicon reference system. X-axis identifies the task and	

associated joint angle. F/E = flexion/extension, Ab/Ad = abduction/adduction, LaF = lateral flexion, Rot = rotation. Black dots indicate medians, empty circles indicate outliers, bold line indicates quartiles, and whiskers indicate non-outlier maximums and minimums. (Figure 3 of Wang et al., 2022 {Wang, 2022 #1933}) ..... 73

Figure 4.5 Distributions of (a) neck joint angle RMSE and (b) neck joint angle bias across subjects for the IMU system (Xsens) and markerless system (Kinect) compared to the Vicon reference system. X-axis identifies the task and associated joint angle. F/E = flexion/extension, Ab/Ad = abduction/adduction, LaF = lateral flexion, Rot = rotation. Black dots indicate medians, empty circles indicate outliers, bold line indicates quartiles, and whiskers indicate non-outlier maximums and minimums. (Figure 4 of Wang et al., 2022 {Wang, 2022 #1933}) ..... 74

Figure 4.6 Distributions of (a) torso angle RMSE and (b) torso angle bias across subjects for the IMU system (Xsens) and markerless system (Kinect) compared to the Vicon reference system. X-axis identifies the task and associated joint angle. F/E = flexion/extension, Ab/Ad = abduction/adduction, LaF = lateral flexion, Rot = rotation. Black dots indicate medians, empty circles indicate outliers, bold line indicates quartiles, and whiskers indicate non-outlier maximums and minimums. (Figure 5 of Wang et al., 2022 {Wang, 2022 #1933}) ..... 75

## List of Abbreviations

3D	three dimensional
ADLs	activities of daily living
AMULA	Activities Measure for Upper Limb Amputees
CAPPFUL	Capacity Assessment of Prosthetic Performance for Upper Limb
DOFs	degrees of freedom
DfC	Deviation from Chance
HAPTIX	Hand Proprioception and Touch Interfaces
JHFT	Jebsen-Taylor Hand Function test
IMU	inertial measurement unit
mSHAP	modified Southampton Hand Assessment Procedure
OM	outcome measures
QoM	quality of motion
RMSE	root mean square error
SHAP	Southampton Hand Assessment Procedure
tBBT	targeted Box and Blocks Test
UL	upper limb
wLIF	weighted Liner Indices of Function

## Chapter 1: Introduction

According to Zeigler-Graham (2008), roughly 500,000 Americans were estimated to suffer some degree of upper limb (UL) loss in 2005, of which 41,000 were major losses beyond fingers. By 2050, the number of yearly cases is expected to increase in proportion to the increasing population[1]. Major UL amputations can be perceived as devastating damage that reduces autonomy by disrupting the ability to perform activities of daily living during work and socialization[2]. The needs of UL amputees vary depending on the levels of limb loss, with unilateral amputees depending on UL prostheses as an aid to the sound limb and bilateral amputees using the prostheses as the main way to interact with the environment[2]. However, the state of prosthesis technology has yet to fully meet the needs of amputees: over 85% of bilateral amputees do not return to work[2] and the rates of prosthesis rejection rates may be greater than 1 in 5[3]. Factors that have been cited for prosthesis rejection include: lack of comfort, lack of functional gain, awkwardness of use, fine control difficulties, and limited usability[2-4]. Additionally, UL amputees suffer from disproportionate rates of overuse related musculoskeletal pain and injury[5-11].

Performance-based outcome measures become a critical component of the evidence necessary to show effectiveness of the technology and the benefits to the prosthesis user. These types of outcome measures are typically used to assess function during the performance of actions relevant to activities of daily living (ADLs) and have the potential to provide unbiased and reproducible assessment of function. However, very few of these measures consider quality of motion (QoM) during functional tasks[12]. Quality of motion can be defined as the normality of task

performance, the smoothness and independence of motion, or as the correctness of a motion[12]. It is important to take quality of motion into account because of the propensity of individuals with UL amputations to employ compensatory movement patterns, which concentrates the workload on the remaining limb and alters the kinematics of the rest of the body[13-15]. These alterations in body kinematics may contribute to the overuse-related musculoskeletal pain and injuries prevalent in the UL amputee population[5-11].

One potential method to quantitatively assess QoM uses motion capture technology, which involves the recording and analysis of motion to produce kinematic information such as body trajectories and joint angles. There are various mechanisms of action for the motion capture systems on the market: 3D optoelectric, markerless, and inertial measurements. 3D optoelectric motion capture systems use multiple cameras to track the position of markers placed on a moving body to relate the position of orientation of body segments[16-23]. Markerless systems depend on image processing algorithms to track the frame-to-frame changes indicative of motion [24-31]. Inertial measurement systems track the linear acceleration and rotational velocity in three directions and use processing algorithms to interpret the changes measured as movements over time[32-38]. All the systems are capable of producing the quantitative kinematic data needed for motion-capture based outcome measures, but accuracy assessments of motion tracking in the upper limb across all systems and insight regarding feasibility of clinical implementation for each of these systems are lacking in the literature.

Motion capture-based outcome measures have the potential to fill the gaps identified in the evaluation of functional capabilities and quality of motion[6, 39-41]. There have been several studies utilizing quantitative motion capture to examine QoM for the upper limb prosthesis user population[7, 13-15, 42, 43]. However, these studies have had narrow scopes of analyses and vary greatly in the kinematic features analyzed. Several issues obstruct the clinical, regulatory, and industry adoption of motion capture. The normative kinematic ranges of many commonly used performance-based outcome measures have yet to be established. The deviations from normative motion and the kinematic characteristics useful for the measurement of QoM is thus unclear. To address the paucity of normative clinical data for common outcome measures and the lack of coordinated datasets from which to examine deviations from normative motion in a clinical population of interest, the first Specific Aim of this dissertation focuses on the development of such kinematic databases. With the kinematic data from both healthy controls and individuals representing a clinical population of interest, it is possible to apply advanced mathematical methods (e.g., machine learning) to discern differences between these populations. With the differences identified, it would then allow for targeted developments in rehabilitation and device design. The goal of Specific Aim 2 is to apply machine learning to datasets of normative and simulated disability motion for the identification of kinematic features associated with compensatory motion. Once the kinematic features have been identified, the ability to detect the features of interest becomes vital as the accessibility and technical specifications of the motion capture systems available influences the adoption and utilization of motion capture.

By examining available systems for the ability to detect the kinematic characteristics of interest, it will be possible to encourage the greater adoption of motion capture into research and rehabilitation. The goal of Specific Aim 3 is to examine the performance of three motion capture systems with varying mechanisms of action using motions and features identified by Specific aim 2. A detailed description of each specific aim and the corresponding chapter in this dissertation follows.

### *1.1 Specific Aim 1: Development of Kinematic Databases*

Those few performance-based outcome measures that incorporate subjective evaluation of quality of movement assess this metric by asking the administrator to compare the movements of the prosthesis user to those of a person with a sound, intact hand [44, 45]. Although these scoring approaches provide more insight into the functional abilities of individuals using upper limb prosthesis technology, the broad definition of “normal movement” and the subjective nature of the scoring can make it difficult to know which areas of the body to focus on evaluating, and the magnitude of the deviation from the normative movement ranges given the lack of quantitative normative baselines.

As mentioned above, previous motion studies of QoM have isolated single features of motion and made narrowly defined comparisons to healthy, able-bodied individuals. Additionally, those studies vary greatly in the kinematic parameters analyzed – from joint angles and range of motion[13-15, 43, 46] to velocity changes[7, 47], rendering trend interpretations and cross study conclusions challenging. Overall, there has yet to be a kinematic database of performance-based outcome measure motions, normative and otherwise, much less a publicly available

database. Publicly available kinematic databases will speed the development of new motion capture outcome measures and the clinical adoption of objective performance-based outcome measures by increasing access to data and reducing duplicative efforts.

Thus, the first aim of this dissertation was to generate coordinated kinematic databases of normative and UL prosthesis user movements to allow the establishment of normative baselines, the evaluation of factors relevant to quality of motion, and eventually allow the quantification of QoM. In Chapter 2, we generate a standardized normative motion database by recording able-bodied participants as they performed standard tasks from performance-based outcome measures. We then generate a standardized database of simulated disability motion data by recording able-bodied participants performing tasks with a prosthesis simulator meant to simulate the loss of distal degrees of freedom (DOFs) in the UL. To ensure skillful use of the UL prosthesis simulator devices, in Chapter 2 we also describe the training protocol used for training the able-bodied participants on the use of the UL prosthetic devices.

### 1.2 Specific Aim 2: Application of Machine Learning to Identify Salient Kinematic Characteristics

After the generation of coordinated kinematic databases, it is necessary to analyze and interpret the data collected to identify kinematic features of interest that can be used to direct future avenues of investigation. In Chapter 3, we apply the k-means clustering machine learning algorithm to the Chapter 2 kinematic data previously gathered to examine the departures from a normative baseline. By

examining those DOFs, it will be possible to identify tasks with distinctive differences for use in the motion capture system comparison performed in Chapter 4.

Previous motion capture evaluations of movement in UL prosthesis users were typically completed for a single terminal device at a time, making the device related influences of varying prosthesis technologies on motion unclear. Consider two available technologies for this clinical population: the voluntary open body-powered hook controlled through body movements and the DEKA arm controlled with inertial measurement units attached to the feet [48-51]. With different prosthetic components and technology that provide different DOFs of control, one might anticipate kinematic differences in response to the available DOFs and control mechanism[52]. However, it is not yet clear where in the body and during what types of tasks these kinematic differences occur relative to “normal” movement and whether administrators should focus on certain areas of the body based on the type of prosthetic technology being used.

The identification of upper body movements as normal or not normal can be characterized as a binary classification problem. If upper body movements are quantified into discrete features that describe the kinematic trajectories for a given DOF, clustering analysis can be used to systematically determine differences between two groups. The application of clustering analysis to identify movement differences between groups is not novel. Some studies have used input from inertial measurement units and accelerometers to classify different upper limb movements[53, 54] or different gait patterns[55]. Other studies have applied clustering analysis and other machine learning techniques to motion capture data to

classify different full body actions in healthy individuals[56] or severity of crouch gait in children with cerebral palsy[57]. Electromyography data of the abdominal and erector spinae muscles has also been used as input to clustering algorithms to classify patterns of muscle activity during gait in healthy controls[58]. While a few clustering studies have focused on the upper limb prosthesis user population, the application of clustering analysis to compare movement of individuals using multiple prosthetic devices to the movements of healthy individuals has not been done.

The second aim of this dissertation was to identify DOFs that inform abnormal movement for several tasks using unsupervised machine learning (clustering methods). In Chapter 3, we applied the K-means clustering machine learning algorithm to the Chapter 2 kinematic data previously gathered to examine the departures from a normative baseline. By examining those DOFs, it will be possible to elucidate the variations in movement approach across several upper-limb prosthesis devices with varying DOFs as compared to healthy controls and identify standard tasks with distinctive kinematic features that would be useful for the comparison of the motion capture systems performed in Chapter 4.

### *1.3 Specific Aim 3: Comparison of Motion Capture Systems*

Even when kinematic databases have been established and informative DOFs and tasks have been identified, the clinical implementation of motion capture in rehabilitation may be challenging due the technical requirements for most commercial gold standard motion capture systems. A large proportion of studies investigating human motion use 3D optoelectric motion capture systems that track the position of markers placed on anatomical landmarks of the body to relate the position and

orientation of body segments. These systems are advantageous given their high resolution and accuracy, as well as their length of use in research[16-23] compared to more recently developed mechanisms of motion capture[26, 31, 59-62]. However, these 3D optoelectric systems are too bulky for use outside of the clinic, have restrictive operating environment requirements, and require high levels of training to collect and analyze data[26, 31]. As such, there has been interest in other systems, such as the Microsoft Kinect or inertial measurement unit-based systems, that have less restrictive operating environment requirements[25, 29].

There have been several previous studies comparing motion capture systems that have focused on one-to-one comparisons of a single test system and a gold standard system[33, 36, 63-69], the lower limbs[28, 34, 68, 70-73], or have relied on mechanical testing devices to ensure the greatest replicability of the ground truth[64, 74-76]. However, these approaches lack applicability and generalizability to the tracking of motion in the upper limbs, specifically upper limb prosthesis users.

To better understand the performance of various motion capture systems in quantifying upper limb movement in the prosthesis user population, Chapter 4 of this dissertation compares kinematics of users trained on the use of an UL prosthesis simulator simultaneously recorded from three systems that vary in motion capture mechanisms: a marker-based system, a markerless system, and an IMU system. The trained participants performed standardized tasks selected through the results from Chapter 3. The kinematic data generated from three systems was compared with RMSE and Bias values using the marker-based system as the standard. This simultaneously acquired dataset will clarify the technical capabilities of the selected

motion capture systems and provide insight into the ability of those systems to identify the differences from normative motion previously elucidated in the second aim of this project.

## Chapter 2: Establishment of Kinematic Databases

### *2.1 Introduction*

Motion capture is a promising method for measuring performance in an objective and quantitative manner due to its mechanism of action, the description of object movements with mathematical expressions of changes over time. However, one limitation that has slowed the adoption of motion capture for use in clinical evaluation, rehabilitation, or device evaluation is the unknown range of normative kinematic variation, especially in the upper limb (UL). Without an established range, it is unclear what is typical vs. atypical performance. Previous studies attempting to examine movement quality in the UL prosthesis population with motion capture have varied greatly in prosthesis devices studied, the tasks and motions selected, the comparisons made to able bodied motion, and the kinematic parameters analyzed, ranging from joint angles to velocity changes [13-15, 43, 46] [7, 47], which renders cross study trends and conclusions challenging. Other studies have focused on well-defined movements such as reach-to-target tasks for ease of analysis and processing [77-81]. These well-defined approaches are not necessarily representative of the strategies or motions present during the performance of ADLs.

The establishment of publicly accessible standardized database of normative UL motion during performance-based outcome measure tasks is necessary for the establishment of quantitative normative performance kinematic baselines. Currently, there is limited consensus on how to quantitatively measure differences from normative performance to assess quality of motion within existing performance-based outcome measures [12]. Performance-based outcome measures have previously

assessed quality of motion subjectively through comparisons of the movements to those of a person with a sound, intact hand[44, 45], or consider factors such as “normality”, “smoothness”, or “independence” of performance[12]. All these subjective approaches require expertise for consistent judgement, and do not provide quantitative descriptions of normal motion, much less the magnitude of the kinematic deviations from normal motion.

A publicly accessible database reduces the duplication of efforts within the field and lowers the technological burdens associated with the collection of motion data for kinematic research. (I.e., the pre-requisites of needing access to a motion capture lab and human subjects research experience to collect data for a research question.) Lowering the barriers to entry for upper limb kinematic research will stimulate research activity within the field. With the establishment of kinematic baselines, it becomes possible to quantitatively assess variations in motion and examine the factors that influence quality of motion.

To examine the differences between a normative baseline, movement patterns elicited during use of an assistive device, and movement patterns results from limited degrees of freedom, it is also necessary to establish databases of motion under those conditions. The solution proposed for this quandary is the use of able-bodied participants performing under conditions of simulated disability. The use of able-bodied participants allows for an increase in sample sizes as compared to the samples sizes possible with UL amputee participants, a controlled level of device exposure and training as compared to UL amputees which may vary widely in these factors, and allows the isolation of device related influences on motion[82]. To simulate the

loss of distal DOF found in UL amputees, wrist braces and adaptive bypass devices can be used. Wrist braces restrict the DOFs available for use, while adaptive bypass devices allow able-bodied participants to use UL prosthesis terminal devices. In order to ensure consistent skillful use of the UL prosthesis device, the implementation of a common training protocol is necessary.

With the normal and device use motion databases, it will be possible to investigate the most informative UL DOFs and outcome measure tasks with machine learning – which will be presented in the following chapter for Significant Aim 2. The analysis of the data performed in chapter 3 for Significant Aim 2 will then be used to select tasks and motions that are useful for characterizing the technological capabilities of motion capture systems of varying mechanisms in chapter 4 for Significant Aim 3. The details of the data collection for the normative and simulated disability databases are presented in this chapter, as well as the prosthesis training approach taken to ensure skillful device use

## 2.2 *Methods*

### 2.2.1 Functional Tasks

Participants performed a subset of tasks from the following outcome measures: the Jebsen-Taylor Hand Function test (JHFT)[83], the targeted Box and Blocks Test (tBBT)[83, 84], the Capacity Assessment of Prosthetic Performance for Upper Limb (CAPPFUL)[44], and the Activities Measure for Upper Limb Amputees (AMULA) [85, 86]. The outcome measures tasks were chosen either due to previous use in kinematic studies[83, 84, 87] or due to validation in the upper limb prosthesis

user population[44, 45]. Tasks selected from these outcome measures were chosen as ones that would elicit a wide range of movements representative of those performed during activities of daily living. A standard template was used to place each object for a given task in the same location for each participant. At least two trials of each selected task were performed

Table 2.1: Description of tBBT and tasks from the JHFT, AMULA, and CAPPFUL

Task name	Description
JHFT 1 – Writing	Write the standard sentence, 24 letters long, presented in cursive. Performed seated.
JHFT 2 – Page Turn	Flip over five 3x5 cm notecards arranged in a row with any technique, starting with the leftmost card and moving across. Performed seated.
JHFT 3 – Small Objects	Pick up six small objects (2 paperclips, 2 bottle caps, & 2 pennies) arranged two inches apart on the dominant side of the subject, and place in an empty can individually, starting with the right most object. Performed seated.
JHFT 4 – Simulated Feeding	Scoop with a spoon five kidney beans arranged two inches apart on the dominant side of the subject, and place in an empty can individually, starting with the right most bean. Performed seated.
JHFT 5 – Stacking Checkers	Stack one on top of another, four standard wooden checkers centered in front of the subject. Performed seated.
JHFT 6 – Light Objects	Lift 5 empty cans individually about 1” onto a board, starting with the rightmost can. Performed seated
JHFT 7 – Heavy Objects	Lift 5 filled cans individually about 1” onto a board, starting with the rightmost can. Performed seated
AMULA 10 – Fork	Grasp fork and bring to mouth, move fork back to table and release fork. Performed seated
AMULA 16 – Doorknob	Reach, grasp, and turn door knob. Release doorknob. Performed seated.
AMULA 24 – Reach	Lift arm overhead to grasp empty cup on shelf and bring down arm with cup in hand. Performed seated.
CAPPFUL 4 – Dice	Pick up three dice from a plate, touch to chin, and return to plate. Performed standing
CAPPFUL 8 – Bottle	Empty a squeeze bottle of water into a cup. Performed seated.
CAPPFUL 11 – Picture	Modified task – Reach overhead to grasp two rings suspended in the air on a pulley system, bring rings down to waist, then control the placement of rings back in their suspended position. Performed seated.
tBBT	Transport 16 blocks, one at a time, over a partition using only the dominant hand, starting with the innermost left block and moving across each row placing the block in its mirrored position. Performed either seated or standing.

### 2.2.2 General Participant Information

Able-bodied participants with no upper limb disability or impairment and no prior prosthesis experience were included in this study. The study was approved by the FDA IRB (Protocol 16-071). All participants provided written informed consent prior to participating in the study.

Each participant performed a set of standardized tasks under several possible conditions: Normative (Norm), Brace (BC), Body Powered Bypass (BP Bypass), DEKA Bypass (DK Bypass), or Myoelectric Bypass (MY Bypass). Some participants performed the set of standardized tasks under multiple conditions. As an example, some participants performed under the Norm, Brace, and BP Bypass conditions while other participants only performed under the MY Bypass condition. Other participants performed under the DK Bypass and Norm conditions.

In the brace condition (Figure 2.1), a motion restriction that reproduced some of the DOF limitations found in conventional prosthetic devices was induced on able-bodied participants[13, 88]. In the bypass conditions, adaptive bypass devices allowed trained able-bodied participants to use upper limb prosthesis terminal devices (Figure 2.2A, B, C). Bypass devices are a well-accepted approach to assess skill acquisition, training efficacy, and device use performance[8, 89-92]. Participants were trained until a learning curve performance plateau set to 90% of peak performance was reached, in accordance with the protocol of Bloomer et al 2018[82]. Further details on the training, the participants, and the devices within each of these condition groups are provided below.



Figure 2.1. Brace Condition. Induces limitations on wrist and hand DOFs through a cock-up splint, Coban wrap, and paper tape.



Figure 2.2. Upper limb prosthesis bypass devices. A) Body Powered Bypass device, right side configuration with body-powered voluntary open Hosmer 5x split hook terminal device (Arm Dynamics, Dallas, TX). B) DEKA Bypass device, right-hand radial configuration with powered wrist (Next Step Bionics,

Manchester, NH). C) Myoelectric Bypass device, right-hand radial configuration TouchBionic i-limb Ultra with manual wrist (OSSUR, NJ, USA). (Figure modified from Figure 1 of Wang et al., 2021[93])

### 2.2.3 Bypass Training and Condition Descriptions

The original bypass training protocol was designed by Bloomer et al (2018)[82] to facilitate a controlled presentation of the bypass prosthesis devices to able-bodied participants and enable efficient acquisition of prosthesis use skills. Participants completed ten two-hour training sessions with either the Body Powered (BP) bypass or the DEKA (DK) bypass. Each training session included tasks for three standardized training categories, 1) Object manipulation, 2) Free training, and 3) Activities of Daily Living. The task presentation order was randomized within each training category during each session. Participant performance during each session was scored with a modified Southampton Hand Assessment Procedure (mSHAP) outcome measure and the Box and Blocks Test (BBT) outcome measure. A learning curve was fitted to the session scores, which allowed for the identification of learning rates and learning plateau values. Motion capture sessions were performed at the midpoint (after five training sessions) and endpoint (after the tenth session) of the training sessions. The data from the endpoint motion capture sessions were used in this chapter.

Based on the results from the original training protocol, a modified accelerated protocol was used to train the Myoelectric (MY) bypass users. The training endpoint was set as either the achievement of a learning plateau set at 90% of the predicted peak performance, or the completion of ten two-hour training sessions. The termination of training was based on whichever endpoint was achieved first. Due

to the nature of a leaning plateau, it was not expected for participants to exhibit significant changes in performance with additional training sessions after reaching the plateau performance point. Participant performance during each session was scored for the SHAP and the mSHAP, as well as the BBT. The learning curve was fitted to the mSHAP scores for comparability with the previous training program results from Bloomer et al (2018). Due to the instability of the predicted plateau session over time and the difficulty of fitting a curve to less than 3 points of data, participants completed at least one training session post plateau achievement to ensure that the performance plateau was adequately captured. The motion capture session was performed after the training endpoint was achieved.

#### **2.3.2.1 Normative (Norm) Condition**

No devices were used in the Norm condition, and no training was provided. A convenience sample of 34 participants performed under the Norm condition (9 females, 23 males; mean age  $27.41 \pm 9.89$  years). 27 of the 34 participants were right hand dominant and all participants performed the standard tasks with the right hand.

#### **2.3.2.2 Brace (BC) Condition**

For the Brace condition (Figure 2.1), able bodied participants had wrist and hand function restricted through use of a cock up split and Coban wrap. This resulted in limited wrist flexion/extension and ulnar/radial deviation. All fingers were restrained except for the index and middle fingers. The index and middle fingers were further wrapped with paper tape to reduce possible flexion, sensitivity, and dexterity. A convenience sample of 22 participants performed under the Brace condition (7

females, 15 males; mean age  $26.45 \pm 8.63$  years). 19 of the 22 participants were right hand dominant, and all participants performed the standard tasks with the right hand.

### **2.3.2.3 Body-Powered (BP) Bypass Condition**

In the BP Bypass condition (Figure 2.2A), a forearm brace adaptor with a perpendicular handlebar allowed the use of a body-powered voluntary open Hosmer 5x split hook terminal device, with manual locking wrist rotation, set in-line with the length of the forearm. On average, the length of the bypass prosthesis was 9.25 cm longer than the intact limb. The body-powered bypass device was provided by Arm Dynamics (Dallas, TX). The in-line terminal device configuration was chosen due to the mechanical and kinematic requirements of the cable actuation with the figure eight harness.

A convenience sample of 6 participants (3 females, 3 males; mean age  $28.67 \pm 2.67$  years) were trained with the BP Bypass device. All participants self-reported as right hand dominant. During standard task performance, the BP Bypass was set to a right-side configuration for all participants.

### **2.3.2.4 DEKA (DK) Bypass Condition**

For the DK Bypass condition (Figure 2.2B), a forearm brace adaptor provided by Next Step Bionics (Manchester, NH) with a perpendicular handlebar allowed the use the right-hand radial configuration motorized DEKA device with powered wrist (DEKA Inc.). Just as the device is controlled by upper limb amputees, able-bodied participants used inertial measurement units attached to the dorsum of the foot to control grip changes, opening and closing of the device, and wrist rotation. This

terminal device was mounted to the forearm adaptor with a medial offset of 10° from the subject's forearm.

A convenience sample of eight participants (3 females, 5 males; mean age  $31.13 \pm 14.49$  years) were trained with the DK Bypass device. Six participants self-reported as right hand dominant, one participant self-reported as indeterminant in hand dominance, and one participant self-reported left hand dominant. All participants performed standard tasks with the right-hand radial configuration DK Bypass.

#### **2.3.2.5 Myoelectric (MY) Bypass Condition**

A forearm brace adaptor with a perpendicular handlebar provided by Next Step Bionics allowed the use of a right-hand TouchBionic i-limb Ultra (OSSUR, NJ, USA) myoelectric terminal device with manual wrist adjustment. The device was mounted to the brace with a medial offset of 15° from the subject's forearm (Figure 2.2C). In accordance with upper-limb amputee control configurations, myoelectric sensors were placed on antagonist pairs of radial and ulnar muscles on the forearm to control the opening and closing of the device. Grip changes were controlled with the TouchBionic my i-limb™ app on an iPod Touch™ (Figure 2.3). This adaptive bypass device (MY Bypass) allowed trained able-bodied participants to use a commercial upper limb prosthesis terminal device.

10 able bodied participants with no upper limb disability or impairment were included. The participants were selected through convenience sampling (5 females, 5 males; mean age  $29.6 \pm 7.1$  years). 9 of the 10 participants were right hand dominant

( $92.53 \pm 10.62$  laterality), one was left hand dominant ( $-100$  laterality) per the Edinburgh handedness survey[94].



Figure 2.3 My i-limb grip selection screenshot (Touch Bionics, Apple App Store, 2020) (Figure modified from Figure 1 of Wang et al., 2022[95])

#### 2.2.4 Motion Analysis

The state-of-the-art motion capture system selected for the creation of the kinematic databases was the Vicon™ passive marker optoelectric system with 10 infrared cameras and 1 digital video camera (VICON, Oxford, UK). This system was used to acquire and pre-process motion data.

The Bonita B10 and Vero infrared cameras were set to a sampling rate of 100Hz. Prior to each data collection session, the motion analysis system was calibrated according to manufacturer guidelines. Twenty-seven retro-reflective markers were placed on the upper body of each participant at the bony anatomical landmarks of the upper body in accordance to the Vicon Upper-Body Plug-In-Gait body model documentation (“Upper body modeling with Plug-in Gait,” 2019) (Figure 2.4A). Briefly, head markers were placed on the right/left temple and right/left back of the head; torso markers were placed on the spinous process of C7 and T10 vertebrae, right scapula, xiphoid process, and sternal notch; arm markers were placed on the acromio-clavicular joint, lateral surface of upper arm, lateral epicondyle of the elbow joint, lateral surface of lower arm, medial and lateral sides of the wrist joint, and on the third metacarpal; hip markers were placed on the right/left anterior superior iliac torso and right/left posterior superior iliac torso. The Plug-In-Gait upper body model was then calibrated to the dimensions of the participant to create the wrist, forearm, upper arm, head, neck, torso, and pelvic model segments. For the BP Bypass, the medial and lateral wrist joint markers were placed in line with the grip bar on the shell of the device at the locations of the red circles on Figure 2A, and the third metacarpal marker was placed on the portion of the split hook below the rubber band. For the DK and MY Bypasses, the medial and lateral wrist joint markers were placed on the wrist of the device with the base of the device thumb acting as the location reference. The third metacarpal market was placed on the corresponding location on the devices with the index finger acting as the location reference.

### 2.2.5 Data Cleaning and Processing

Joint angles were calculated from the Vicon upper body model using YXZ Euler angles derived from relative orientation comparisons of two segments (VICON Plug-In-Gait, Oxford, UK). The DOFs processed in this aim of the dissertation include right and left elbow flexion/extension; right and left shoulder flexion/extension, abduction/adduction, and internal/external rotation; torso flexion, lateral flexion, and rotation; and neck flexion, lateral flexion, and rotation.

The angle data were then filtered using a 4<sup>th</sup> order, zero lag, low pass Butterworth filter at 6 Hz. Data from each trial were further segmented into segments, with the number of segments depending on the number of objects manipulated in a given task (Figure 2.4B). For example, the JHFT Task 2 -Page turning required the participant to turn over five notecards, which resulted in five segments. In general, segment start was defined as the moment just before an object was touched and segment end defined as the moment following object release. A standard template was used to place each object for a given task in the same location for each subject, but the objects themselves may be distributed across the front of the participant or to the side of the participant depending on the task. To adequately compare kinematic trajectories across participants within a given condition, the analysis was limited to the last segment within each trial.



## 2.4 *Discussion*

During the bypass training, several factors appeared to influence the rate of task completion. One factor was the visibility of the object being manipulated. Participants generally completed tasks more quickly when the object was highly visible, either due to the bypass terminal device design (i.e. BP Bypass) or the training task parameters. This could be attributed to the lack of alternative feedback mechanisms for fine tuning device control and object position manipulation. Another factor was the mass of the bypass. As the training tasks were completed multiple times, the DK bypass participants, who were using a bypass with greater mass, tended to tire more quickly compared to the BP Bypass participants. A support frame was implemented for the DK bypass participants in an effort to counterbalance the greater mass. However, the inertia from the greater mass may still have influenced the task performance strategies chosen by the participants. In addition, perceived fatigue and the effects of fatigue on skill acquisition and retention were not factors that were specifically monitored and could be avenues of future investigation.

During the data collection, several unexpected factors influenced the rate of data collection and processing. One factor was that only a single machine had a Vicon Nexus license key. This resulted in data processing becoming a rate limiting bottleneck. Data collection sessions averaged about two hours in length; the data collected in a single session could take up to 4 hours of cleaning and annotation. Although the time required for cleaning and annotation could be substantially reduced with additional experience and additional efforts made during recording sessions to ensure high quality data, the time ratio of collection to processing never dropped

below 1:1. This factor was aggravated when several motion capture research projects were concurrently collecting and processing data and multiple lab members needed the same machine.

Other factors that influenced data processing rates were the environmental conditions of the capture environment and the efforts taken to ensure that the participant assumed a clean clear starting pose for each task. Regarding the environmental conditions, although the infrared cameras used to track the passive markers were not sensitive to the ambient light levels per se – high level levels from the incandescent lab lights resulted in transient background reflections that masking and threshold adjustments only partially alleviated. Transient background reflections occasionally resulted in undesirable merging of markers with different markers and reflections with markers. These errors needed manual detection and manual adjustments to address. Low light levels alleviated the transient background reflections but rendered the output of the system's video camera difficult to interpret. As the video was used to determine the placement of interaction annotations for each task, low light videos occasionally required multiple replays to determine consistent frames for the annotations.

Regarding the clean clear starting poses, initially there were several issues with marker labeling and spurious outputs from the Vicon joint angle calculation algorithms when markers were missing in the initial frames of a task recording. This was partially alleviated after a Vicon software version update which allowed for virtual placeholder markers that could substitute for the missing markers. However, the issue was most ideally addressed by ensuring all markers were visible prior to

recording initiation by coordinating body position adjustments with the participant. The most frequently problematic markers were as follows: the anterior hip markers, which were frequently obscured from the cameras by the task table and by body anatomy; the right wrist markers, which were frequently obscured by other portions of the bypass; the sternal notch and C7 markers, which were obscured by head position or hair. The use of a backless stool avoided obscuration issues for the remaining posterior body markers. However, the trade-off from prioritizing marker visibility through body position adjustments was that each task for each participant had a slightly different starting pose and consistent joint angles could not be assumed.

Lastly, available hard drive storage was another unexpected factor that affected data collection. Although the text files that stored the reflective marker positions in space were not especially large, the associated video files were still quite large even when set to half the frame rate of the infrared cameras. When the dedicated hard drive partition in the recording machine filled to capacity during a task recording, the Vicon Nexus program would either freeze or crash. This factor ended up limiting both the maximum number of trials per recording session, as well as the ability to perform back-to-back recording sessions.

The standard training protocol developed by Bloomer et al (2018)[82] successfully allowed the controlled and efficient implementation of able-bodied bypass users in the research setting. This in turn allowed the collection of kinematic data for multiple bypass devices, leading to the creation of kinematic databases for normative and device use motion data. The kinematic databases have been used in other studies to establish normative kinematic ranges for performance-based outcome

measure tasks and has allowed kinematic comparisons of various methods to simulate the loss in distal DOF found in upper limb amputees[52, 83, 84, 87, 88, 96]. The data collected will be used with machine learning clustering methods in the next chapter to identify the features and tasks that are most informative of the differences between normative and characteristic motions elicited during use of an upper limb prosthesis device. A comparison of the various methods to simulate upper limb disability will be performed to examine the influences of available distal DOFs upon body kinematics.

## Chapter 3: Application of Machine Learning to Identify Salient Kinematic Characteristics

### *3.1 Introduction*

In the previous chapter, databases of motion data for normative and simulated losses of DOF were generated under a standardized protocol, enabling a robust analysis of kinematic data across conditions. This analysis is focused on the determination of consistent kinematic characteristics for compensatory motions that result from the loss of distal degrees of freedom in the upper extremity. The interpretation of motion capture results can be simplified through the identification of kinematic features and multi-condition trends. This in turn can reduce the knowledge barriers involved in the adoption of motion capture as a method for assessing rehabilitative progress.

This chapter examines the degrees of freedom associated with compensatory movements in the upper limb prosthesis user population through the application of unsupervised machine learning. The machine learning algorithm selected for the evaluation of multiple features of movement for each individual and each prosthetic device type is the K-means clustering algorithm. The K-means algorithm is a robust and interpretable unsupervised algorithm for which the details of the features selected, and a more detailed explanation of the implementation is described below in Methods: Data Analysis. In brief, a binary classification between device and non-device motion was performed on six features calculated from the kinematic data collected in the previous chapter. The results from the clustering were analyzed per

joint DOF per standardized task with a novel metric called the Deviation from Chance to assess the accuracy of the clustering.

Previous machine learning studies with this clustering approach have focused on motion classification to aid in the recognition of representative kinematic patterns[53, 55-58], and the application of the results towards the assessment of upper limb rehabilitative progress through the frequency of characteristic motion performance[53] rather than focusing on the kinematic characteristics. By comparison, the results of this work will elucidate the variations in movement approaches and distinctive differences in motion across several UL prosthesis devices with varying available DOFs compared to participants with non-limited DOFs. In addition, the results of this work can provide cross device guidance for the evaluation of joints and movements typically involved in device-use motion and may aid rehabilitative efficacy by providing guidance on task selection and directed focus on the differences identified.

The goals of this chapter are to 1) utilize unsupervised machine learning to create an approach to identify informative features and tasks, and 2) elucidate the variations in motion quality and compensatory motions across several upper-limb prosthetic devices with varying DOFs. The information gathered about the most predictive characteristics and motions will inform the evaluation of the motion capture systems in the next chapter by reducing the analytical load required to examine multiple systems.

## 3.2 *Methods*

### 3.2.1 Participants Selected

A total of 24 non-disabled participants with no upper limb disability or impairment and no prior prosthesis experience were included in this portion of the study. All participants included were selected from the previously described dataset in Chapter 2. The study was approved by the FDA IRB (Protocol 16-071). All participants provided written informed consent prior to participating. Each participant performed a set of standardized tasks under one of several conditions: Normative (Norm), Body Powered Bypass (BP Bypass), or DEKA Bypass (DK Bypass). To avoid confounding effects of the same individual being trained on two different prosthetic devices each participant selected only participated in one condition. This served to increase the rigor of the comparison performed by limiting the participants' task familiarity. Limiting the participant selection in this manner also increased the variation within the motion envelope across the participant population by increasing the number of unique participants.

As described in the previous chapter, in the bypass conditions, adaptive bypass devices allowed trained non-disabled participants to use upper limb prosthesis terminal devices (Figure 3.1A, B). Bypass devices are a well-accepted approach to assess skill acquisition, training efficacy, and device use performance[8, 89-92]. The use of bypass devices was chosen in this study to isolate the influence of the upper limb terminal device on motion[82, 96], as prosthesis users vary in terms of favored terminal devices, device training, and usage experience. Recruitment of individuals using the DEKA arm is also difficult since very few individuals throughout the

country are trained on and using this device. In accordance with the protocol of Bloomer et al. [82] described in the previous chapter, participants were trained for 20 hours on each bypass prosthetic device. Recommendations on training length for actual upper limb prosthesis users vary from 5 hours to several months [97, 98], thus 20 hours of training is a reasonable approximation to training that would be received in a clinic. Further details on the participants and the devices within each of these condition groups are provided below.



Figure 3.1 Upper limb prosthesis bypass devices. A) Body Powered Bypass device, right side configuration with body-powered voluntary open Hosmer 5x split hook terminal device. B) DEKA Bypass device, right-hand radial configuration with powered wrist. (Figure 1 of Wang et al., 2021[93])

### **3.1.2.1 Normative (Norm) Condition**

No devices were used in the Norm condition, and no training was provided. A convenience sample of 12 participants performed each task under the Norm condition (four females, eight males; mean age  $26.91 \pm 9.84$  years). 11 of the 12 participants self-reported right-hand dominance, and all participants performed the standard tasks with the right hand. It was determined through examination of data distributions that left-hand and right-hand dominant individuals did not consistently differ in joint movement during tasks. Therefore, to maintain a higher sample size, left-handed individuals were included in the analysis.

The 12 participants were randomly assigned to two separate groups of six to serve as controls for the 6 BP Bypass and the 6 DK Bypass participants. The randomization was performed ten times to examine the effects of the variance in the normative condition. Further details of the randomization will be provided in the K-means clustering section below. None of the participants included in the Norm condition participated in any of the bypass conditions.

### **3.1.2.2 Body-Powered (BP) Bypass Condition**

A convenience sample of 6 participants (3 females, 3 males; mean age  $28.16 \pm 2.67$  years) were trained with the BP Bypass device. All participants self-reported right-hand dominance. During standard task performance, the BP Bypass was set to a right-side configuration for all participants.

### **3.1.2.3 DEKA (DK) Bypass Condition**

A convenience sample of 6 participants (2 females, 4 males; mean age  $27.67 \pm 7.13$  years) were trained with the DK Bypass device. 5 participants self-reported

right-hand dominance, 1 participant self-reported left-hand dominance. All participants performed standard tasks with the right-hand radial configuration DK Bypass. It was determined through examination of data distributions that left-hand and right-hand dominant individuals did not consistently differ in joint movement during tasks. Therefore, to maintain a higher sample size, left-handed individuals were included in the analysis.

### 3.2.2 Functional Tasks

Data for two outcome measures were chosen: the Jebsen-Taylor Hand Function test (JHFT) and the targeted Box and Blocks Test (tBBT)[83, 84]. These tasks were chosen as ones that would elicit a wide range of movements representative of those performed during activities of daily living, and also have established normative ranges of movement[83, 84, 88]. As previously described, the JHFT consists of seven activities of daily living (ADL) tasks performed in a seated position: 1) Writing, 2) Page Turning, 3) Picking Up Small Objects, 4) Simulated Feeding, 5) Stacking Checkers, 6) Moving Large Light Objects and 7) Moving Large Heavy Objects[83]. The tBBT involves the controlled transport of 16 blocks arranged in a 4 by 4 array from one side of a divided box to the other side[84]. This task was performed in both a standing position and a seated position[84]. Participants performed two trials of each task. Standard templates were used to place each object for a given task in the same location for each participant.

### 3.2.3 Data Analysis

The YXZ Euler angle data was generated and pre-processed for specific joints/DOFs in the previous chapter. The joint angles/DOFs analyzed in this chapter include right and left elbow flexion/extension; right and left shoulder flexion/extension, abduction/adduction, and internal/external rotation; torso flexion, lateral flexion, and rotation; and neck flexion, lateral flexion, and rotation.

Although a standard template was used to place each object for a given task in the same location for each subject, the objects themselves may be distributed across the front of the participant or to the side of the participant depending on the task. To adequately compare kinematic trajectories across participants within a given condition, the analysis was limited to the last segment within each trial.

K-means clustering was selected as the unsupervised machine learning method for this study due to the binary nature of the classification problem (i.e., Norm vs a Bypass), and the simplicity of the algorithm's decision-making approach. Specific features, of the joint angle trajectories were calculated to characterize the movement and serve as input into the K-means clustering algorithm. Given the current lack of consensus on the definition of movement quality as it pertains to evaluation of upper limb prosthesis users [99], several features describing different aspects of movement were selected for this analysis: peak angle, range of motion (RoM), joint trajectory path distance (PDist), mean joint angle, peak angle velocity, and number of zero crossings. The peak angle was calculated as the maximum measured joint angle value. The RoM was calculated as the difference between the maximum angle and the minimum angle value. The PDist was calculated according

to Equation 3.1, wherein the absolute difference between each joint angle component sample point was calculated and summed across all samples taken (1 to  $n$  points) for a given DOF. All trajectories were interpolated to be the same array length  $n$ , so no additional normalization to PDist was done.

$$P_{\text{dist}} = \sum_1^n |(x_{n+1} - x_n)|$$

Equation 3.1

Mean angle was calculated as the average of the joint angle over the task segment. The maximum value of the derivative of each joint angle served as the peak angle velocity. Smoothness was measured from zero crossing, where zero crossing is defined as the number of times angle velocity crossed zero[100, 101]. The peak angle and RoM were selected as clinically accepted, accessible, and interpretable features of movement[7, 15, 30, 37, 77, 83, 84, 88, 102, 103] and represent the movement envelope within which an individual performs a given task. PDist was selected as an additional summary metric to characterize movements as it has been previously used in the literature to examine compensatory motions in individuals with upper limb loss[7] , and has been used as a method to examine motion efficiency [104, 105]. Max normalization was applied for each feature.

Understanding one of the limitations of K-means clustering to be the dependence of the output on cluster center initialization, cluster center initialization used the K-means++ algorithm (Statistics and Machine Learning Toolbox, MATLAB) with the squared Euclidean as the distance metric. To further improve consistency in results by avoiding local minima, the clustering process was

implemented with five replicates, with the algorithm returning the solution with the lowest total sum of distances for all five replicate processes.

K-means clustering analyses were performed between the normative condition data and each bypass condition data (i.e. Norm vs. BP Bypass and Norm vs. DK Bypass), for each task and DOF, resulting in a total of 126 K-means analyses for one bypass condition (9 tasks x 14 DOFs per condition). For each analysis, ten iterations were performed, with randomized Norm controls assigned for each iteration. That is, each k-means iteration for a given task and DOF had the twelve normative participants randomly assigned into either the BP Bypass control group or the DK Bypass control group. This approach was implemented to account for variation in normal movement patterns, and to provide an estimate of the classification accuracy range. A flowchart of the data collection, processing, and analysis is shown in Figure 3.2. In total, 2,520 K-means were performed (9 tasks x 14 DOFs x 10 iterations x 2 conditions).

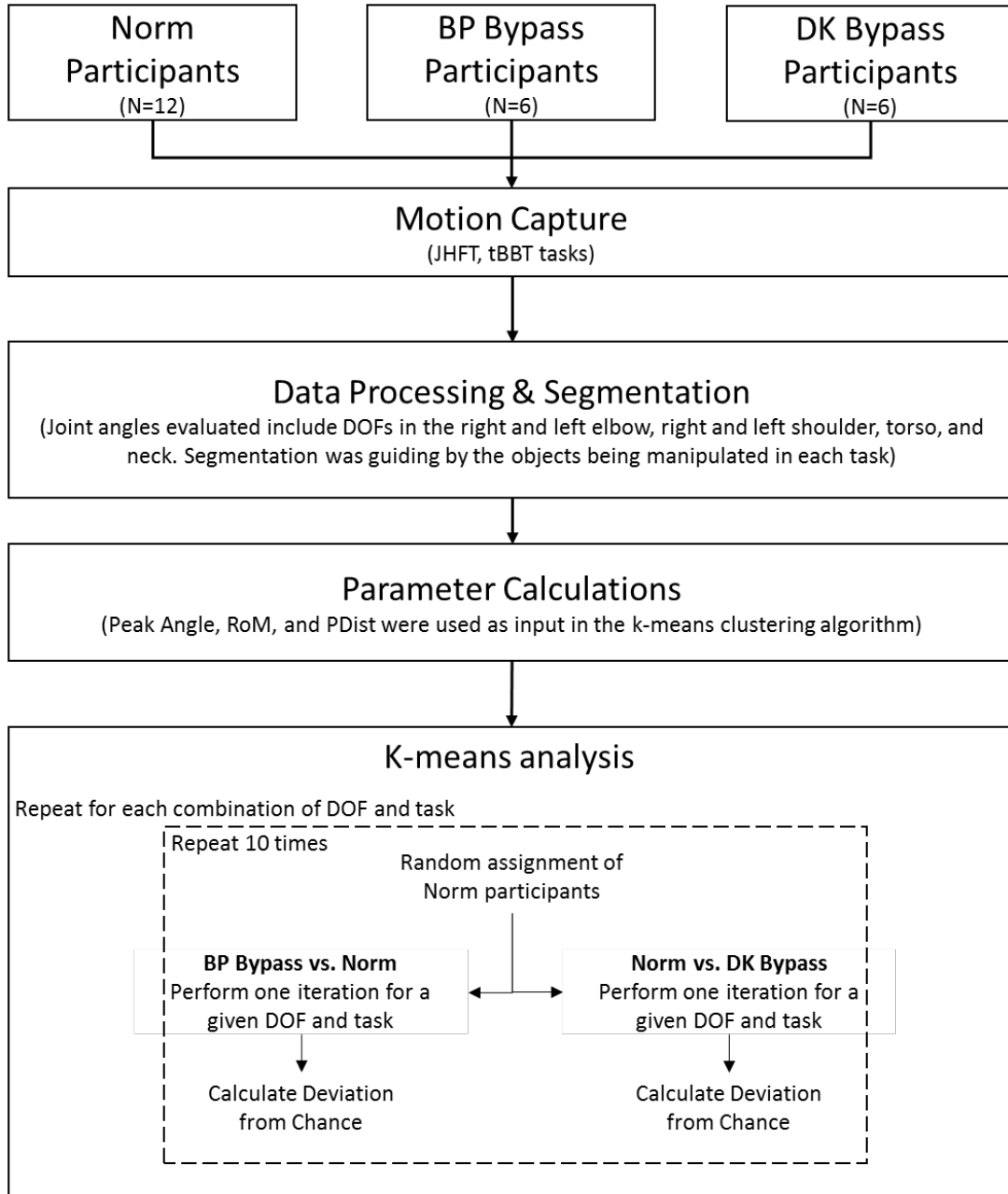


Figure 3.2 Flowchart of data collection and processing and the calculation of deviation from chance (DfC) metric. (Figure 2 of Wang et al., 2021[93])

### 3.2.4 Evaluation of algorithm performance – Deviation from Chance (DfC) metric

Although the true category of each data point was known (i.e., Norm or Bypass), the unsupervised approach employed in this study assigns an arbitrary category to every “cluster” that is formed. Thus, when determining accuracy of the classification, a new accuracy metric was used that provides the accuracy of clustering regardless of the actual labeling of any cluster, if the data points of any given cluster are maintained as a single cluster. The new metric utilized in this paper measured the absolute difference of the accuracy from random chance, which is 50% for a binary classification. We refer to this metric as the deviation from chance or DfC (Equation 3.2). The DfC ranges from 0 to 50, with a result of 0 indicating that a particular DOF was not informative in distinguishing the Norm and Bypass conditions (i.e., classification accuracy matches that of random chance) and a result of 50 indicating a particular DOF was highly informative in distinguishing the Norm and Bypass conditions. A threshold for this DfC metric was selected to be 25, half of the maximum possible value, as an initial value. More or less strict requirements can be placed on the identification of DOFs that distinguish the Norm and Bypass conditions by increasing or decreasing this DfC threshold, respectively.

$$DfC = \left| \text{Kmeans labeling accuracy \%} - \left( \frac{100}{\# \text{ Labeling Categories}} \right) \right|$$

Equation 3.2

### 3.2.5 Statistical Analysis

To determine the DfC values for a given DOF/task that are significantly higher than the DfC threshold of 25, a one-sided Wilcoxon ranksum test was performed between the DfC values resulting from the 10 iterations for a given task/DOF and the threshold ( $\alpha = 0.05$ ). Since the goal of this work is to identify the individual DOFs and tasks that elicit significantly different movement from normative movement during use of a bypass prosthesis, an adjustment for multiple comparisons was not done. However, a table of p-values for this analysis is included in supplementary material (Supplemental Table 1).

The distributions of all features used in the k-means analyses are also plotted for each DOF and task (Supplemental Figure 1 – 14). For informational purposes, a Wilcoxon ranksum test between each bypass condition and the norm condition was done with a significance level set at  $\alpha = 0.05$ . While a comparison of clustering approaches to conventional statistical approaches is beyond the scope of this chapter, these data are provided for transparency purposes.

### 3.3 Results

The average DfC metric from the K-means analyses are plotted for each individual joint and task, with error bars on the bar plots indicating the standard deviation of the 10 k-means iterations (Figure 3.3). Asterisks in the bar plots indicate that a given DOF/task for a condition resulted in a significantly higher DfC values than the threshold. This figure allows for identification of tasks that separate normative movement from bypass device movement as a function of each analyzed DOF. The threshold for DfC was denoted through the red dotted line at 25 (Figure

3.3). In general, the tasks that exceeded the threshold varied across the bypass conditions and the DOFs within each joint. The results were consistent with previous studies in showing that tasks and joint DOF involved in abnormal movement are device specific. However, certain patterns did emerge and will be discussed in the Discussion section.

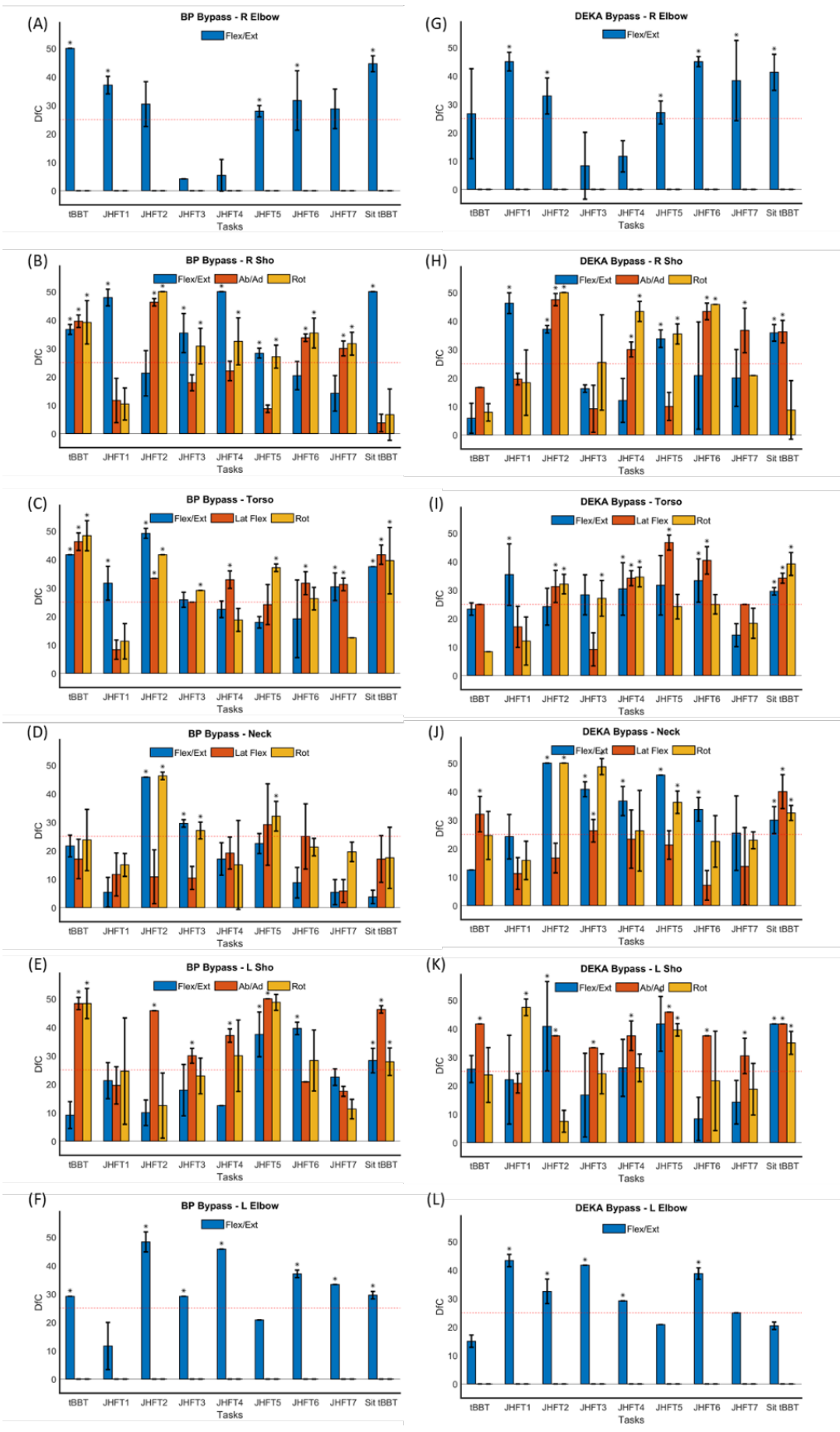


Figure 3.3 Average and standard deviation from chance (DfC) for all tasks, DOFs, and bypass condition comparisons: A-F) Body Powered Bypass v. Norm Joint results, G-L) DK Bypass v. Norm Joint Results. Tasks JHFT1 - Writing, JHFT2 - Page Turning, JHFT3 - Picking Up Small Objects, JHFT4 - Simulated Feeding, JHFT5 - Stacking Checkers, JHFT6 - Moving Large Light Objects and JHFT7 - Moving Large Heavy Objects Distributions significantly greater than the threshold at DfC = 25 (red dotted line) denoted by a \* ( $p < 0.05$ ). (Figure 3 of Wang et al., 2021[93])

To get a better sense of which tasks and DOFs were associated with the greatest distinguishability between normative movement and bypass condition movement, the K-means results that were significantly greater than the DfC threshold were summarized for each bypass condition. Out of the 126 k-means analyses for the BP bypass condition (9 tasks x 14 DOFs) performed, 62 significantly exceeded the threshold. For those 62 analyses, the frequency of appearance of a particular task (Table 3.1A) or DOF (Table 3.1B) was determined and presented as a percentage. The same summary was done for the DK bypass condition, with 64 out of 126 analyses significantly exceeding the threshold, and the frequency of a particular task (Table 3.1A) or DOF (Table 3.1B) was determined.

Table 3.1 Percentage of times a (A) task and (B) DOF were associated with deviations from chance distributions significantly greater than the threshold. (Table modified from Table 1. of Wang et al., 2021[93])

(A)	Task Frequency (%)	
	BP Bypass	DK Bypass
tBBT	16.1	3.1
JHFT1 - write	4.8	7.8
JHFT2 - page turn	14.5	17.2
JHFT3 - small objects	11.3	9.4
JHFT4 – simulated feeding	8.1	12.5
JHFT5 – stacking checkers	12.9	14.1

JHFT6 - light cans	9.7	12.5
JHFT7 - heavy cans	8.1	4.7
Sit-tBBT	14.5	18.8

<b>(B)</b>	DOF Frequency (%)	
<b>DOF</b>	<b>BP Bypass</b>	<b>DK Bypass</b>
R Elbow - Flex/Ext	8.1	9.4
L Elbow - Flex/Ext	11.3	7.8
R Sho - Flex/Ext	9.7	6.3
R Sho - Ab/Ad	6.5	7.8
R Sho - Rot	11.3	6.3
L Sho - Flex/Ext	4.8	4.7
L Sho - Ab/Ad	9.7	12.5
L Sho - Rot	4.8	4.7
Neck - Flex/Ext	3.2	9.4
Neck - Lat Flex	0.0	4.7
Neck - Rot	4.8	6.3
Torso - Flex/Ext	8.1	6.3
Torso - Lat Flex	9.7	7.8
Torso - Rot	8.1	6.3

The most frequent tasks with high DfC values for both the BP bypass and DK bypass conditions were JHFT2 – Page Turning, occurring in 14.5% and 17.2% of the significant results, respectively (Table 3.1A). Some tasks were found to elicit more significant DfC values for one bypass condition, but not the other. For example, 16.1% of the significant results were elicited by tBBT in the BP bypass condition compared to only 3.1% for this same task in the DK bypass condition.

When all DOFs are combined, the right shoulder and torso appear more often in the significant results across both bypass conditions, indicating these joints are most informative for distinguishing movement between the Norm and Bypass conditions (Table 1B). Interestingly, left shoulder abduction/adduction appears often in the significant results for both the BP (9.7%) and DK (12.5%) bypass conditions. While each DOF tends to be equally represented in the significant results across bypass conditions, there is a large discrepancy in the neck DOFs, with these DOFs appearing more often when distinguishing movement between the Norm condition and DK bypass condition.

### *3.4 Discussion*

The goals of this work were to utilize unsupervised machine learning to identify features that will inform abnormal movement for several tasks and elucidate the variations in movement approach across two different upper-limb prosthesis devices with varying DOFs as compared to non-disabled controls. To achieve those goals, specific features of movement derived from motion capture data from individuals with no upper limb impairment or disability under normative conditions and individuals using two upper limb bypass prosthesis devices (body-powered hook and DEKA arm) were used as input into a K-means clustering algorithm. While a few studies have focused on the application of clustering algorithms to the upper limb prosthesis user population, the use of these clustering methods to compare movement of individuals using these two prosthetic devices to the movements of non-disabled individuals has not been done. Although patterns emerged, there was no single DOF that was universally distinctive across tasks and Bypass conditions (Figure 3.3) and

no single task that consistently elicited distinctive movements between the Norm and Bypass conditions (Figure 3.3). This result is not unexpected, however, based on previous studies that have indicated compensation patterns for this clinical population are both task and device dependent[13, 52]. The BP Bypass results, with highly distinct torso and shoulder angles, were consistent with the results from Metzger et al. 2012 which had 7 of the 10 participants using a body powered device[7]. Additionally, the compensatory motions of the head and torso found by Hussaini et al. 2017 in prosthesis users equipped with single DOF electric hand terminal devices[14] also corresponded well with the distinct joint angles identified in the BP Bypass condition. With a more robust approach to characterizing movement that simultaneously incorporates multiple features of movement into advanced clustering algorithms to identify differences, the results presented here still build on existing knowledge and can be used to inform the development of scoring methodology for upper limb performance-based outcome measures. A discussion of the clinical implications of the results as well as limitations and future work follows.

According to Table 3.1B, the right shoulder and torso are more frequently associated with high DfC values, meaning differences in normative and bypass prosthesis user movement are greater for these body regions. Figure 3.3B and H indicate that tasks requiring a lot of wrist motion, such as JHFT2 - page turning and JHFT6 – moving large, light objects, will challenge shoulder abduction and internal rotation for both BP and DK Bypass prosthesis users, but not so much shoulder flexion. This information could be used to devise more targeted approaches for the assessment of “normal” movement for tasks typically requiring wrist manipulation.

Instead of simply asking an observer to make a subjective assessment of the normalcy of movement, instructions could be provided to closely observe how far the upper arm goes out to the side or how much rotation is required of the upper arm to complete a task. Similarly, instructions could be provided to focus more on torso rotation as opposed to torso forward flexion or lateral flexion for tasks that require small object manipulation. Figure 3.3C and I indicate for tasks such as JHFT3 – small objects and JHFT5 - stacking checkers, torso rotation is the DOF that differs most consistently between non-disabled controls and bypass prosthesis users.

As mentioned previously, the type of device being used may also be an important factor to consider when assessing normalcy of movement and the impact of the device on compensatory movement. Figure 3.3B, for example, shows that right shoulder flexion/extension during JHFT4 – simulated feeding is significantly different between non-disabled control movement and BP Bypass prosthesis user movement. However, Figure 3.3H shows that right shoulder abduction/adduction and rotation are the DOFs that distinguish non-disabled control movement from DK Bypass prosthesis user movement for this same task. Another interesting observation showing the potential impact of device on movement can be seen in the neck DOFs in Table 3.1B and DfC plots in Figure 3.3D and J. Of all the DOFs that appeared in the results significantly higher than the DfC threshold of 25 for the BP bypass condition, only 8.1% included neck DOFs. Conversely, 20.3% of the significant results for the DK bypass included neck DOFs. This implies neck movements of individuals using the DK bypass prosthesis are more often different from the non-disabled control group. The result can be explained by considering the visibility of objects being

manipulated by the terminal device of these two prosthetic systems, with body-powered hooks more typically known for good visibility of objects [3].

Understanding how the device impacts the movement of the user is important to assessing the normalcy of the observed movement, and the results presented here serve as a preliminary source for elucidating such an impact for two types of upper limb prosthetic devices.

Due to the binary nature of the classification problem (i.e., Norm vs a Bypass), and the simplicity of the algorithm's decision-making approach, K-means clustering was selected for this study. K-means clustering is a partitioning algorithm that divides data into groups of at least one value with each data value assigned to exactly one group, by minimizing the mean distance of the data value from an assigned cluster center value in repeated rounds of reassignment as necessary[106, 107]. Alternate partitioning algorithms, model-based algorithms, or density-based clustering algorithms may provide greater separation between conditions. The features selected (peak angle, range of motion, path distance, mean angle, peak angle velocity, and zero crossings) were selected for their ease in translation to actual motion and understandability. This study aimed to use a minimally burdensome easily understandable machine learning approach to examine motion data for useful differences, so no dimensionality reduction approaches were applied. The identification of features most informative to the difference between normative and bypass prosthesis user movement was out of scope for this paper, but such an analysis may help contribute to consensus on the definition of movement quality.

Even with only six features characterizing movement, the K-means clustering approach was able to identify distinctive joint DOFs for several ADL tasks over two methods of simulated upper limb prosthesis use. With the development of more compact, easily implementable motion analysis systems such as 3D optical marker-based motion capture, inertial measurements units, or markerless motion capture that can be used in the home or clinic, the widespread collection of quantitative movement data is becoming more of a reality. Although limited in generalizability to actual prosthesis users, this dataset can be used to inform the development of larger, more applicable datasets to be incorporated into a supervised machine learning algorithm for the real-time identification of abnormal or compensatory movement based on movement data input.

Key limitations of this study include the limited sample size due to the high training requirements for skillful bypass device use, the use of non-disabled participants, the unilateral nature of the tasks selected, as well as the limited interaction zones required for task performance. While the use of uniformly trained non-disabled participants limits the sources of kinematic variation to those of the device and potentially allows for a larger participant pool, the generalizability of these results to individuals with upper limb loss remains to be seen. Furthermore, the unilateral nature of the tasks selected allowed the examination of device induced changes in kinematics but may not be fully representative of device use patterns outside of the lab environment. Lastly, all tasks were performed in a frontal central interaction zone, which reflects the task space of performance-based outcome

measure tasks in common use[99]. However, device induced kinematic changes outside of this interaction zone were not captured.

For the purposes of simultaneous motion capture in SA3, the following tasks were chosen: 1) JHFT Task 2 – Page Turn, 2) JHFT Task 3 – Pick up objects, 3) JHFT7 – Heavy Cans, and 4) Standing tBBT. These tasks were chosen based on the distinctiveness across conditions, the variance in required object manipulations, and the variance in task performance space. Additional tasks were chosen from the upper limb prosthesis population validated performance-based outcome measures of AMULA and CAPPFUL to increase the task performance zones involved and to include bilateral tasks. The AMULA tasks chosen were AMULA Task 10 – Fork, AMULA Task 16 – Doorknob, AMULA Task 24 – Overhead Reach. The CAPPFUL tasks chosen were CAPPFUL Task 4 – Dice, CAPPFUL Task 8 – Bottle Squeeze, and CAPPFUL Task 11 – Picture Hang / Ring Pull. Based on the analysis results from this section, the joints of interest for analysis in these tasks are right elbow, right shoulder, neck, and torso.

## Chapter 4: Comparisons of Motion Capture Systems

### *4.1 Introduction*

Motion analysis is a useful method to quantitatively and objectively assess human motion by providing kinematic information (e.g., joint angles, body trajectories, hand velocity, etc.) during task performance. A large proportion of studies investigating human motion use 3D optoelectric motion capture systems. These systems track the position of markers placed on anatomical landmarks of the body to relate the position and orientation of body segments. These systems are advantageous given their high resolution and accuracy, as well as their long history of use in research[16-23] compared to more recently developed mechanisms of motion capture[26, 31, 59-62]. While useful in many clinical populations, assessment of motion in the upper limb prosthesis user population is beneficial as the output of such analyses can aid in rehabilitation by providing more specific details about how a standard task is performed, as well as providing insights into the influence of upper limb prosthesis devices on motion. This is relevant given the upper limb prosthesis user population is known to employ compensatory movements during the performance of everyday tasks to work around lost degrees of freedom (DOF). Given recent technical developments in upper limb prosthesis devices with greater numbers of controllable DOFs [46, 48, 52], many research groups have investigated user movement with these devices using 3D optoelectric motion capture systems[7, 46, 49, 52, 96, 108]. However, the adoption of 3D optoelectric motion capture into the clinic has been slow due to the restrictive operating environment required, high costs, and

longer set-up times required to collect data from optoelectric motion capture systems [26, 31].

Barriers to the use of optoelectric motion capture systems have prompted interest in other systems that have less restrictive operating environment requirements[25, 29]. The Microsoft Kinect is a markerless motion capture sensor system that has been of great interest in research due to the low cost[24, 25] and robustness of the sensors[26-31]. Due to the markerless motion capture mechanism, the set-up time is reduced and the potential for erroneous subject preparation is lower compared to marker-based motion capture systems that are dependent on accurate and consistent identification of anatomical landmarks. Alongside marker and markerless systems, battery and gyroscopic sensor miniaturization and the rapid decrease in technology costs has rendered inertial measurements a new avenue for motion capture research[32-38]. Due to the non-optical mechanism of inertial measurement unit (IMU) motion capture, the operating environment requirements are less restrictive compared to those required for optoelectric systems.

There have been several previous studies comparing motion capture systems that have focused on one-to-one comparisons of a single test system and a gold standard system[33, 36, 63-69], studied the lower limbs[28, 34, 68, 70-73], or relied on mechanical testing devices to ensure the greatest replicability of the ground truth[64, 74-76]. For the one-to-one system comparisons, the parameters examined, motions selected, and populations tested varied greatly, rendering cross system conclusions impractical. Regarding studies in the lower limb, the analyses lack applicability and generalizability to the tracking of motion in the upper limbs,

specifically upper limb prosthesis users. Compared to the lower limbs, the acyclic motions and the multiple redundant DOFs in the upper limb make upper limb motion analysis more challenging. Furthermore, the few studies assessing upper limb function have focused on a limited task space to simplify capture and analysis[12]. Lastly, while the use of a mechanical testing device provides a highly consistent ground truth, it is not fully representative of system performance during human motion given the avoidance of soft tissue artifacts, sensor motion artifacts, and self-occlusion induced errors.

To better understand the performance of various motion capture systems in quantifying upper limb movement in the prosthesis user population, this study compares kinematics (i.e., joint angles) derived from three systems that vary in cost and motion capture mechanisms: a marker-based systems, an IMU system, and a markerless system. Able-bodied individuals using a bypass prosthesis device performed several tasks as movement of the upper body was tracked simultaneously across all three systems. The results of this study can be used to identify consistencies and limitations of various motion capture systems in tracking movements similar to those performed by the upper limb prosthesis user population, which could facilitate the wider adoption of motion capture into rehabilitation.

#### *4.2 Methods*

The data for the MY Bypass users was selected for analysis because the myoelectric terminal device was considered a device with characteristics that were intermediate compared to the body powered hook and the DEKA arm. Like the body powered hook, the myoelectric terminal device has a manual wrist DOF. Like the

DEKA arm, the myoelectric terminal device has powered fingers with pre-programmed grips. As such, this device was considered a useful starting point for generalizing the application of the salient features identified in Chapter 3.

#### 4.2.1 Participants Selected

As previously detailed in Chapter 2, 10 able bodied participants with no upper limb disability or impairment were included in this section of the study. The demographics of the participants for this chapter was previously specified in Chapter 2 and will be repeated here for convenience of reference. There were 5 females and 5 males with a mean age of  $29.6 \pm 7.1$  years. 9 of the 10 participants were right hand dominant ( $92.53 \pm 10.62$  laterality), one was left hand dominant ( $-100$  laterality) per the Edinburgh handedness survey[94].

A bypass prosthetic device was used by able-bodied individuals to elicit similar movement patterns as an upper limb prosthesis user [8, 89-92, 96]. A forearm brace adaptor with a perpendicular handlebar provided by Next Step Bionics allowed the use of a right-hand OSSUR (previously TouchBionics) i-limb Ultra (OSSUR, Foothill Ranch, CA, USA) myoelectric terminal device with manual wrist adjustment. The device was mounted to the brace with a medial offset of  $15^\circ$  from the subject's forearm (Figure 4.1A). In accordance with upper-limb amputee control configurations, myoelectric sensors were placed on antagonist pairs of extensor and flexor muscles on the forearm to control the opening and closing of the device. Grip changes were controlled with the TouchBionic my i-limb<sup>TM</sup> on an iPod Touch<sup>TM</sup> (Apple Inc., Cupertino, CA, USA) (Figure 4.1B). This adaptive bypass device (MY

Bypass) allowed trained able-bodied participants to use a commercial upper limb prosthesis terminal device.

Following the training protocol previously specified in Chapter 2, all participants were trained with the right-hand MY Bypass until a learning plateau of 90% peak performance had been achieved [56].

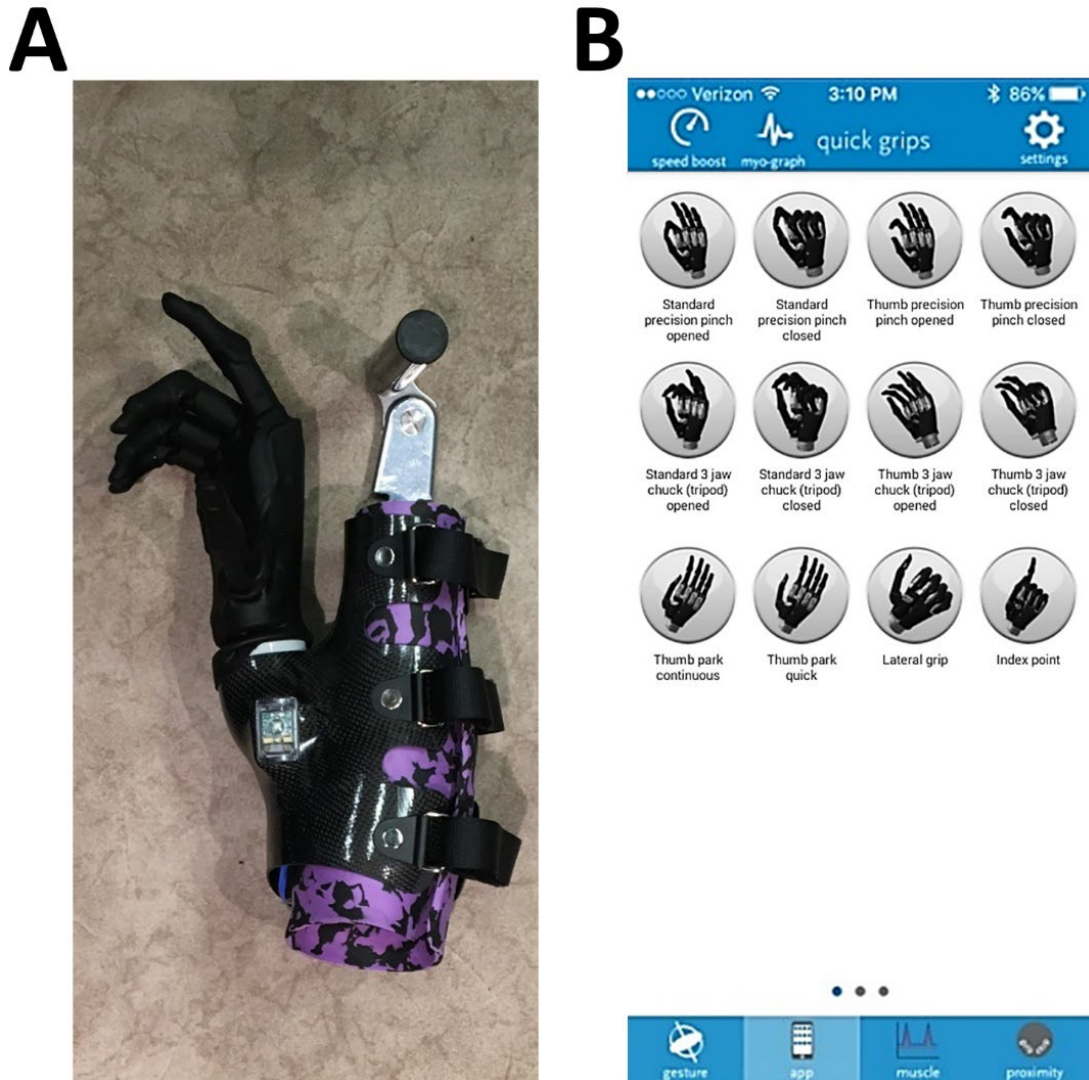


Figure 4.1 A) Right-hand Ossur (TouchBionics) i-limb Ultra myoelectric terminal device. Medial offset = 15°; B) my i-limb grip selection screenshot (Touch Bionics, Apple App Store, 2020). (Figure 1 of Wang et al., 2022[95])

#### 4.2.2 Functional Tasks

When fully trained, participants performed the Targeted Box and Blocks Test (tBBT)[84] as well as tasks selected from the Jebsen-Taylor Hand Function Test (JHFT) [83, 109], Activities Measure for Upper Limb Amputees (AMULA)[85, 86], and Capacity Assessment of Prosthetic Performance for Upper Limb (CAPPFUL)[44] outcome measures while simultaneously recorded by three motion analysis systems. With the motivation to determine the limitations of the motion analysis systems, tasks were selected from the outcome measures that would elicit a wide range of movements representative of those performed during activities of daily living. These outcome measures have also been used in previous kinematic studies[83, 84, 87] and most are validated in the upper limb prosthesis user population[44, 45].

A brief description of each task used in this chapter can be found in Table 4.1. Tasks 2, 3, and 7 from the JHFT were performed in a seated position and are referenced in this manuscript as JHFT – Page Turn, JHFT – Small Objects, and JHFT – Heavy Objects, respectively. Tasks 10, 16, and 24 from the AMULA were performed in the seated position and are referenced as AMULA – Fork, AMULA – Doorknob, and AMULA –Reach, respectively [85, 86]. Tasks 4, 8, and 11 from the CAPPFUL were also performed and are referenced as standing task CAPPFUL– Dice, and seated tasks CAPPFUL– Bottle and CAPPFUL–Picture [44]. A standard template was used to place each object for a given task in the same location for each participant. The tBBT was performed in the standing position[84]. Participants performed three trials of each task.

Table 4.1 Description of tBBT and subtasks from the JHFT, AMULA, and CAPPFUL performed in the current chapter (Table modified from Table 1 of Wang et al., 2022[95])

Task name	Description
JHFT – Page Turn	Flip over five 3x5 cm notecards arranged in a row with any technique, starting with the leftmost card and moving across. Performed seated
JHFT – Small Objects	Pick up six small objects (2 paperclips, 2 bottle caps, & 2 pennies) arranged two inches apart on the dominant side of the subject, and place in an empty can individually, starting with the right most object. Performed seated
JHFT – Heavy Objects	Lift 5 filled cans individually about 1” onto a board, starting with the rightmost can. Performed seated
AMULA – Fork	Grasp fork and bring to mouth, move fork back to table and release fork. Performed seated.
AMULA – Doorknob	Reach, grasp, and turn door knob. Release doorknob. Performed Seated
AMULA – Reach	Lift arm overhead to grasp empty cup on shelf and bring down arm with cup in hand. Performed standing
CAPPFUL – Dice	Pick up three dice from a plate, touch to chin, and return to plate. Performed standing.
CAPPFUL – Bottle	Empty a squeeze bottle of water into a cup. Performed seated.
CAPPFUL – Picture	Modified task – Reach overhead to grasp two rings suspended in the air on a pulley system, bring rings down to waist, then control the placement of rings back in their suspended position. Performed seated
tBBT	Transport 16 blocks, one at a time, over a partition using only the dominant hand, starting with the innermost left block and moving across each row placing the block in its mirrored position. Performed standing

### 4.2.3 Motion Analysis Systems

Motion analysis involved the simultaneous recording of motion data from three systems: optical marker-based system (VICON, Oxford, UK), an inertial measurement unit (IMU)-based system (Xsens Awinda MTw, El Segundo, CA, USA), and a markerless system (dual Microsoft Kinect V1s with iPi Recorder). The Vicon optical marker-based system was selected as the reference system based on its popularity and usage in the literature[30, 64-66, 72, 73, 76, 102, 110-112]. The IMU-based [32-36, 67-71, 113-115] and markerless systems [24, 25, 27, 29-31, 66, 72-75,

116, 117] were selected due to popularity in the literature and due to their differing mechanisms of motion capture.

The sensors of the three systems were not expected to mutually interfere due to the independent locations of the sensor placements and the differences in the recording mechanisms. Excepting the sternum location alone, all other IMUs and retroreflective markers were mounted directly on the body (Figure 4.2). The sternum location required the sternum reflective marker to be mounted on the sternum IMU sensor for the tracking accuracy of the Vicon software.

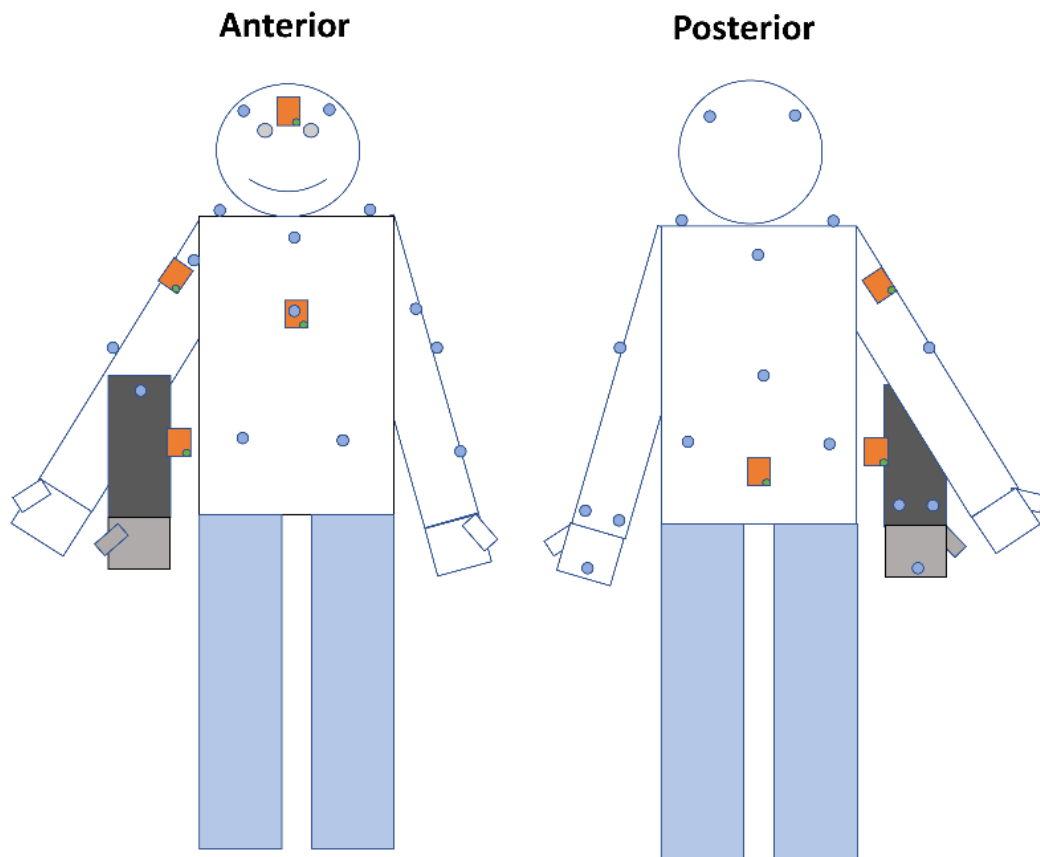


Figure 4.2 Illustration of sensor locations with the anterior view on the left and posterior view on the right. Orange boxes represent IMU sensors. Blue dots represent retroreflective markers. The black box represents the bypass device and the location relative to the forearm of the participant. The grey boxes represent the myoelectric terminal device. (Figure A1. of Wang et al., 2022[95])

During the data cleaning and processing phase, review of the exported data showed that the markerless system's software and background subtraction mechanism detected neither the retroreflective markers used by the optical system-based system nor the IMU sensors. The IMU sensors were not retroreflective and were not detected by the optical marker-based system.

#### **4.3.2.1 Optical Marker-Based System – Vicon Nexus**

A ten-camera passive marker Vicon™ motion analysis system consisting of eight Bonita B10 and two Vero v1.3 cameras was used to acquire and pre-process motion data (VICON, Oxford, UK). The motion capture cameras were set to a sampling rate of 100Hz. Prior to each data collection session, the system was calibrated according to manufacturer guidelines. Twenty-seven retro-reflective markers were placed on the upper body of each participant at the bony anatomical landmarks of the upper body in accordance with the Vicon Upper-Body Plug-In-Gait body model documentation. The Plug-In-Gait upper body model was then calibrated to the dimensions of the participant to create the wrist, forearm, upper arm, head, neck, thorax, and pelvic model segments. The Vicon was set as the primary recording system and controlled the initiation and termination of recordings with a voltage duration sync pulse output.

#### **4.3.2.2 IMU System - Xsens Awinda**

Five (IMUs) for the Xsens Awinda were placed either at bony anatomical landmarks or the midpoints of moving body segments on the head, right arm, and torso (Figure 2). The head sensor was placed in the center of the subject's forehead. The torso sensor was on the xiphoid process of the sternum. The pelvis sensor was

placed at the midpoint between the left and right posterior superior iliac spine. The upper arm sensor was placed on the midpoint of the upper arm. The forearm sensor was placed on the anterior midpoint of the bypass. The system was set to a sampling rate of 100Hz. Prior to each data collection session, all sensors were set to zero at the origin of the recording volume on the floor, as defined by the Vicon calibration to ensure consistent initial sensor outputs. The Xsens was set as the secondary recording system with initiation and termination of recordings automatically controlled through a voltage duration sync pulse from the Vicon system, leading to the synchronization of the two data streams from these systems.

#### **4.3.2.3 Markerless system – Kinect V1 iPiSoft**

Two Kinect V1 cameras (Microsoft, Seattle WA, USA) were used with the iPi Soft markerless motion capture software (iPi Soft, Moscow, RU) to acquire and pre-process motion data. The Kinect V1 was selected due to the limitations of the native Microsoft SDK which did not allow for multiple Kinect V2 data streams into a single computer. This limitation did not apply to the Kinect V1, which allowed for larger capture volumes and improved capture results when multiple Kinect V1 sensors were used[118]. Additionally, the Azure Kinect was both not commercially available and not supported by the iPi software at time of experiment. The Kinect cameras were positioned approximately  $\pm 45^\circ$  from the midline of the subject at a distance of approximately 6 feet. The camera tripods were placed in the same position for each subject. The point of aim for the Kinect cameras was determined through the calibration procedures for the Kinect system and may vary depending on the experimental conditions.

The system was set to 30 Hz, the maximum sampling rate of the cameras. Prior to each data collection session, the system was calibrated according to the software manufacturer's guidelines. Initiation and termination of recordings were manually controlled by the operator of the motion analysis systems. Data synchronization and resampling to 100Hz with the built-in MATLAB function *resample* was achieved through a post-processing automated MATLAB script. This was done to create time series data that was sampled at the same rate to compare each distinct time point across systems.

#### 4.2.4 Data Analysis

Joint angles over time were generated for all three systems. The joint angle data from the Vicon system was set as the reference system given its high resolution and accuracy[16-23], as well as previous history of use as reference systems in research[30, 64-66, 72, 73, 76, 102, 110-112]. Root mean square error (RMSE) (Equation 4.1) and bias (Equation 4.2) were calculated for the IMU and markerless datasets. In equations 1 and 2,  $i$  is the index for each frame in a given joint movement trajectory.

$$\text{RMSE} = \sqrt{\left(\frac{1}{n}\right) \sum_{i=1}^n (\text{testSystem}_i - \text{Vicon}_i)^2}$$

Equation 4.1

$$\text{Bias} = \left(\frac{1}{n}\right) \sum_{i=1}^n (\text{testSystem}_i - \text{Vicon}_i)^2$$

Equation 4.2

A description of the joint angle calculations from each system used in the above equations is provided below.

To assess consistency of measurements from each system, the intraclass correlation coefficient (ICC) was calculated using a two-way mixed effects model (ICC(3,1)). Each participant performed three trials of the same task. These three trials were used to determine the ICC of a discrete kinematic parameters derived from the joint trajectory (range of motion) for each task/DoF combination and for each motion system evaluated in our study. The use of discrete kinematic parameters, such as RoM, was used to avoid artificially low ICC values due to slight misalignments in the trajectories across trials within a subject.

#### **4.4.2.1 Optical Marker-Based System**

Joint angles were calculated in accordance with the methods previously described in Chapter 2. YXZ Euler angles were derived from relative orientation comparisons of two segments (VICON Plug-In-Gait, Oxford, UK). Joint angles analyzed in this chapter include right elbow flexion/extension; right shoulder flexion/extension, abduction/adduction, and internal/external rotation; torso flexion, lateral flexion, and rotation; and neck flexion, lateral flexion, and rotation.

As previously described in Chapter 2, the recorded data from each task was processed and manually segmented in Vicon Nexus into object interactions with the beginning of a segment defined as when the terminal device approached the object, and the end of a segment when the terminal device released the object. For tasks with multiple objects, such as the six objects in JHFT – Small Objects, this resulted in multiple segments. Although the locations of the task objects are standardized with

placement templates, the individual objects may be distributed in the task space. Therefore, to reduce variability introduced in joint kinematics due to object distribution, the analysis was limited to the last segment, or last object interaction, within each trial.

#### 4.4.2.2 IMU System

The joint angles for the IMU-based system were calculated based on relative sensor orientation. The parent sensor is the sensor used to define a local coordinate system for a given body segment, which will be called the parent body segment. The child sensor is the sensor that measures the motion of a different body segment, which will be called the child segment. The method described below defines the motion of the child body segment relative to the local coordinate system defined by the parent sensor as measured through Euler decomposition.

Table 4.2. Definitions of Parent and Child Segments for each joint of Interest. (Modified from Table A1. Of Wang et al., 2022[95])

<b>Joint</b>	<b>Parent</b>	<b>Child</b>
Elbow	Upper Arm	Forearm
Shoulder	Torso	Upper Arm
Neck	Torso	Head
Torso	Torso	Pelvis

First, the quaternion outputs of the parent and child sensors are transformed into standardized local coordinate systems. The known locations of each sensor upon the body are used to define three element vectors which correspond to the Superior-Inferior (SI), Medial-Lateral (ML), and Anterior-Posterior (AP) axes of the sensor that align with the body. These vectors can be called SICalVec, MLCalVec,

APCalVec, respectively. These three element vectors are used to transform the coordinate systems of the sensors from sensor-based local coordinates to body-based local coordinates through quaternion conjugations.

The first step to determining the Euler angles is taking the standardized SI, ML, and AP axes of the child sensor. These axes are defined relative to the body of the participant, so the SI axis of the sensor corresponds to the SI axis of the participant's body. The ML axis of the sensor corresponds to the ML axis of the body, and the AP axis corresponds to the AP axis of the body. These axes are used to produce the three vectors  $\text{ProjectedVector}_{\text{SI}}$ ,  $\text{ProjectedVector}_{\text{ML}}$ ,  $\text{ProjectedVector}_{\text{AP}}$ , which are defined by projecting the SI, ML, and AP axes of the child sensor onto the standardized local coordinate system defined by the parent sensor, X-Y-Z.

The first rotation of the Euler decomposition, labeled  $\text{Rotation}_Y$ , as it rotates the child sensor's projected SI axis in the local coordinate system's original Z-X plane, which is described as follows in Equation 4.3. This rotation also results in a new interim coordinate system with axes labeled X', Y', Z'.

$$\text{Rotation}_Y = \tan^{-1} \left( \frac{\text{ProjectedVector}_{\text{SIComponent3}}}{\text{ProjectedVector}_{\text{SIComponent1}}} \right)$$

Equation 4.3

The second rotation of the Euler decomposition is performed about the new X' axis that results from Equation 4.3. This can be found in the Z'-Y plane, which is identical to the Z'-Y' plane as Equation 4.3 did not involve the local coordinate system's y-axis. The  $\text{ProjectedVector}_{\text{SI}}$  component along the z' axis can be found from the components of the original z-x plane using the Pythagorean theorem. This is used to define  $\text{ProjectedVector}_{\text{SIComponentZ}'}$  in Equation 4.4.

ProjectedVector<sub>SSIComponentZ'</sub> is then used to find the second rotation Euler rotation about the new X' axis with Equation 4.5. This also results in a new coordinate system with axes labeled X'',Y'',Z''.

$$\text{ProjectedVector}_{\text{SIComponentZ}'} = \sqrt{(\text{ProjectedVector}_{\text{SIComponent1}}^2 + \text{ProjectedVector}_{\text{SIComponent3}}^2)}$$

Equation 4.4

$$\text{Rotation}_{\text{X}'} = \tan^{-1} \left( \frac{\text{ProjectedVector}_{\text{SI Component 2}}}{\text{ProjectedVector}_{\text{SIComponentZ}'}} \right)$$

Equation 4.5

To determine the third Euler Angle about Z'', first a quaternion is defined (Equation 4.6) to describe rotation about axis Y from the X,Y,Z coordinate system, also known as the ML axis. MLCalVec is a three-element vector describing the ML axis of the parent sensor, which was pre-defined by the known orientations of the individual IMU sensors on the body. This vector is the same vector previously used to transform the individual sensor coordinate systems into uniform body-based coordinate systems.

$$\text{Quaternion}_{\text{rotationY}} = \left[ \cos \left( \frac{\text{Rotation}_y}{2} \right); \sin \left( \frac{\text{Rotation}_y}{2} \right) * \text{MLCalVec}_{\text{component1}}; \sin \left( \frac{\text{Rotation}_y}{2} \right) * \text{MLCalVec}_{\text{component2}}; \sin \left( \frac{\text{Rotation}_y}{2} \right) * \text{MLCalVec}_{\text{component3}} \right]$$

Equation 4.6

Quaternion<sub>rotationY</sub> is then used to rotate the X axis from the X,Y,Z coordinate system to find the X' axis through quaternion conjugation as described in (Equation 4.7). The X' Axis vector is then projected onto the coordinate system defined by ProjectedVector<sub>SI</sub>, ProjectedVector<sub>ML</sub>, and ProjectedVector<sub>AP</sub> to produce

ProjectedX'Axis. The third Euler Angle about Z'' is found with the components of ProjectedX'Axis as described in (Equation 4.8).

$$X'Axis=(Quaternion_{rotationY}*Quaternion_{XAxis})*Quaternion_{rotationY}^{-1}$$

Equation 4.7

$$Rotation_{Z''}=\tan^{-1}(ProjectedX'Axis_{Component2}/ProjectedX'Axis_{Component3})$$

Equation 4.8

To reiterate in brief, the right elbow flexion/extension was calculated between the forearm and upper arm sensors. Right shoulder angles were calculated between the sternum and upper arm sensors. Neck angles were calculated from the head and sternum sensors. Torso angles were calculated between the sternum and pelvis sensors.

The IMU sensor orientations were output as quaternions and decomposed into axial vector components that corresponded to the three axes of the sensor units in unit quaternions. Then, the axial vector components were used to generate the individual Euler joint angle components through decomposition. The decomposition used the known initial orientations of the sensor unit locations on the body to define a superior-inferior axis for each sensor, with the other two axes defined through orthogonality. The angles defined through the pairs of sensors sought to mimic the output of the Vicon YXZ Euler angle outputs. However, the shoulder angles suffered from computational errors and the XYZ rotation order was used instead to best match the Vicon outputs. This approach matched what was found in a recent study [36]. The planar surface sensor calibrations and known body placement locations were used for the alignment of sensor axes to body segment axes. The initial values of the Vicon

outputs were used to initialize the values of the derived Xsens angles to limit the variance from the calibration approach. In some instances, joint angles from the Xsens IMU system were inverted to match the conventions of the Vicon reference system angle values. The resultant angles were then visually examined for computational anomalies that violated anatomical angle limits due to gimble lock. Trajectories with computational anomalies were manually removed from the analysis.

Since the data from the optical marker-based and IMU systems were synchronized, the IMU data was segmented for analysis using the segmentation event markers from the optical marker-based system. As previously mentioned, analysis was limited to the last segment of each task.

#### **4.4.2.3 Markerless System**

The joint angles for the dual Kinects were calculated with the Biomech add-on toolbox for iPi studio using YXZ Euler angles derived from the relative orientation comparisons of two skeletal rig segments (iPi Soft, Moscow, RU). To derive joint angles comparable to those generated from the optical marker-based system, re-zeroing operations were performed on the outputs of the Biomech toolbox. In some instances, joint angles from the Kinect system were inverted to match the conventions of the Vicon reference system angle values. For the right elbow angles, due to the obscuration of the MY Bypass device caused by the actual right arm, the Kinect prioritized arm tracking over bypass tracking. An offset of  $15^\circ$ , equal to the medial offset of the device, was applied to these elbow angles to provide a more accurate estimate.

The data from the markerless system were synced with the optical marker-based and IMU systems post-capture with an automated MATLAB script. To aid in this synchronization, all subjects started each trial with their hands at their side and subsequently moved their arms into a “motor-bike” pose. The MATLAB script detected time points in each system where the joint angle rate of change, or joint angle derivative, in the right shoulder exceeded a preset threshold (determined through pilot experiments). The data from each system were aligned to this detected time point. As previously mentioned, analysis was limited to the last segment of each task.

#### *4.3 Results*

The distributions of RMSE and bias values across all trials and subjects for the two comparison systems relative to the reference system are shown as boxplots for each joint in Figure 4.3 - Figure 4.6. In each figure, the values for the IMU system are shown in red; values for the markerless system are shown in blue. Within each distribution, white circles with a black dot indicate the median of the distribution.

The markerless system tended to slightly overestimate the right elbow angle while the IMU system was inconsistent and greater in magnitude in the bias measurement (Figure 4.3B). Larger errors were seen with the IMU system for right elbow flexion: the median RMSE values for the markerless system were between 14.4° and 31.2° while the median RMSE values for the IMU system were between 23.8° and 62.6°. The AMULA - Reach task had the highest median RMSE values across both systems (Figure 4.3A). This task resulted in a relatively low bias value

across the tasks for the markerless system at 8.4°, and the most positive bias value for the IMU system at 59.1°.

Conversely, with the right shoulder, the IMU system had lower median RMSE values and tended to have lower variance for RMSE and bias compared to the markerless system (Figure 4.4A and B). The median RMSE values across tasks and DOFs for the IMU system were all under 30° while median RMSE values at the shoulder for the markerless system were above 30°. The markerless system tended to underestimate shoulder flexion/extension and shoulder rotation while overestimating shoulder adduction/abduction. In contrast, the IMU system tended to overestimate shoulder rotation and underestimate shoulder abduction/adduction across tasks.

Compared to the markerless system, the median bias values for the IMU system tended to be closer to zero across all tasks and DOFs (Figure 4.4B). The tasks with the lowest RMSE values and the bias values closest to zero varied depending on the joint angle component. For the IMU system, JHFT – Page Turn had the lowest median RMSE for shoulder flexion/extension at 5.1° and the task's median bias was the closest to zero for all tasks in the shoulder flexion/extension component at 0.02°.

The AMULA – Reach task had the lowest median IMU RMSE for shoulder abduction/adduction at 7.2°, and the corresponding median bias was 1.3°. CAPPFUL – Bottle had the lowest median IMU RMSE for shoulder rotation at 9.2°. For the markerless system: the lowest median shoulder flexion/extension RMSE value was in the AMULA - Fork task (18.5°), the lowest median shoulder abduction/adduction RMSE value was in the JHFT – Page task (30.8°), and the smallest median shoulder rotation RMSE value was in the CAPPFUL – Picture task (28.2°). The bias values

closest to zero for all tasks in the markerless system were in: AMULA - Fork for shoulder flexion/extension ( $-7.0^\circ$ ), CAPPFUL – Bottle for shoulder abduction/adduction ( $-3.1^\circ$ ), and CAPPFUL - Bottle for shoulder rotation ( $-2.6^\circ$ ).

With the neck angle measurements (Figure 4.5A and B), the IMU system tended to have slightly lower RMSE values and comparable variance compared to the markerless system. For the IMU system, neck rotation in the AMULA – Reach was a notable outlier in the variance even though the median RMSE value of  $13.9^\circ$  was in line with the magnitude of the neck rotation values found in other tasks. Similarly, the markerless system had the largest median RMSE value in AMULA – Reach neck rotation at  $29.04^\circ$ . The IMU system was more closely clustered around zero for the bias values compared to the markerless system. The median RMSE and bias values that were closest to zero were distributed across the JHFT – Heavy Objects, CAPPFUL – Bottle, and CAPPFUL - Dice tasks for the three components of the neck across the two systems. In the IMU system, the median RMSE values ranged from  $6.6^\circ$  to  $14.7^\circ$  while bias values ranged from  $-13.7^\circ$  to  $4.9^\circ$ ; for the markerless system the median RMSE values ranged from  $4.2^\circ$  to  $28.3^\circ$  and the median bias values ranged from  $-25.6^\circ$  to  $23.6^\circ$ .

With the torso angle measurements (Figure 4.6A and B), the IMU system tended to have slightly lower median RMSE values compared to the markerless system. However, the IMU system had much greater variance in torso rotation RMSE values in the CAPPFUL - Dice and tBBT tasks. The markerless system had the greatest median RMSE values and greatest RMSE variance in torso flexion for the JHFT – Page Turn and JHFT – Small Objects tasks. For both systems, the task with

the lowest median RMSE values for all torso components was CAPPFUL – Bottle. For the IMU, the torso flexion/extension was  $5.30^\circ$ , the torso lateral flexion was  $2.9^\circ$ , and the torso rotation was  $3.2^\circ$ . For the markerless system, the torso flexion/extension was  $6.9^\circ$ , the torso lateral flexion was  $2.3^\circ$ , and the torso rotation was  $2.6^\circ$ . With the IMU system, the median RMSE values ranged from  $3.2^\circ$  to  $15.8^\circ$  and the bias values ranged from  $-10.7^\circ$  to  $10.3^\circ$ ; with the markerless system, the median RMSE values ranged from  $2.3^\circ$  to  $24.1^\circ$  and the bias values ranged from  $-22.5^\circ$  to  $14.0^\circ$ .

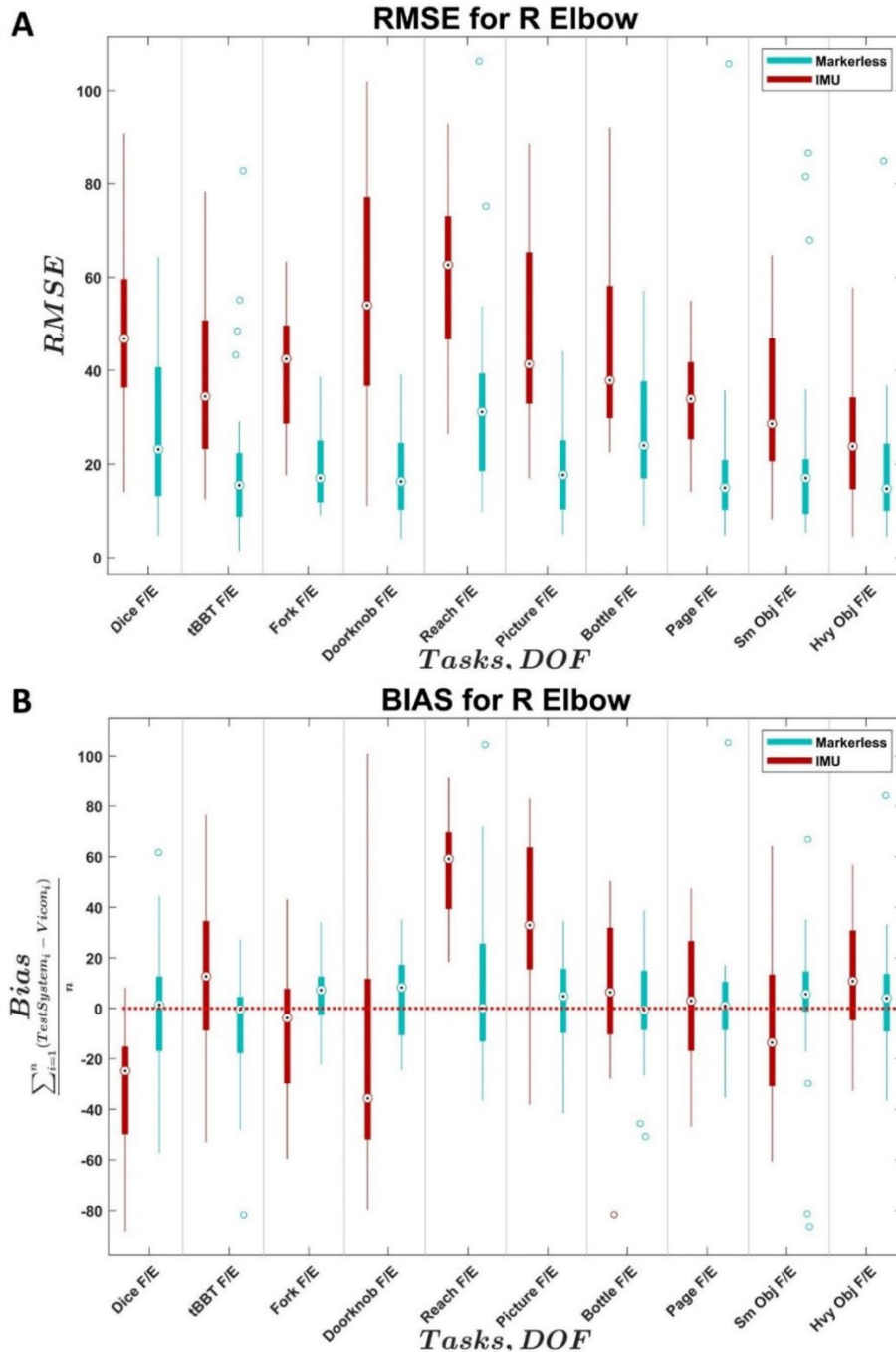


Figure 4.3 Distributions of (a) right elbow flexion RMSE and (b) right elbow flexion bias across subjects for the IMU system (Xsens) and markerless system (Kinect) compared to the Vicon reference system. X-axis identifies the task and associated joint angle. F/E = flexion/extension, Ab/Ad = abduction/adduction, LaF = lateral flexion, Rot = rotation. Black dots indicate medians, empty circles indicate outliers, bold line indicates quartiles, and whiskers indicate non-outlier maximums and minimums. (Figure 2 of Wang et al., 2022[95])

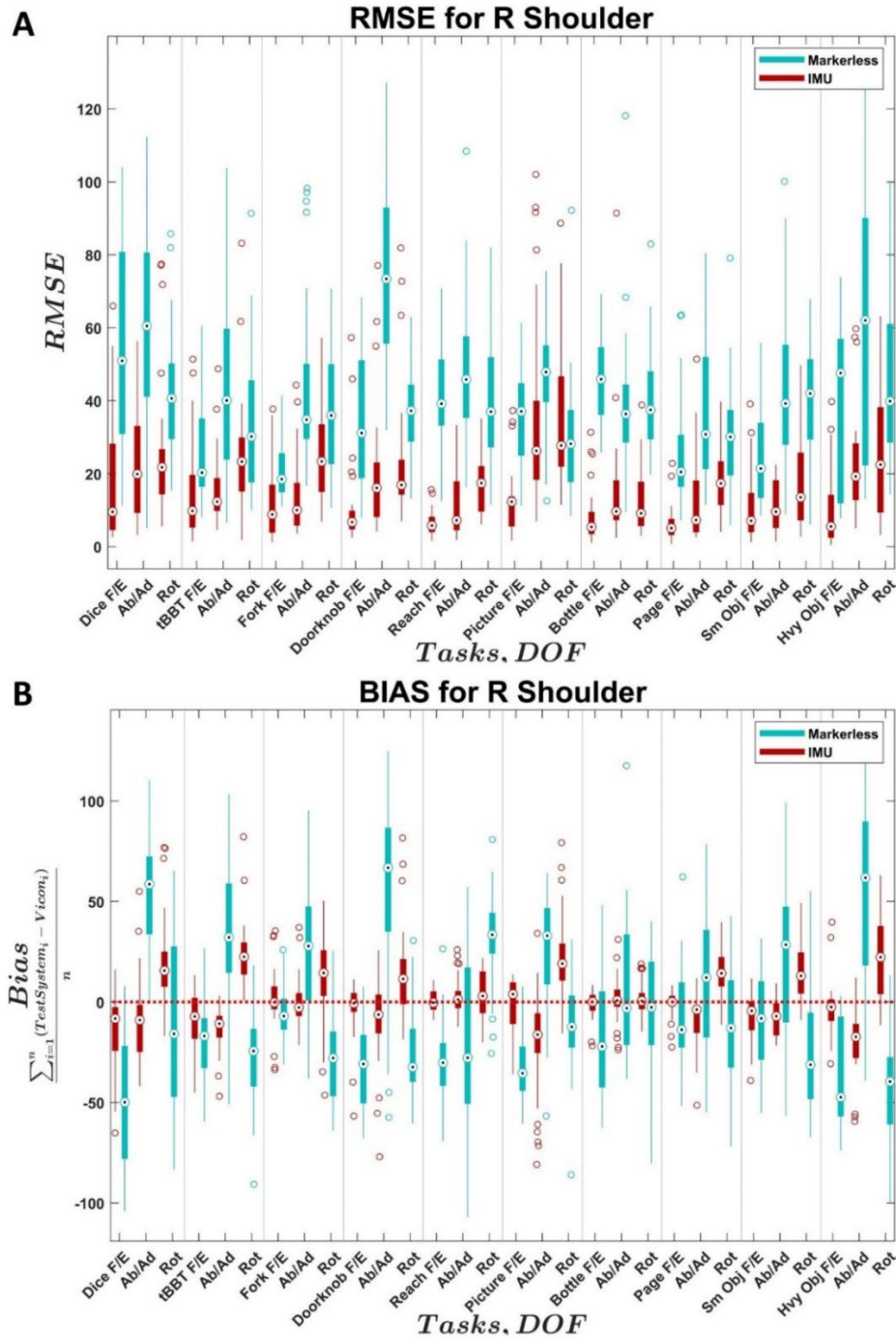


Figure 4.4 Distributions of (a) right shoulder joint angle RMSE and (b) right shoulder joint angle bias across subjects for the IMU system (Xsens) and markerless system (Kinect) compared to the Vicon reference system. X-axis identifies the task and associated joint angle. F/E = flexion/extension, Ab/Ad = abduction/adduction, LaF = lateral flexion, Rot = rotation. Black dots indicate medians, empty circles indicate outliers, bold line indicates quartiles, and whiskers indicate non-outlier maximums and minimums. (Figure 3 of Wang et al., 2022[95])

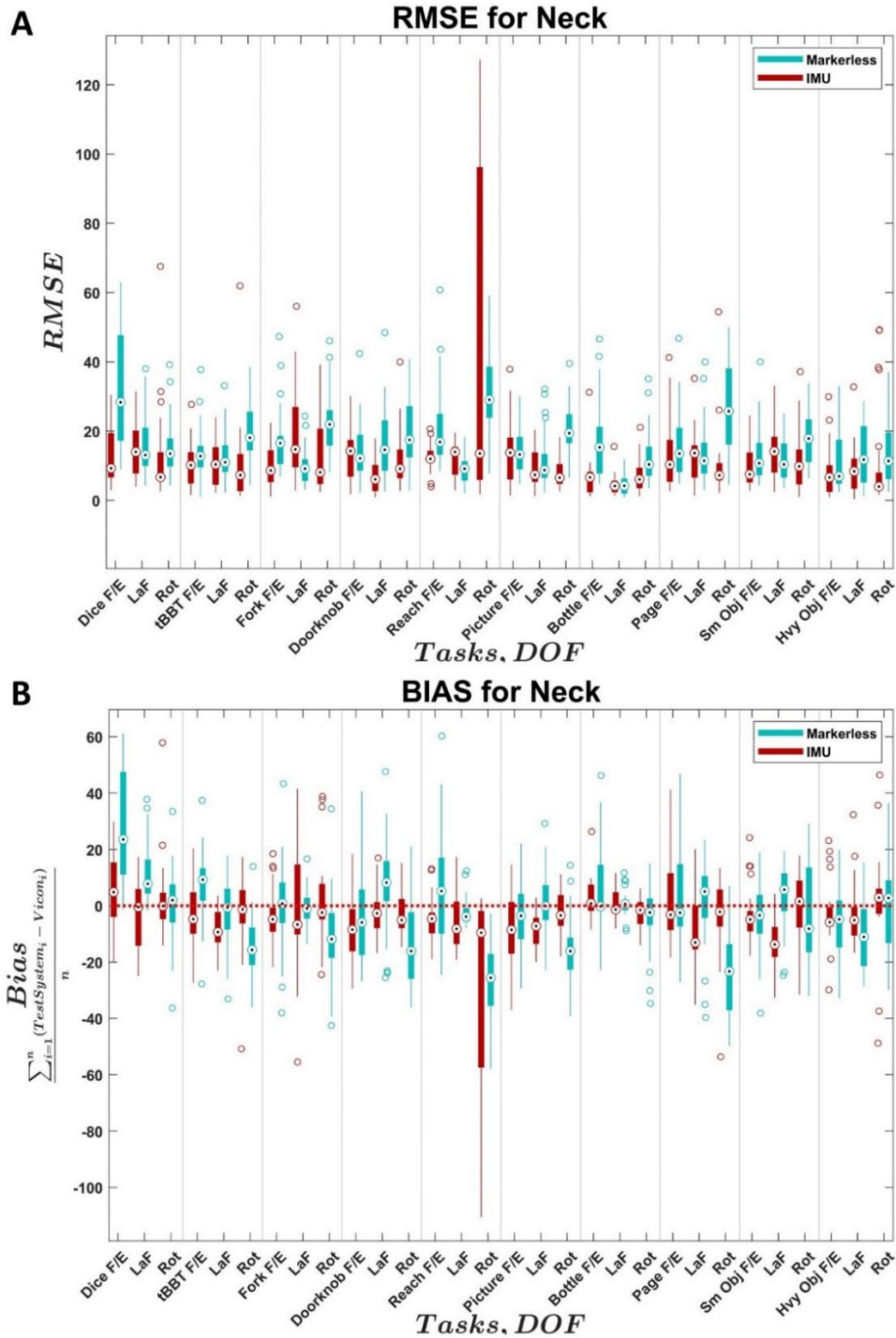


Figure 4.5 Distributions of (a) neck joint angle RMSE and (b) neck joint angle bias across subjects for the IMU system (Xsens) and markerless system (Kinect) compared to the Vicon reference system. X-axis identifies the task and associated joint angle. F/E = flexion/extension, Ab/Ad = abduction/adduction, LaF = lateral flexion, Rot = rotation. Black dots indicate medians, empty circles indicate outliers, bold line indicates quartiles, and whiskers indicate non-outlier maximums and minimums. (Figure 4 of Wang et al., 2022[95])

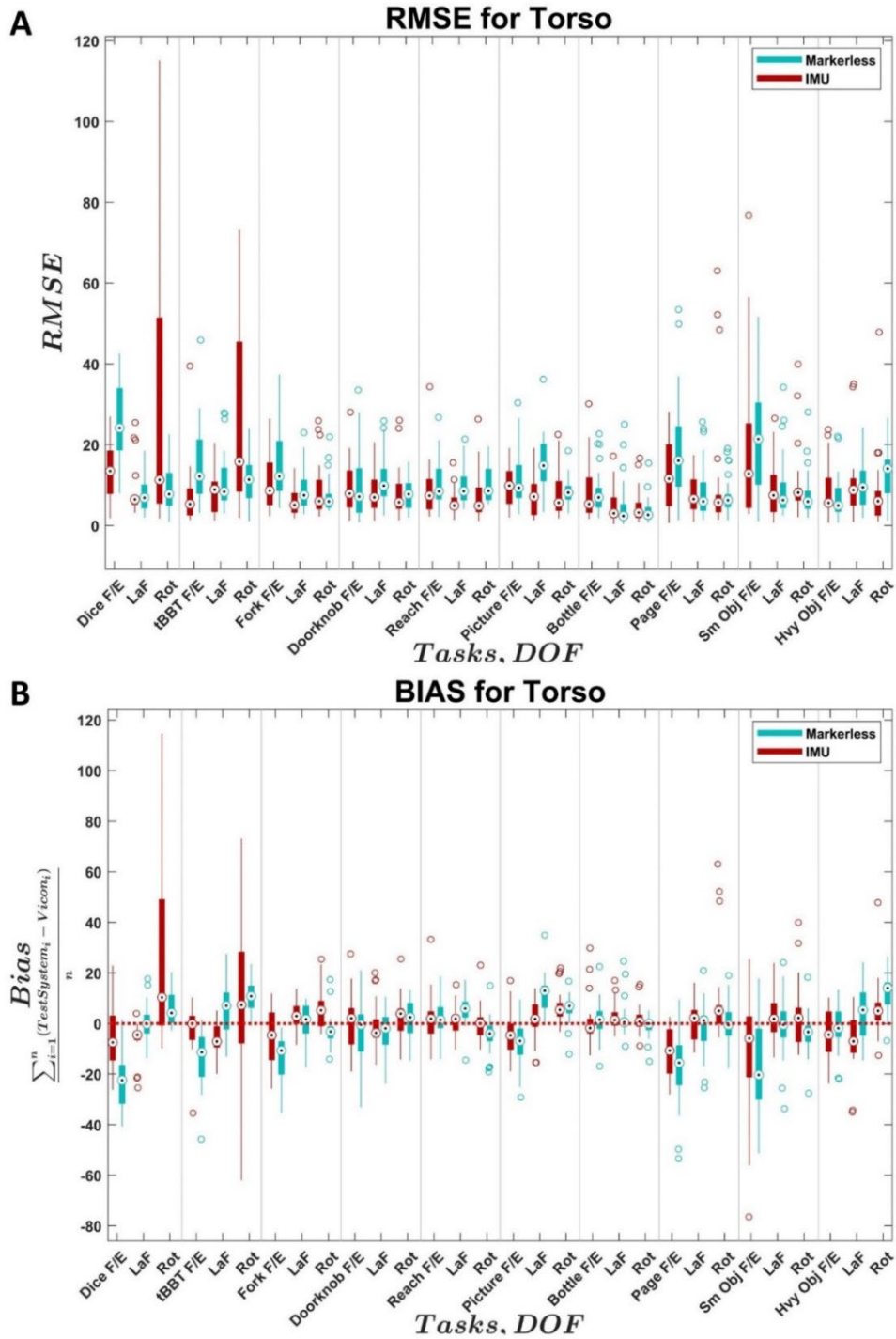


Figure 4.6 Distributions of (a) torso angle RMSE and (b) torso angle bias across subjects for the IMU system (Xsens) and markerless system (Kinect) compared to the Vicon reference system. X-axis identifies the task and associated joint angle. F/E = flexion/extension, Ab/Ad = abduction/adduction, LaF = lateral flexion, Rot = rotation. Black dots indicate medians, empty circles indicate outliers, bold line indicates quartiles, and whiskers indicate non-outlier maximums and minimums. (Figure 5 of Wang et al., 2022[95])

Table 4.3 shows the ICC(3,1) along with the 95% confidence interval for each system, DOF, and task combination. ICC values less than 0.4 were considered weak correlation; values between 0.4 and 0.74 were considered moderate, and values greater than 0.75 were considered strong[119]. To facilitate the qualitatively comparison of ICC across systems, the table is color coded according to the weak, moderate, and strong definitions. In general, the Vicon and IMU systems have moderate to strong correlations across trials for all subjects. There does not appear to be any trend based on the task or DoF. The Kinect system generally has poor reliability with weaker ICC values.

Table 4.3 ICC values with 95% confidence intervals for each DoF, task, and motion system comparison. Red cells indicate a weak correlation (ICC < 0.4). Yellow cells indicate a moderate correlation (0.4 ≤ ICC < 0.75). Green cells indicate a strong correlation (ICC ≥ 0.75) (Table modified from Table 2 of Wang et al., 2022[95])

Joint/DoF	Tasks	ICC (Kinect)	95% CI	ICC (Vicon)	95% CI	ICC (Xsens)	95% CI
Right Elbow F/E	CAPPFUL4	0.73	[0.42 0.92]	0.88	[0.6 0.98]	0.88	[0.59 0.98]
	tBBT	0.21	[-0.15 0.66]	0.76	[0.32 0.96]	0.66	[0.17 0.94]
	AMULA10	0.31	[-0.071 0.72]	0.72	[0.34 0.93]	0.91	[0.75 0.98]
	AMULA16	0.19	[-0.18 0.66]	0.47	[0.025 0.84]	0.85	[0.59 0.96]
	AMULA24	0.86	[0.64 0.96]	0.68	[0.2 0.94]	0.80	[0.42 0.97]
	CAPPFUL11	0.69	[0.35 0.9]	0.36	[-0.073 0.79]	0.79	[0.46 0.95]
	CAPPFUL8	0.47	[0.077 0.81]	0.95	[0.85 0.99]	0.82	[0.53 0.96]
	JHFT2	0.33	[-0.05 0.73]	-0.16	[-0.38 0.36]	0.18	[-0.21 0.69]
	JHFT3	0.19	[-0.16 0.64]	0.54	[0.096 0.87]	0.41	[-0.029 0.81]
	JHFT7	0.40	[-0.014 0.79]	0.63	[0.21 0.9]	0.69	[0.3 0.92]
Right Shoulder F/E	CAPPFUL4	0.66	[0.31 0.89]	0.92	[0.75 0.98]	0.91	[0.73 0.98]
	tBBT	0.22	[-0.14 0.66]	0.56	[0.12 0.87]	0.57	[0.14 0.88]
	AMULA10	0.50	[0.1 0.82]	0.65	[0.24 0.91]	0.69	[0.3 0.92]
	AMULA16	0.33	[-0.077 0.75]	0.73	[0.4 0.92]	0.58	[0.18 0.87]
	AMULA24	0.73	[0.4 0.92]	0.88	[0.7 0.97]	0.92	[0.79 0.98]
	CAPPFUL11	0.42	[0.024 0.78]	0.87	[0.68 0.96]	0.80	[0.54 0.94]

	CAPPFUL8	0.16	[-0.19 0.61]	0.98	[0.93 0.99]	0.78	[0.49 0.93]
	JHFT2	-0.12	[-0.34 0.33]	0.67	[0.3 0.9]	0.66	[0.29 0.9]
	JHFT3	0.66	[0.31 0.89]	0.78	[0.48 0.94]	0.75	[0.43 0.93]
	JHFT7	0.23	[-0.15 0.69]	0.80	[0.5 0.95]	0.81	[0.52 0.96]
Right Shoulder Ab/Ad	CAPPFUL4	0.47	[0.072 0.8]	0.66	[0.25 0.91]	0.63	[0.21 0.9]
	tBBT	0.10	[-0.22 0.57]	0.42	[-0.02 0.82]	0.64	[0.22 0.9]
	AMULA10	0.38	[-0.014 0.76]	0.71	[0.33 0.93]	0.90	[0.7 0.98]
	AMULA16	0.50	[0.081 0.83]	0.76	[0.44 0.93]	0.51	[0.094 0.84]
	AMULA24	0.83	[0.57 0.95]	0.90	[0.74 0.97]	0.91	[0.77 0.97]
	CAPPFUL11	0.46	[0.065 0.8]	0.85	[0.63 0.96]	0.89	[0.72 0.97]
	CAPPFUL8	0.51	[0.11 0.82]	0.91	[0.76 0.97]	0.90	[0.75 0.97]
	JHFT2	0.37	[-0.021 0.75]	0.69	[0.33 0.91]	0.79	[0.49 0.94]
	JHFT3	0.39	[0.0016 0.77]	0.79	[0.49 0.94]	0.86	[0.64 0.96]
	JHFT7	-0.01	[-0.3 0.5]	0.50	[0.062 0.85]	0.42	[-0.017 0.82]
Right Shoulder Rot	CAPPFUL4	0.78	[0.49 0.93]	0.92	[0.75 0.98]	0.79	[0.47 0.95]
	tBBT	0.11	[-0.21 0.58]	0.61	[0.18 0.89]	0.60	[0.17 0.89]
	AMULA10	0.44	[0.048 0.79]	0.84	[0.56 0.96]	0.97	[0.91 0.99]
	AMULA16	0.15	[-0.2 0.64]	0.77	[0.46 0.94]	0.51	[0.099 0.84]
	AMULA24	0.44	[0.022 0.81]	0.92	[0.78 0.98]	0.89	[0.71 0.97]
	CAPPFUL11	0.49	[0.096 0.82]	0.73	[0.42 0.92]	0.79	[0.52 0.94]
	CAPPFUL8	0.84	[0.61 0.95]	0.56	[0.17 0.85]	0.70	[0.36 0.9]
	JHFT2	0.78	[0.49 0.93]	0.18	[-0.19 0.65]	0.56	[0.15 0.86]
	JHFT3	0.35	[-0.033 0.75]	0.66	[0.28 0.9]	0.78	[0.48 0.94]
	JHFT7	-0.11	[-0.35 0.38]	0.53	[0.089 0.86]	0.45	[0.0077 0.83]
Neck F/E	CAPPFUL4	0.54	[0.15 0.84]	0.52	[0.0014 0.9]	-0.10	[-0.38 0.56]
	tBBT	-0.03	[-0.3 0.45]	0.17	[-0.26 0.76]	0.05	[-0.32 0.69]

	AMULA10	0.30	[-0.082 0.71]	0.60	[0.14 0.91]	0.60	[0.14 0.91]
	AMULA16	0.55	[0.14 0.86]	0.28	[-0.14 0.75]	0.42	[-0.019 0.82]
	AMULA24	0.52	[0.11 0.84]	0.96	[0.9 0.99]	0.97	[0.91 0.99]
	CAPPFUL11	0.31	[-0.075 0.72]	0.54	[0.13 0.85]	0.86	[0.63 0.96]
	CAPPFUL8	0.72	[0.4 0.91]	0.76	[0.38 0.95]	0.58	[0.11 0.9]
	JHFT2	0.31	[-0.089 0.74]	0.69	[0.31 0.92]	0.20	[-0.19 0.7]
	JHFT3	0.29	[-0.084 0.71]	0.68	[0.19 0.94]	0.36	[-0.14 0.85]
	JHFT7	-0.02	[-0.3 0.49]	0.76	[0.41 0.94]	0.86	[0.62 0.97]
Neck LaF	CAPPFUL4	-0.23	[-0.39 0.17]	0.75	[0.3 0.96]	0.86	[0.54 0.98]
	tBBT	0.23	[-0.13 0.67]	0.49	[-0.029 0.89]	0.37	[-0.13 0.85]
	AMULA10	0.59	[0.22 0.86]	0.64	[0.18 0.92]	0.79	[0.43 0.96]
	AMULA16	0.26	[-0.13 0.71]	0.23	[-0.17 0.72]	-0.12	[-0.36 0.41]
	AMULA24	0.69	[0.33 0.91]	0.93	[0.81 0.98]	0.93	[0.79 0.98]
	CAPPFUL11	0.44	[0.048 0.79]	0.85	[0.62 0.96]	0.90	[0.74 0.98]
	CAPPFUL8	0.62	[0.25 0.87]	0.74	[0.34 0.94]	0.67	[0.23 0.92]
	JHFT2	0.11	[-0.23 0.61]	0.66	[0.25 0.91]	0.63	[0.21 0.9]
	JHFT3	0.48	[0.087 0.81]	0.85	[0.53 0.98]	0.92	[0.71 0.99]
	JHFT7	0.09	[-0.24 0.58]	0.39	[-0.048 0.81]	0.48	[0.034 0.84]
Neck Rot	CAPPFUL4	-0.05	[-0.31 0.42]	0.91	[0.69 0.99]	0.13	[-0.28 0.74]
	tBBT	0.13	[-0.2 0.59]	0.71	[0.25 0.95]	0.47	[-0.051 0.88]
	AMULA10	0.60	[0.23 0.87]	0.89	[0.66 0.98]	0.56	[0.09 0.89]
	AMULA16	0.25	[-0.13 0.71]	0.31	[-0.12 0.76]	0.38	[-0.057 0.8]
	AMULA24	0.59	[0.19 0.87]	0.93	[0.8 0.98]	0.99	[0.98 1]
	CAPPFUL11	0.54	[0.16 0.84]	0.89	[0.7 0.97]	0.80	[0.52 0.95]
	CAPPFUL8	0.51	[0.12 0.82]	0.60	[0.14 0.9]	0.71	[0.29 0.94]
	JHFT2	0.27	[-0.12 0.71]	0.60	[0.18 0.89]	0.15	[-0.22 0.67]

	JHFT3	0.36	[-0.028 0.75]	0.91	[0.68 0.99]	0.69	[0.21 0.94]
	JHFT7	0.09	[-0.24 0.59]	0.74	[0.37 0.93]	0.68	[0.28 0.92]
Torso F/E	CAPPFUL4	0.82	[0.58 0.95]	0.98	[0.93 1]	0.90	[0.65 0.98]
	tBBT	-0.07	[-0.32 0.4]	0.52	[0.043 0.88]	0.58	[0.12 0.9]
	AMULA10	0.50	[0.11 0.82]	0.70	[0.27 0.93]	0.69	[0.26 0.93]
	AMULA16	0.06	[-0.26 0.56]	0.59	[0.22 0.86]	0.42	[0.032 0.78]
	AMULA24	0.07	[-0.25 0.57]	0.96	[0.87 0.99]	0.93	[0.79 0.98]
	CAPPFUL11	0.46	[0.066 0.8]	0.90	[0.74 0.97]	0.60	[0.23 0.87]
	CAPPFUL8	0.62	[0.25 0.87]	0.83	[0.57 0.95]	0.68	[0.31 0.91]
	JHFT2	0.40	[0.0059 0.77]	0.48	[0.083 0.81]	0.72	[0.4 0.91]
	JHFT3	0.34	[-0.044 0.74]	0.89	[0.73 0.97]	0.90	[0.73 0.97]
	JHFT7	0.70	[0.35 0.91]	0.57	[0.16 0.86]	0.39	[-0.023 0.78]
	Torso LaF	CAPPFUL4	0.67	[0.32 0.89]	0.66	[0.17 0.94]	0.78
tBBT		0.27	[-0.1 0.7]	0.71	[0.29 0.94]	0.66	[0.22 0.92]
AMULA10		0.72	[0.4 0.91]	0.82	[0.49 0.96]	0.35	[-0.11 0.81]
AMULA16		0.19	[-0.18 0.67]	0.90	[0.74 0.97]	0.72	[0.4 0.91]
AMULA24		0.11	[-0.23 0.6]	0.90	[0.73 0.97]	0.89	[0.7 0.97]
CAPPFUL11		0.55	[0.16 0.84]	0.88	[0.7 0.97]	0.95	[0.87 0.99]
CAPPFUL8		0.25	[-0.11 0.68]	0.90	[0.73 0.97]	0.94	[0.82 0.98]
JHFT2		0.28	[-0.093 0.7]	0.61	[0.23 0.87]	0.88	[0.69 0.96]
JHFT3		0.40	[0.01 0.77]	0.57	[0.19 0.85]	0.88	[0.69 0.96]
JHFT7		0.38	[-0.028 0.78]	0.70	[0.34 0.91]	0.33	[-0.076 0.75]
Torso Rot	CAPPFUL4	0.46	[0.063 0.8]	0.40	[-0.11 0.86]	0.50	[-0.023 0.89]
	tBBT	0.27	[-0.1 0.69]	0.73	[0.32 0.94]	0.62	[0.17 0.91]
	AMULA10	0.69	[0.35 0.9]	0.80	[0.45 0.96]	0.85	[0.57 0.97]
	AMULA16	0.36	[-0.046 0.77]	0.63	[0.27 0.88]	0.54	[0.15 0.84]

AMULA24	-0.08	[-0.34 0.42]	0.89	[0.7 0.97]	0.96	[0.89 0.99]
CAPPFUL11	0.62	[0.26 0.88]	0.62	[0.25 0.87]	0.67	[0.33 0.9]
CAPPFUL8	0.49	[0.094 0.82]	0.93	[0.81 0.98]	0.89	[0.7 0.97]
JHFT2	0.06	[-0.25 0.53]	0.68	[0.33 0.9]	0.53	[0.14 0.83]
JHFT3	0.16	[-0.18 0.61]	0.85	[0.63 0.96]	0.63	[0.27 0.88]
JHFT7	0.49	[0.075 0.83]	0.23	[-0.15 0.69]	0.39	[-0.02 0.79]

#### 4.4 *Discussion*

In this study, joint kinematics derived from three motion capture systems of varying costs and mechanisms were compared through simultaneous motion capture of able-bodied participants using an upper limb myoelectric bypass device. By evaluating the ability of each system to capture kinematic changes of simulated upper limb prosthesis users during a variety of standardized tasks, this study provides insight into the advantages and limitations of using different motion capture technology for upper limb functional assessment. Two established metrics of precision and accuracy (RMSE and bias) were calculated as a function of ten different joint degrees of freedom and ten different upper-limb tasks for every time point to assess inter-subject variability and inter-system agreement. Because differences are calculated for every time point, the RMSE values would reflect unstable system related influences given the simultaneous capture setup. Similarly, the bias values would indicate systematic influences on differences over time – allowing for an assessment of joint angle stability. In addition, ICC values were calculated for each system and each task/DoF combination using a two-way mixed effects model (ICC(3,1) to further assess consistency of measurements from each system. A

discussion of advantages and limitations of each system is presented along with considerations for clinical implementation.

Based on the results presented in this study, the IMU system yields more accurate kinematics for shoulder, neck, and torso angles over all DOFS (Figure 4.3 - Figure 4.5) compared to the Kinect (markerless) system's performance over all DOFs. Due to the current level of accuracy and variability, the IMU system is not recommended in the elbow DOF (Figure 4.3). The markerless system is not recommended for use in measuring the elbow or the shoulder DOFs due to high variability and bias (Figure 4.3, Figure 4.4), which are in line with the results from the literature[25, 30, 63], but may provide accurate results for neck and torso DOFs (Figure 4.5, Figure 4.6) when individuals perform the specific tasks analyzed in this study.

For both systems, the tasks requiring the greatest amount of movement (i.e., CAPPFUL - Dice, CAPPFUL - Picture, and tBBT) resulted in the largest RMSE and variability values over the DOFs examined. This implies that both systems struggled with precision during large gross movements, a result in line with previous literature that suggests the markerless system overestimates large motions and underestimates small motions[30].

For DOFs parallel to the recording plane of the cameras (e.g., neck/torso lateral flexion and shoulder abduction/adduction), the markerless system had the best results. Given the mechanism of movement capture for the Kinect V1, which measures infrared reflectivity and subtracts changes from a predefined static background[24, 74, 117], this result is expected [66, 73, 117]. The elbow bias values

(Figure 4.3B) for the markerless system were inconsistent overestimates, which was likely influenced by how the system struggled to detect the bypass device. The markerless shoulder bias values (Figure 4.4B) measured in this study were also notably different from those found in the literature (current study measured approximately  $-25^{\circ}$  compared to an average around  $+10^{\circ}$ ) [28, 30]. Although this difference is large, it may be a more accurate representation of the expected performance of these motion capture systems given the use of complex tasks[120] and human subjects in this study compared to simple ROM measurements[28, 30] and testing machines[75] found in the literature.

The precision of the IMU system was best in the shoulder (Figure 4.4), which is consistent with previous results in the literature[32, 36]. The variability across subjects in the elbow DOF (Figure 4.3) for the IMU system was likely influenced by variations in sensor placement and movement artifacts from the sensor attachment method, which are known factors in the literature[67]. The variability across subjects in the neck and torso angles (Figure 4.5, Figure 4.6) appeared to be heavily task-influenced and the capture accuracy of the systems was likely affected by the varying motions used by the participants to achieve the task. The magnitude of the differences between the IMU-generated angles and the Vicon reference system angles found in the DOFs examined in this study were similar to the magnitude of the differences previously found in the literature for the commercial Xsens software[120] in the shoulder, neck, and back. However, the magnitude of the differences in the elbow are much greater in this study compared to those previously found in the literature. The

source of the errors within the elbow is currently still unclear and warrant further investigation given the results seen in the other angles measured.

In terms of the system stability as measured by the ICC values, the IMU and marker-based systems showed comparable moderate to strong correlations across trials for all subjects. The markerless system generally showed weaker correlations compared to the IMU system and marker-based reference system. Due to the lack of any trends based on the task or DoF, these results can be considered to support the general performance of the three systems. However, it should be noted that the participants were free to choose their own approaches to achieve the tasks and often used different approaches between trials. As such, it is difficult to draw more specific conclusions based on the ICC values due to the inherent variability of the base data. Overall, the marker-based reference system and IMU system showed the greatest stability per the ICC metric.

In terms of capture environment restrictions and operating stability, the IMU system proved more robust and less demanding compared to the markerless system. The IMU system did not require the consideration of issues such as the color and reflectivity of the capture background, the participant clothing, or the participant skin tone, and was not vulnerable to loss of tracking issues due to obscuration from task objects or body parts. The IMU system had comparable costs for the number of sensors used, and less strenuous requirements for data processing, data storage, and data export procedures compared to the markerless system. The markerless system incorporated established calibration procedures, while there exist many approaches for effective calibration of the IMU system. The impact of IMU calibration

procedure on derived joint angles was not the subject of this study but may need further investigation regarding the most effective calibration approach. However, both systems proved lacking in data annotation abilities – with the markerless system holding a slight advantage due to the visual review allowed by the video-based capture data. In this experiment, the availability of reference video and data from the gold standard system served to ameliorate the lack of review and annotation abilities for the IMU system – but for independent use of the IMU system this factor needs additional consideration. Overall, the IMU system may be best for clinical and remote monitoring purposes.

The generalizability of the joint kinematics observed here with able-bodied individuals to those of upper limb prosthesis users is uncertain. However, the movements elicited by able-bodied individuals using a bypass prosthesis are close approximations to the movements of interest, making the results obtained in this study relevant to understanding the utility of different motion capture systems for tracking upper limb prosthesis user movement. The focus on unilateral tasks performed with the MY Bypass device may not be fully representative of device use patterns in daily living and may also be considered a limitation of the current study. While a bilateral task was included, (i.e. CAPPFUL Task 11 – Picture), the task required symmetrical use of the two upper limbs. Motion analysis of tasks with independent use of both upper limbs has yet to be performed under these simultaneous capture conditions and is a future avenue of investigation. Given the current results with unilateral tasks, and other results in the literature[69], it is likely that asymmetrical bilateral tasks may further elucidate the performance capabilities of

the IMU and the markerless motion analysis systems. The limitations and advantages discovered about each system in this study can be used to inform clinical implementation of motion analysis for research and rehabilitation.

## Chapter 5: Conclusions and Future Work

### 5.1 *Conclusions*

In this dissertation, we have examined several factors to fill the gaps previously identified in Chapter 1 related to the evaluation of functional capabilities and quality of motion[6, 39-41]. Namely, this dissertation addresses factors that have influenced the adoption of motion capture into clinical use in rehabilitation such as: the lack of normative kinematic ranges for commonly used performance-based outcome measure, the lack of coordinated datasets of normative and device use kinematic data, the lack of analyses that identify informative tasks and motions, as well as the lack of comparisons examining whether selected motion capture systems are able to detect the most informative tasks and motions. Without normative kinematic ranges, it is difficult to establish departures from normative ranges of motion. Without coordinated datasets, it is difficult to perform comparisons of device use motion against normative motion. Without the identification of informative tasks and motion, and without comparisons of motion capture systems to clarify technical capabilities, it is difficult to implement motion capture into clinical or rehabilitative programs.

To address these gaps, this dissertation has established new kinematic databases of normative and device use motion in Chapter 2. In Chapter 3, to identify informative motions and tasks with a novel metric developed for the purpose, the K-means machine learning algorithm was applied to the new kinematic data previously collected in Chapter 2. In Chapter 4, the tasks and motions identified were used to

compare the technical characteristics of three motion capture systems with three different mechanisms of action.

In Chapter 2: Specific Aim 1 – Development of Kinematic Databases, standardized databases of kinematic data for standardized tasks from several performance- based outcome measures were developed. Both normative baselines and simulated disability motion data have now been published in the literature and are available through the Food and Drug Administration Office of Science and Engineering Labs Division of Biomedical Physics GitHub repository[82-84, 96].In Chapter 3: Specific Aim 2 – Application of Machine Learning to Identify Salient Kinematic Characteristics, the unsupervised K-means clustering algorithm was applied to the previously collected kinematic data and DOFs that inform abnormal movement were identified. With the features selected to characterize movement (RoM, peak angle, path length, mean joint angle, peak angle velocity, and number of zero crossings), the K-means clustering approach was able to identify distinctive joint DOFs for several ADL tasks over three methods of simulated upper limb prosthesis use. The most frequent tasks with high DfC values for both the BP bypass and DK bypass conditions were JHFT2 – Page Turning and the sitting targeted Box and Blocks Test. Some tasks (e.g., standing targeted Box and Blocks) were found to elicit more significant DfC values for one bypass condition, but not the other. When all DOFs are combined, the right shoulder and torso appear more often in the significant results across both bypass conditions, indicating these joints are most informative for distinguishing movement between the Norm and Bypass conditions. Although limited in generalizability to actual prosthesis users, the results of this analysis can be used to

inform the development of larger, more applicable datasets to be incorporated into a supervised machine learning algorithm for the real-time identification of abnormal or compensatory movement based on movement data input.

In Specific Aim 3 – Comparison of Motion Capture Systems, using the tasks and motions identified in Specific Aim 2, the performance of three motion analysis systems with varying mechanisms of action were compared through simultaneous data acquisition. An analysis of the factors that influenced the relative accessibility of the three systems in terms of capture environment requirements, data processing pipelines, and annotation capabilities was also produced. This chapter can serve as a starting point for minimum technical requirements in motion capture systems for use in clinical rehabilitation and highlights the current state of commercially available technology in terms of technical and capture environment requirements that may be barriers to the clinical adoption of motion capture. The results can also be used to guide improvements in the design and algorithms of low-cost, portable motion capture systems to facilitate the wider adoption of these tools in clinical practice.

## *5.2 Future Work*

Future work for this database development effort involves the expansion of these databases by 1) collecting additional data for the current selection of performance-based outcome measure tasks, 2) collecting kinematic data for additional performance-based outcome measures, and 3) collecting data for additional participant populations (i.e., amputee data or additional terminal device data).

Future avenues of investigation for the application of machine learning algorithms to UL kinematic data include increasing the selectivity of the clustering

approach used in this chapter by increasing the threshold value, comparing the results from this chapter with the actual upper limb amputee motion capture data, performing further experiments with larger and more varied interaction zone requirements, and utilizing the distinct tasks identified for further motion capture or rehabilitation experiments.

Future work on the examination of motion capture system performance may focus on investigating the effects of additional Kinect V1 cameras, examining the performance results from more modern Kinect cameras models such as the Azure Kinect, and further refinement of the IMU system joint angle calculations and sensor placements to allow for more reliable capture of challenging task performance zones such as the portion of the lower central zone by the feet and the far left and far right of the lateral zones[12]. Other avenues of future work may also include remote monitoring and additional capture mechanisms such as those employed in visual-inertial systems or single-view pose estimation systems.

With the development of more compact, easily implementable motion analysis systems such as 3D optical marker-based motion capture, inertial measurements units, or markerless motion capture that can be used in the home or clinic, the widespread collection, analysis, and application of quantitative movement data is becoming more of a reality. The work performed in this dissertation serves to aid the adoption of motion capture into clinical use and rehabilitation. The kinematic data collected in this dissertation establishes useful ranges of variation for normative and device use motion. The machine learning applied to the collected kinematic data has aided the identification of informative DOFs and tasks for the comparison of motion capture

systems. The motion capture system comparisons performed clarify factors beyond precision and accuracy that may be useful for system selection.

## Appendices

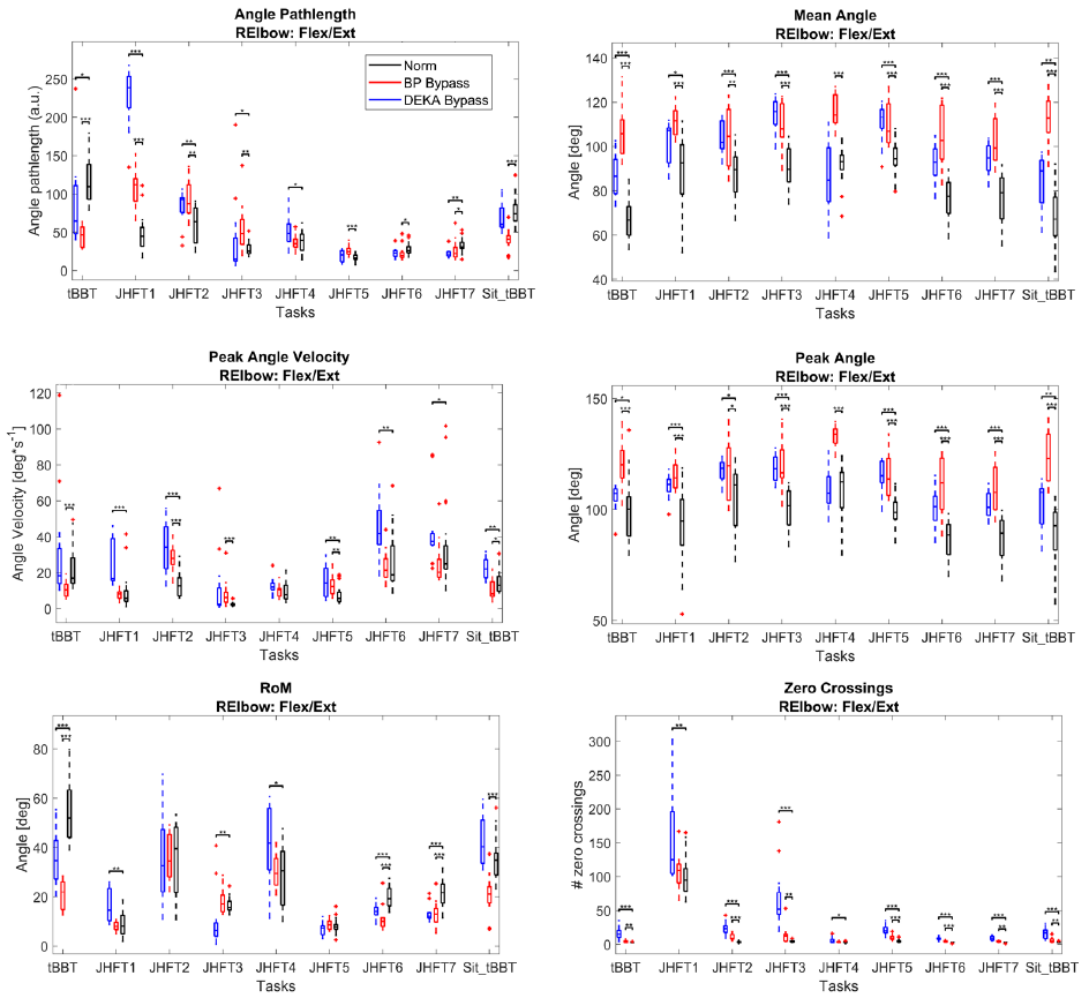
Supplemental Table 1 P-values for the statistical test comparing the Deviation from Chance (DfC) distributions for a given task/DOF to the threshold value (DfC = 25). (From Wang et al., 2021[93])

<b>Task</b>	<b>DOF</b>	<b>BP Bypass (p-value)</b>	<b>DK Bypass (p-value)</b>	
<b>tBBT</b>	R Elbow - Flex/Ext	7.97E-06	0.219	
	L Elbow - Flex/Ext	1.64E-05	1.000	
	R Sho - Flex/Ext	1.64E-05	1.000	
	R Sho - Ab/Ad	2.65E-05	1.000	
	R Sho - Rot	3.08E-05	1.000	
	L Sho - Flex/Ext	1.000	0.519	
	L Sho - Ab/Ad	2.42E-05	2.37E-05	
	L Sho - Rot	1.21E-05	0.803	
	Neck - Flex/Ext	0.994	1.000	
	Neck - Lat Flex	0.999	0.001	
	Neck - Rot	0.220	0.355	
	Torso - Flex/Ext	2.02E-05	0.987	
	Torso - Lat Flex	2.86E-05	1.000	
	Torso - Rot	1.21E-05	1.000	
	<b>JHFT1 - writing</b>	R Elbow - Flex/Ext	2.67E-05	2.86E-05
		L Elbow - Flex/Ext	1.000	2.55E-05
R Sho - Flex/Ext		2.44E-05	2.86E-05	
R Sho - Ab/Ad		0.999	1.000	
R Sho - Rot		1.000	0.960	
L Sho - Flex/Ext		0.983	0.901	
L Sho - Ab/Ad		0.983	0.999	
L Sho - Rot		0.221	2.67E-05	
Neck - Flex/Ext		1.000	0.687	
Neck - Lat Flex		1.000	1.000	
Neck - Rot		1.000	1.000	
Torso - Flex/Ext		0.001	0.001	
Torso - Lat Flex		1.000	0.998	
Torso - Rot		1.000	1.000	

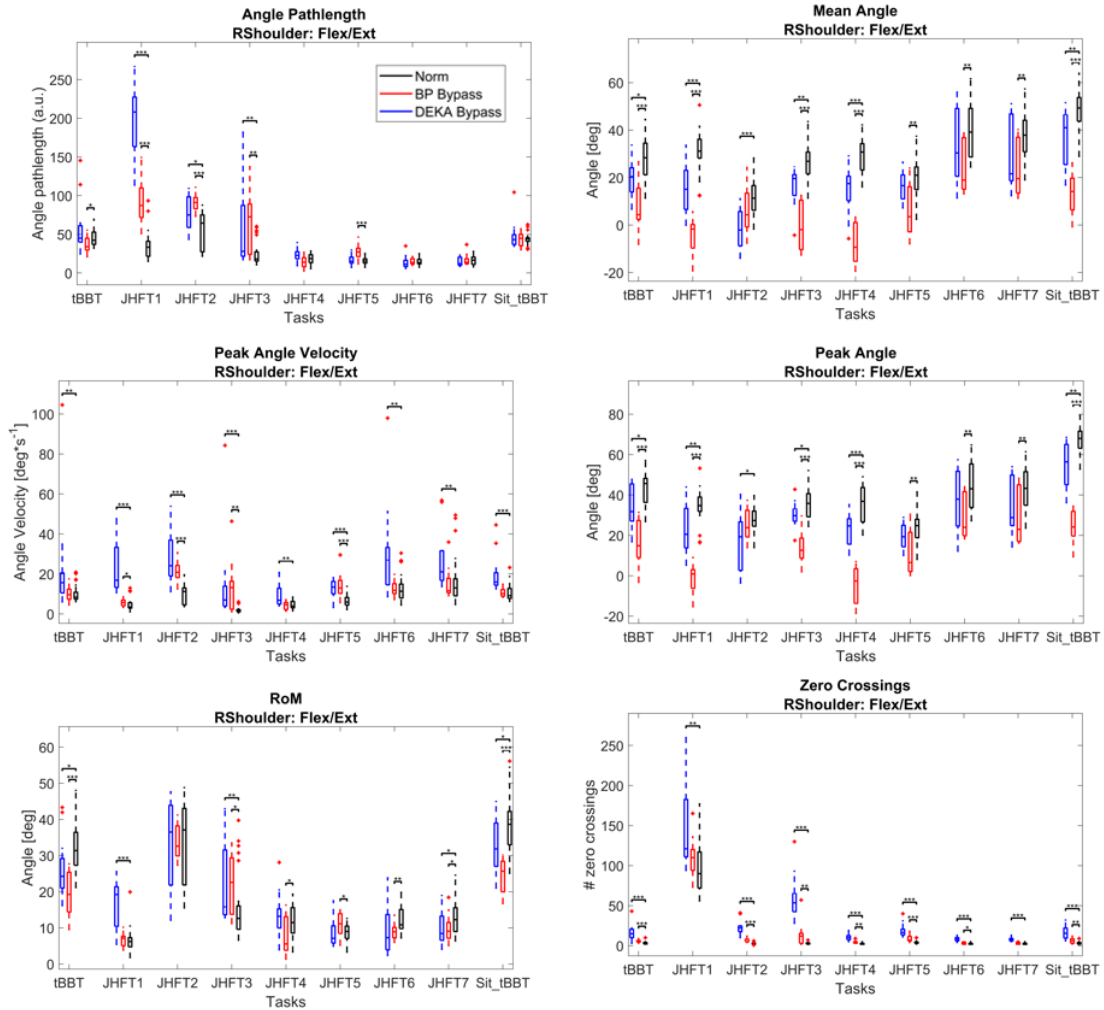
<b>JHFT2 - page turning</b>	R Elbow - Flex/Ext	0.099	0.002
	L Elbow - Flex/Ext	1.64E-05	0.000
	R Sho - Flex/Ext	0.836	1.21E-05
	R Sho - Ab/Ad	2.38E-05	2.73E-05
	R Sho - Rot	7.97E-06	7.97E-06
	L Sho - Flex/Ext	1.000	0.008
	L Sho - Ab/Ad	2.37E-05	7.97E-06
	L Sho - Rot	0.999	1.000
	Neck - Flex/Ext	2.02E-05	7.97E-06
	Neck - Lat Flex	1.000	1.000
	Neck - Rot	2.55E-05	7.97E-06
	Torso - Flex/Ext	1.64E-05	0.989
	Torso - Lat Flex	1.21E-05	0.001
	Torso - Rot	2.28E-05	3.03E-05
	<b>JHFT3 - small objects</b>	R Elbow - Flex/Ext	1.000
L Elbow - Flex/Ext		2.02E-05	1.64E-05
R Sho - Flex/Ext		2.73E-05	1.000
R Sho - Ab/Ad		1.000	1.000
R Sho - Rot		0.015	0.806
L Sho - Flex/Ext		0.998	0.804
L Sho - Ab/Ad		2.07E-05	2.28E-05
L Sho - Rot		0.960	0.960
Neck - Flex/Ext		1.66E-05	2.55E-05
Neck - Lat Flex		1.000	0.034
Neck - Rot		0.014	1.66E-05
Torso - Flex/Ext		0.184	0.084
Torso - Lat Flex		1.000	1.000
Torso - Rot		2.28E-05	0.021
<b>JHFT4 - simulated feeding</b>		R Elbow - Flex/Ext	1.000
	L Elbow - Flex/Ext	1.64E-05	2.37E-05
	R Sho - Flex/Ext	7.97E-06	1.000
	R Sho - Ab/Ad	0.994	0.000
	R Sho - Rot	0.009	2.65E-05
	L Sho - Flex/Ext	1.000	0.355
	L Sho - Ab/Ad	2.09E-05	3.06E-05
	L Sho - Rot	0.221	0.099

	Neck - Flex/Ext	1.000	3.08E-05
	Neck - Lat Flex	0.999	0.517
	Neck - Rot	0.993	0.114
	Torso - Flex/Ext	0.994	0.001
	Torso - Lat Flex	3.03E-05	2.55E-05
	Torso - Rot	1.000	2.73E-05
<b>JHFT5 - stacking checkers</b>	R Elbow - Flex/Ext	0.001	0.005
	L Elbow - Flex/Ext	1.000	1.000
	R Sho - Flex/Ext	0.000	2.88E-05
	R Sho - Ab/Ad	1.000	1.000
	R Sho - Rot	0.047	2.73E-05
	L Sho - Flex/Ext	0.000	0.001
	L Sho - Ab/Ad	7.97E-06	2.28E-05
	L Sho - Rot	1.66E-05	2.37E-05
	Neck - Flex/Ext	0.987	2.28E-05
	Neck - Lat Flex	0.221	0.988
	Neck - Rot	0.001	2.92E-05
	Torso - Flex/Ext	1.000	0.057
	Torso - Lat Flex	0.994	2.86E-05
	Torso - Rot	1.21E-05	0.522
	<b>JHFT6 - light cans</b>	R Elbow - Flex/Ext	0.021
L Elbow - Flex/Ext		1.21E-05	2.07E-05
R Sho - Flex/Ext		0.996	0.676
R Sho - Ab/Ad		2.38E-05	2.92E-05
R Sho - Rot		3.10E-05	1.21E-05
L Sho - Flex/Ext		2.55E-05	1.000
L Sho - Ab/Ad		1.000	7.97E-06
L Sho - Rot		0.345	0.951
Neck - Flex/Ext		1.000	0.000
Neck - Lat Flex		0.355	1.000
Neck - Rot		0.999	0.815
Torso - Flex/Ext		0.951	0.006
Torso - Lat Flex		2.86E-05	2.09E-05
Torso - Rot		0.184	0.519
<b>JHFT7 - heavy cans</b>		R Elbow - Flex/Ext	0.115
	L Elbow - Flex/Ext	2.02E-05	1.000

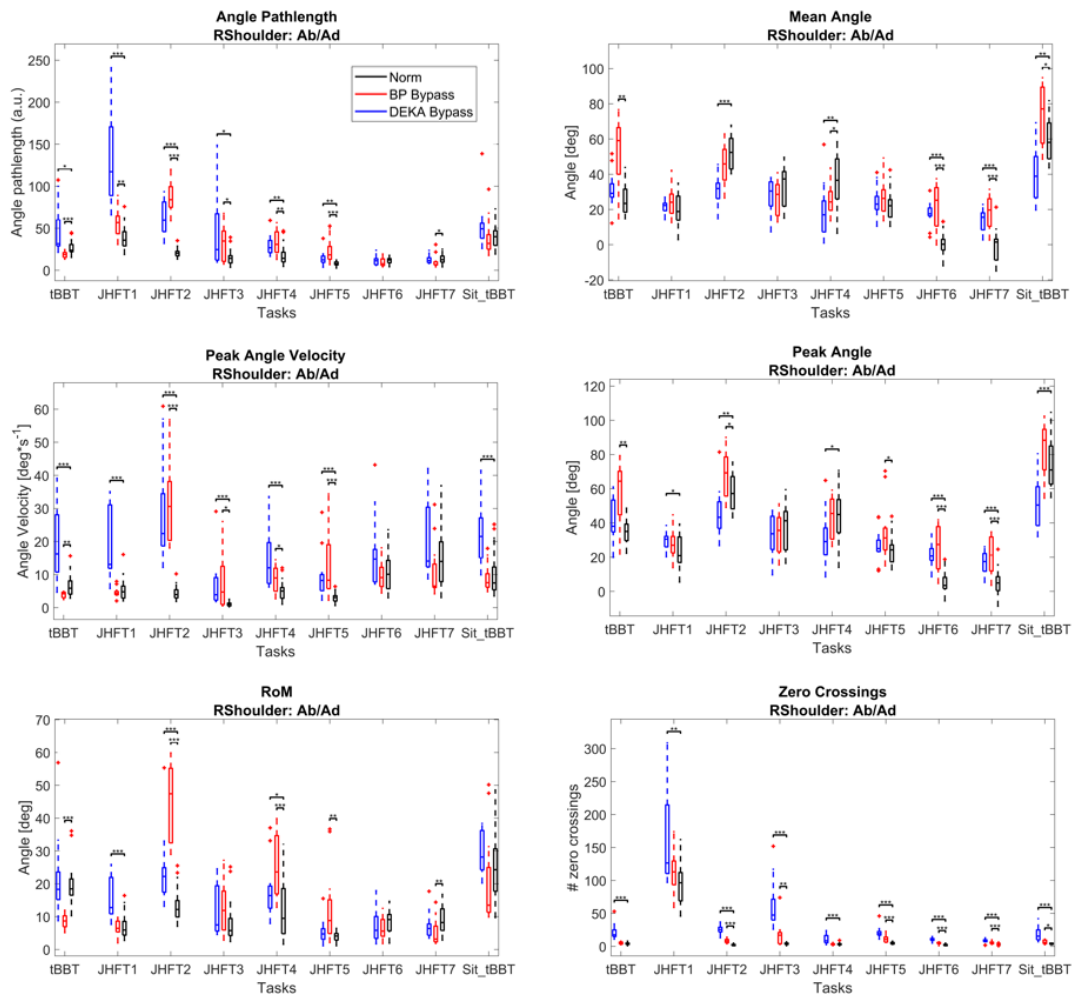
	R Sho - Flex/Ext	1.000	0.901
	R Sho - Ab/Ad	0.000	0.001
	R Sho - Rot	0.000	1.000
	L Sho - Flex/Ext	0.994	1.000
	L Sho - Ab/Ad	1.000	0.007
	L Sho - Rot	1.000	0.952
	Neck - Flex/Ext	1.000	0.221
	Neck - Lat Flex	1.000	0.998
	Neck - Rot	1.000	0.987
	Torso - Flex/Ext	0.002	1.000
	Torso - Lat Flex	2.97E-05	1.000
	Torso - Rot	1.000	1.000
<b>Sit tBBT</b>	R Elbow - Flex/Ext	2.67E-05	3.08E-05
	L Elbow - Flex/Ext	2.55E-05	1.000
	R Sho - Flex/Ext	7.97E-06	2.09E-05
	R Sho - Ab/Ad	1.000	2.88E-05
	R Sho - Rot	1.000	0.998
	L Sho - Flex/Ext	0.015	2.28E-05
	L Sho - Ab/Ad	2.07E-05	2.37E-05
	L Sho - Rot	0.048	2.92E-05
	Neck - Flex/Ext	1.000	0.002
	Neck - Lat Flex	0.993	3.06E-05
	Neck - Rot	0.988	7.82E-05
	Torso - Flex/Ext	7.97E-06	2.55E-05
	Torso - Lat Flex	2.99E-05	2.65E-05
	Torso - Rot	0.001	2.71E-05



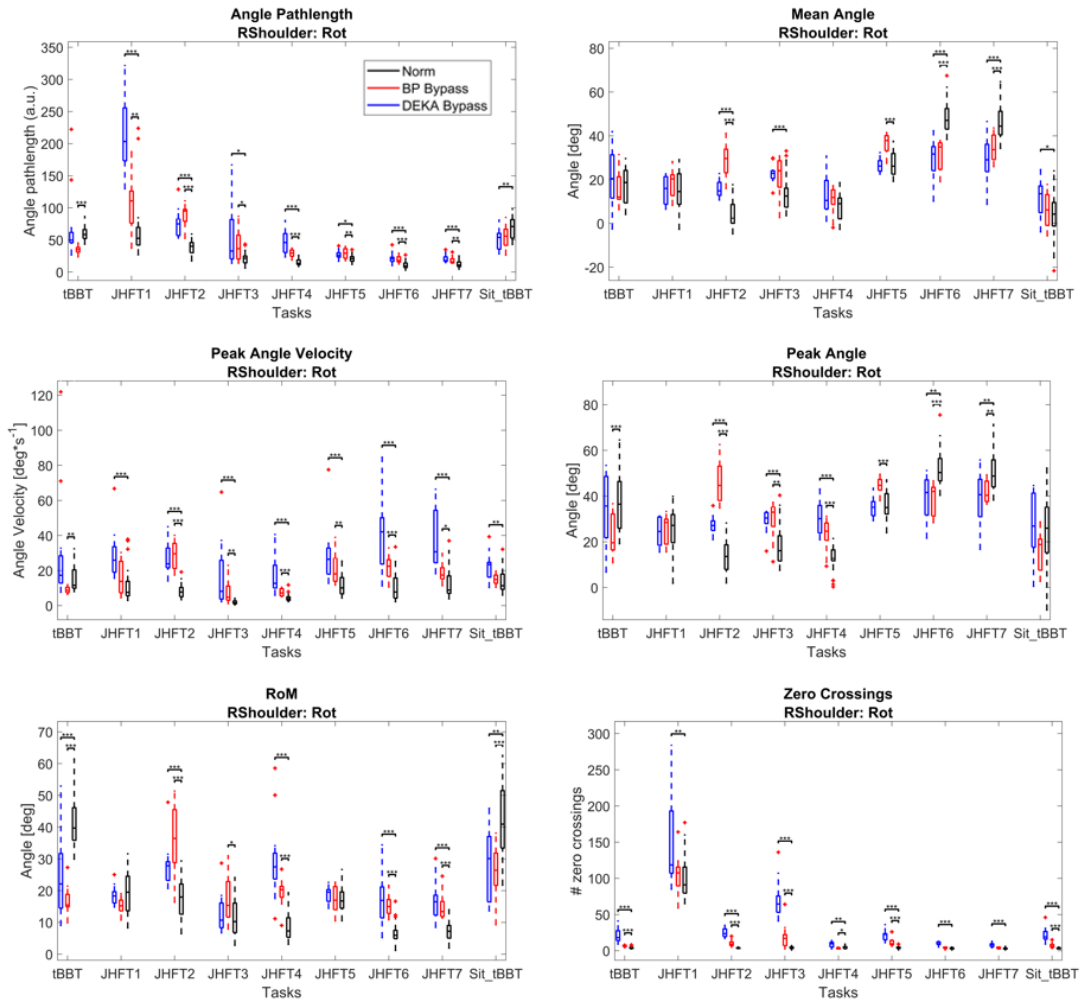
Supplemental Figure 1 Distributions of features for DEKA Bypass (blue), BP Bypass (red), and Norm (black) conditions for right elbow flexion/extension. Tasks JHFT1 - Writing, JHFT2 - Page Turning, JHFT3 - Picking Up Small Objects, JHFT4 - Simulated Feeding, JHFT5 - Stacking Checkers, JHFT6 - Moving Large Light Objects and JHFT7 - Moving Large Heavy. Stars denote statistical significance of Wilcoxon ranksum test between each bypass condition data and the Norm condition data. \*p< 0.05, \*\*p<0.01, \*\*\*p<0.001. (From Wang et al., 2021[93])



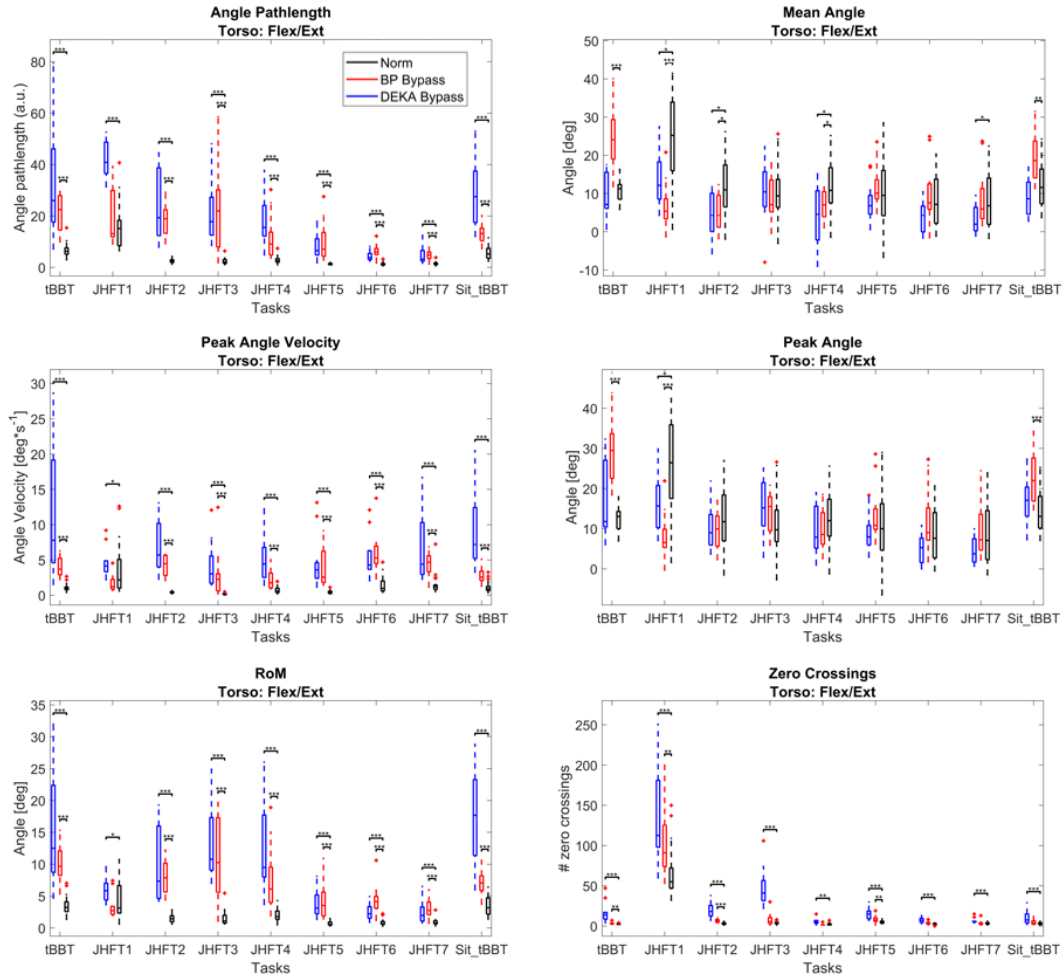
Supplemental Figure 2 Distributions of features for DEKA Bypass (blue), BP Bypass (red), and Norm (black) conditions for right shoulder flexion/extension. Tasks JHFT1 - Writing, JHFT2 - Page Turning, JHFT3 - Picking Up Small Objects, JHFT4 - Simulated Feeding, JHFT5 - Stacking Checkers, JHFT6 - Moving Large Light Objects and JHFT7 - Moving Large Heavy. Stars denote statistical significance of Wilcoxon ranksum test between each bypass condition data and the Norm condition data. \*p < 0.05, \*\*p < 0.01, \*\*\*p < 0.001. (From Wang et al., 2021[93])



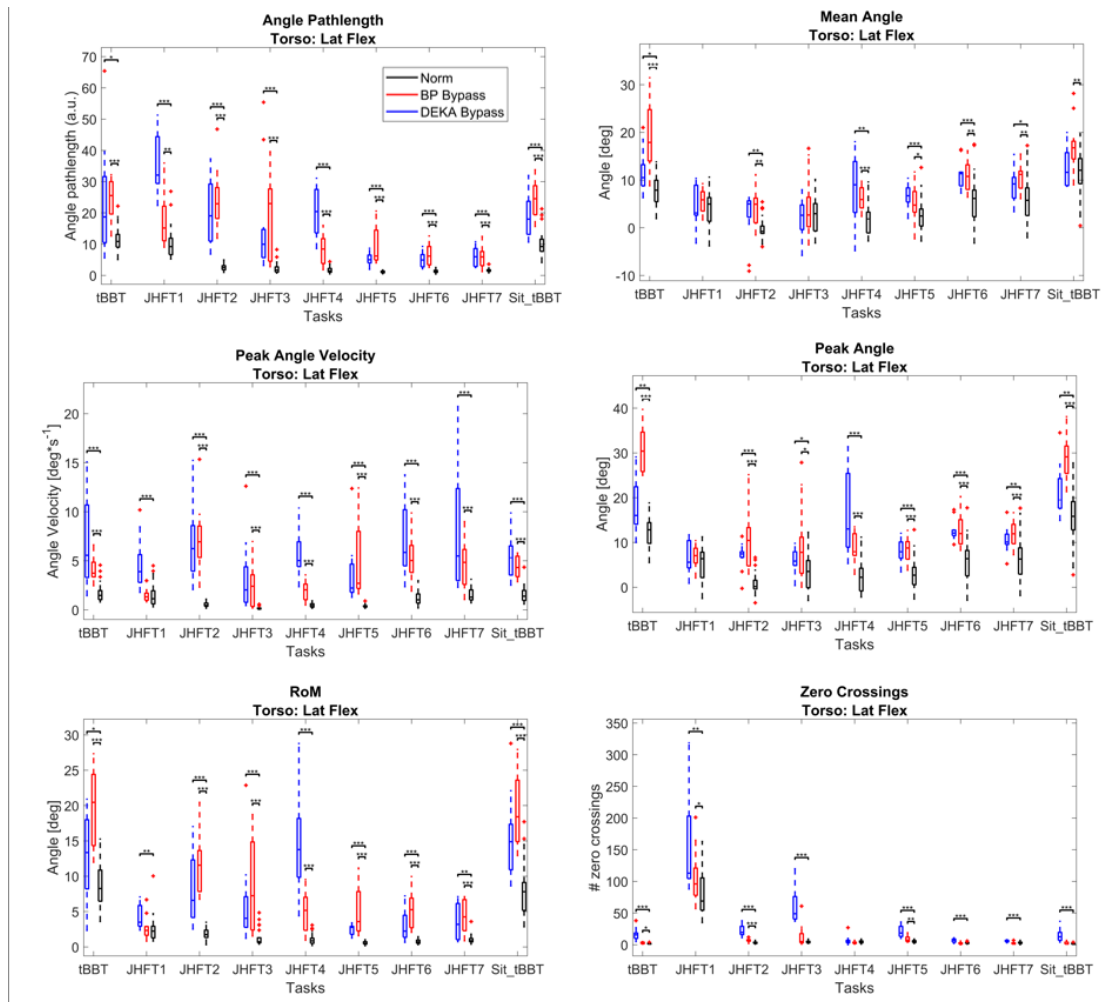
Supplemental Figure 3 Distributions of features for DEKA Bypass (blue), BP Bypass (red), and Norm (black) conditions for right shoulder abduction/adduction. Tasks JHFT1 - Writing, JHFT2 - Page Turning, JHFT3 - Picking Up Small Objects, JHFT4 - Simulated Feeding, JHFT5 - Stacking Checkers, JHFT6 - Moving Large Light Objects and JHFT7 - Moving Large Heavy. Stars denote statistical significance of Wilcoxon ranksum test between each bypass condition data and the Norm condition data. \* $p < 0.05$ , \*\* $p < 0.01$ , \*\*\* $p < 0.001$ . (From Wang et al., 2021[93])



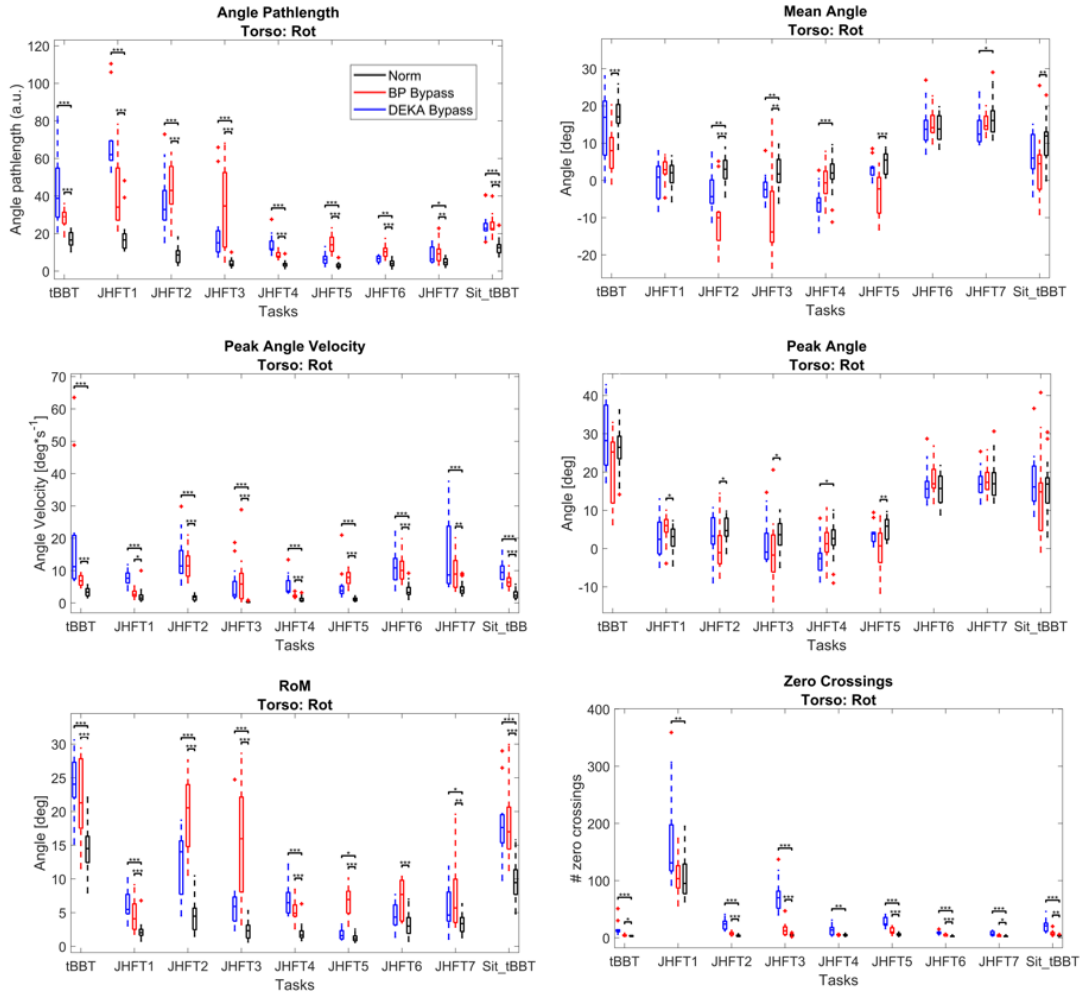
Supplemental Figure 4 Distributions of features for DEKA Bypass (blue), BP Bypass (red), and Norm (black) conditions for right shoulder rotation. Tasks JHFT1 - Writing, JHFT2 - Page Turning, JHFT3 - Picking Up Small Objects, JHFT4 - Simulated Feeding, JHFT5 - Stacking Checkers, JHFT6 - Moving Large Light Objects and JHFT7 - Moving Large Heavy. Stars denote statistical significance of Wilcoxon ranksum test between each bypass condition data and the Norm condition data. \* $p < 0.05$ , \*\* $p < 0.01$ , \*\*\* $p < 0.001$ . (From Wang et al., 2021[93])



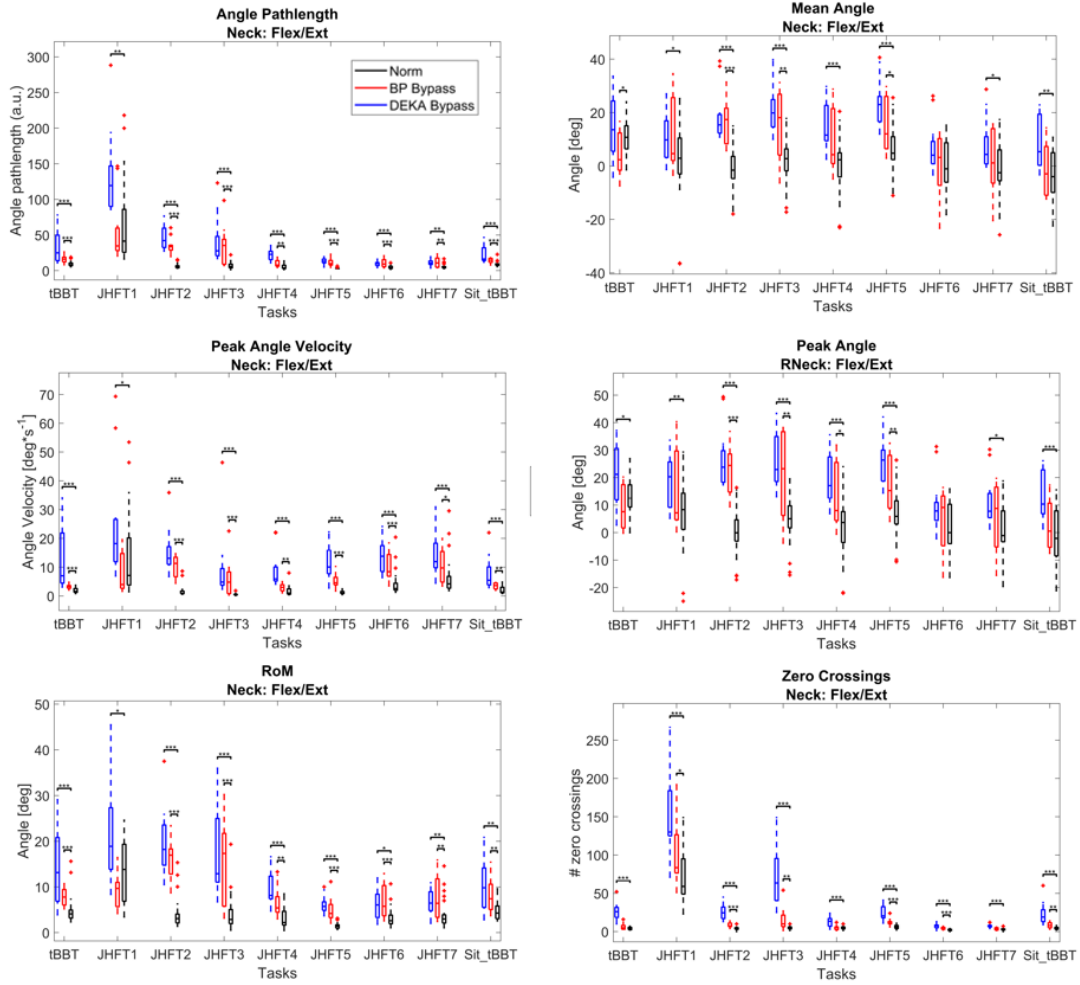
Supplemental Figure 5 Distributions of features for DEKA Bypass (blue), BP Bypass (red), and Norm (black) conditions for torso flexion. Tasks JHFT1 - Writing, JHFT2 - Page Turning, JHFT3 - Picking Up Small Objects, JHFT4 - Simulated Feeding, JHFT5 - Stacking Checkers, JHFT6 - Moving Large Light Objects and JHFT7 - Moving Large Heavy. Stars denote statistical significance of Wilcoxon ranksum test between each bypass condition data and the Norm condition data. \*p<0.05, \*\*p<0.01, \*\*\*p<0.001. (From Wang et al., 2021[93])



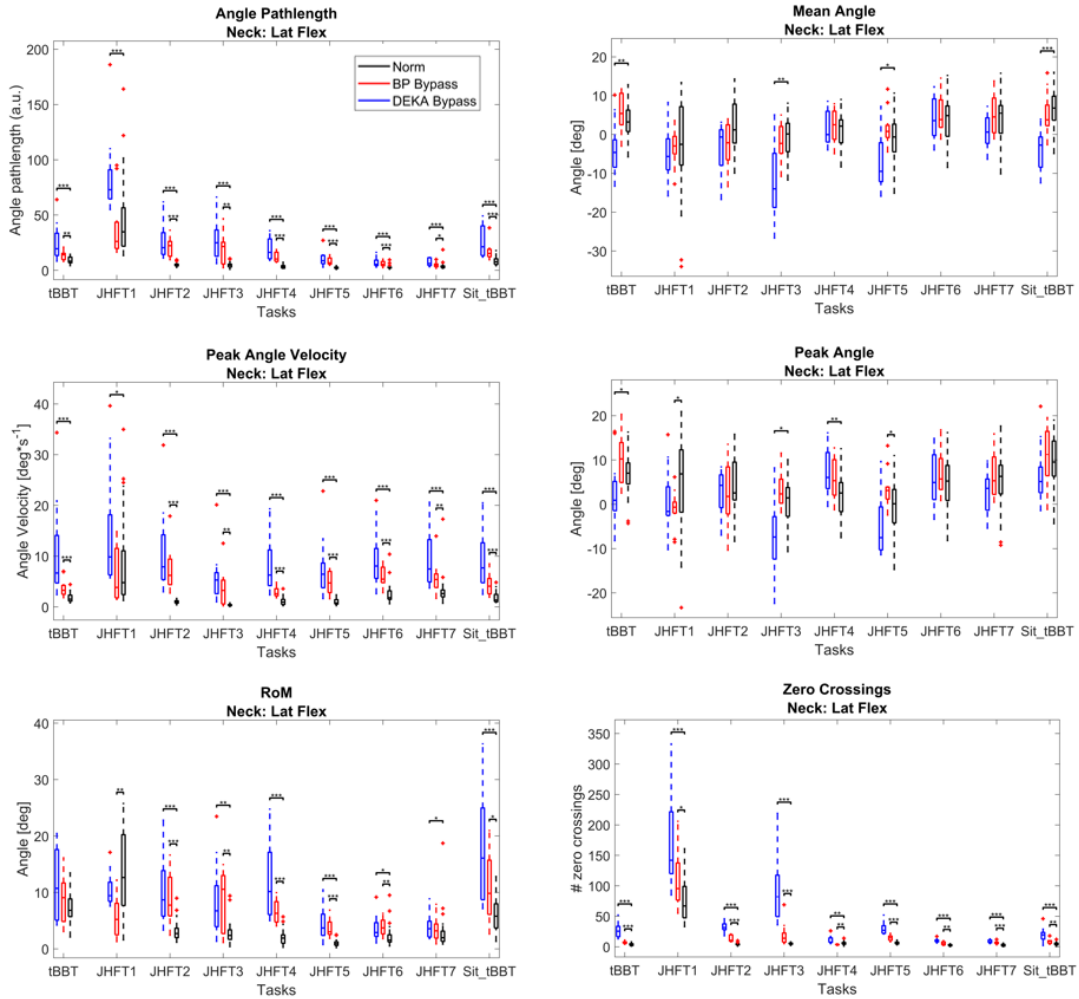
Supplemental Figure 6 Distributions of features for DEKA Bypass (blue), BP Bypass (red), and Norm (black) conditions for torso lateral flexion. Tasks JHFT1 - Writing, JHFT2 - Page Turning, JHFT3 - Picking Up Small Objects, JHFT4 - Simulated Feeding, JHFT5 - Stacking Checkers, JHFT6 - Moving Large Light Objects and JHFT7 - Moving Large Heavy. Stars denote statistical significance of Wilcoxon ranksum test between each bypass condition data and the Norm condition data. \* $p < 0.05$ , \*\* $p < 0.01$ , \*\*\* $p < 0.001$ . (From Wang et al., 2021[93])



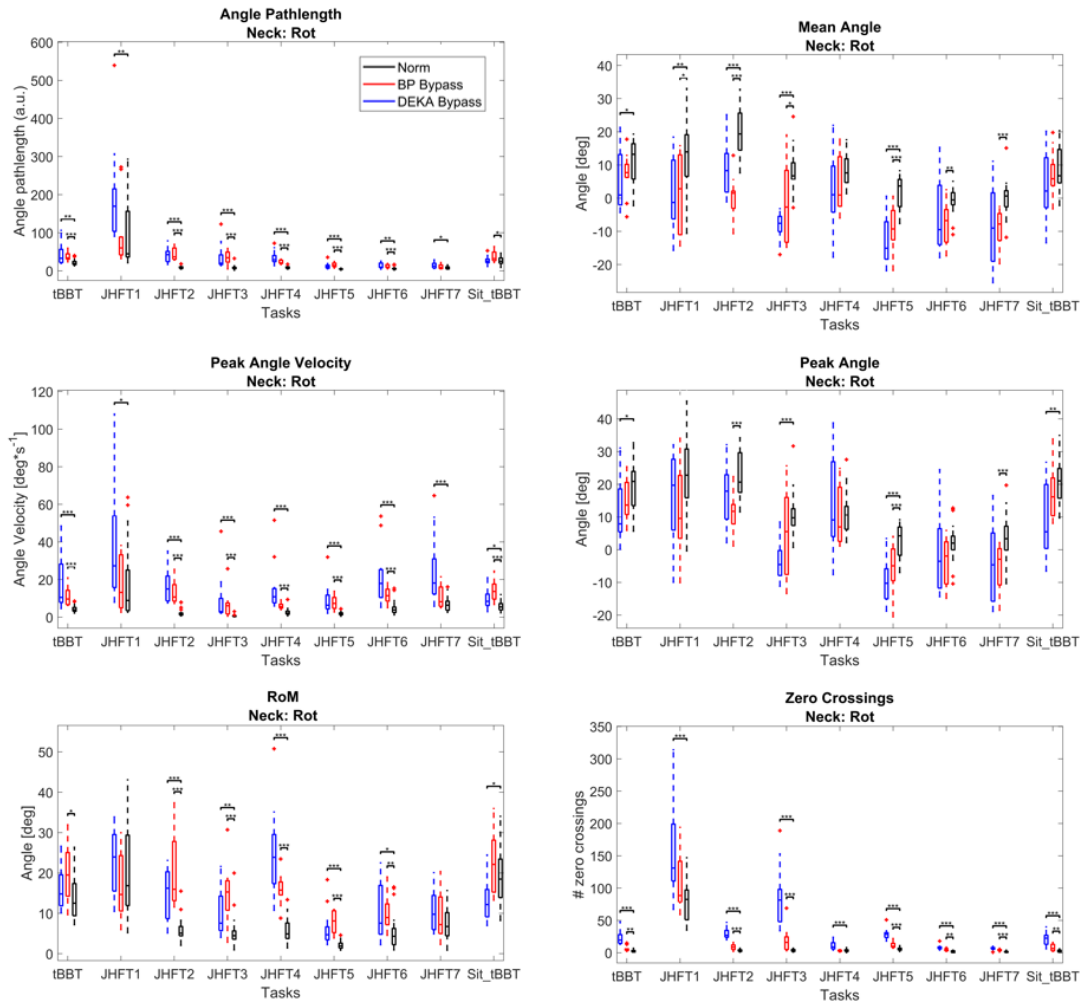
Supplemental Figure 7 Distributions of features for DEKA Bypass (blue), BP Bypass (red), and Norm (black) conditions for torso rotation. Tasks JHFT1 - Writing, JHFT2 - Page Turning, JHFT3 - Picking Up Small Objects, JHFT4 - Simulated Feeding, JHFT5 - Stacking Checkers, JHFT6 - Moving Large Light Objects and JHFT7 - Moving Large Heavy. Stars denote statistical significance of Wilcoxon ranksum test between each bypass condition data and the Norm condition data. \* $p < 0.05$ , \*\* $p < 0.01$ , \*\*\* $p < 0.001$ . (From Wang et al., 2021[93])



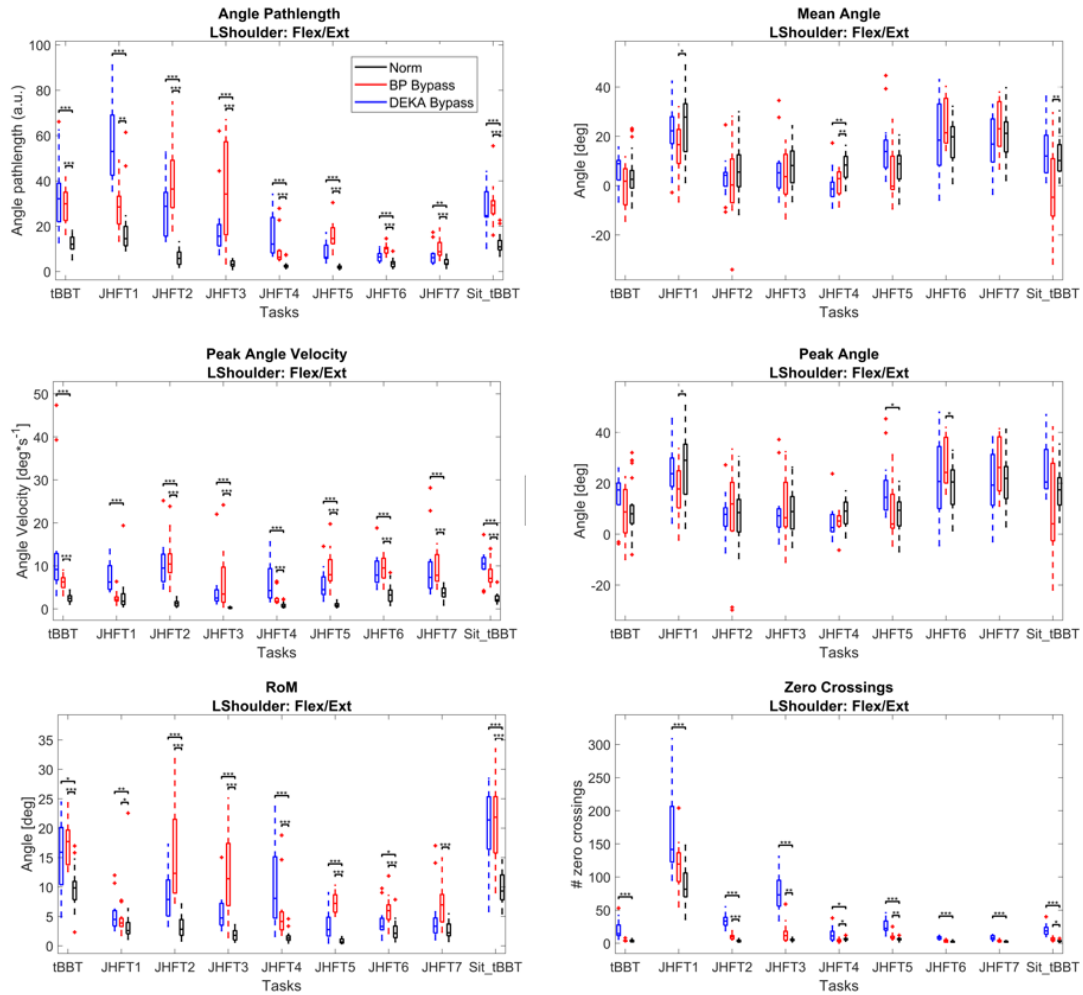
Supplemental Figure 8 Distributions of features for DEKA Bypass (blue), BP Bypass (red), and Norm (black) conditions for neck flexion. Tasks JHFT1 - Writing, JHFT2 - Page Turning, JHFT3 - Picking Up Small Objects, JHFT4 - Simulated Feeding, JHFT5 - Stacking Checkers, JHFT6 - Moving Large Light Objects and JHFT7 - Moving Large Heavy. Stars denote statistical significance of Wilcoxon ranksum test between each bypass condition data and the Norm condition data. \* $p < 0.05$ , \*\* $p < 0.01$ , \*\*\* $p < 0.001$ . (From Wang et al., 2021[93])



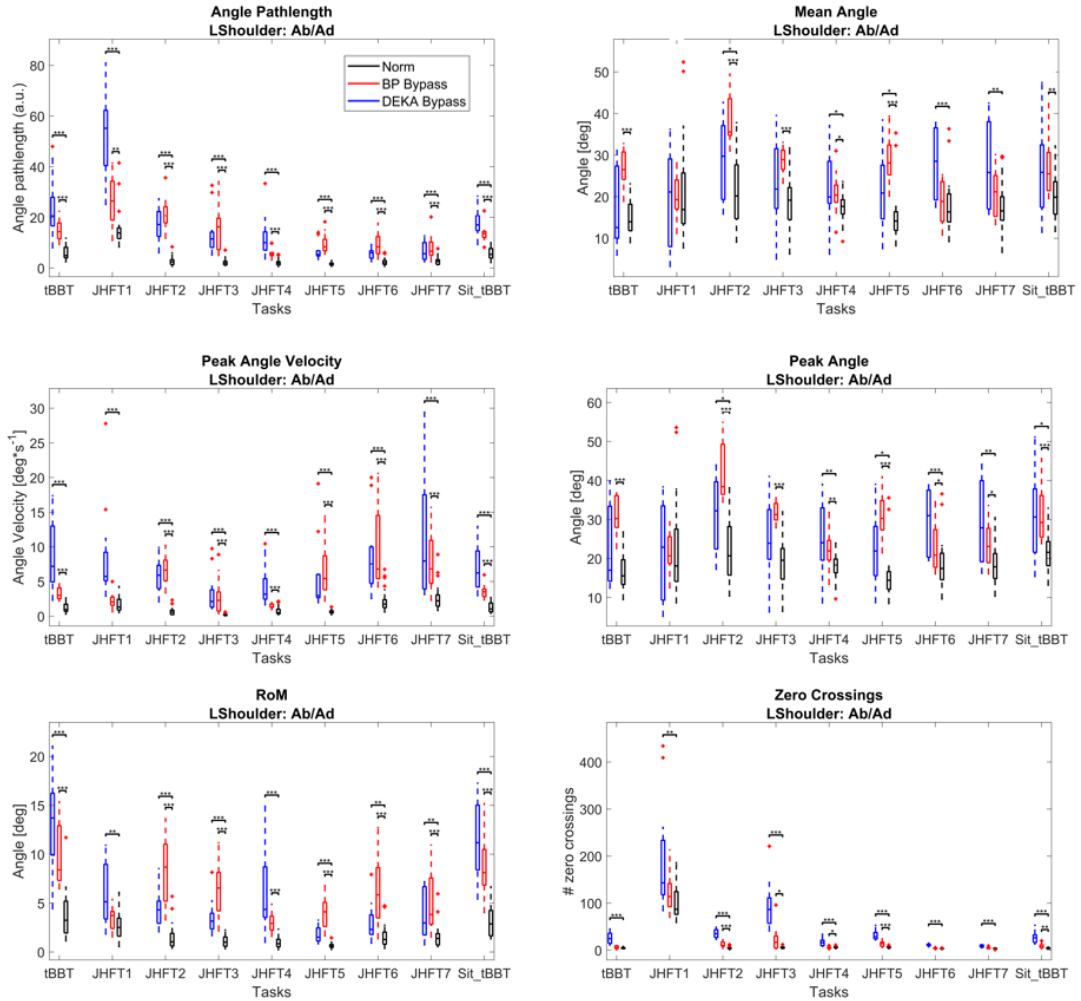
Supplemental Figure 9 Distributions of features for DEKA Bypass (blue), BP Bypass (red), and Norm (black) conditions for neck lateral flexion. Tasks JHFT1 - Writing, JHFT2 - Page Turning, JHFT3 - Picking Up Small Objects, JHFT4 - Simulated Feeding, JHFT5 - Stacking Checkers, JHFT6 - Moving Large Light Objects and JHFT7 - Moving Large Heavy. Stars denote statistical significance of Wilcoxon ranksum test between each bypass condition data and the Norm condition data. \* $p < 0.05$ , \*\* $p < 0.01$ , \*\*\* $p < 0.001$ . (From Wang et al., 2021[93])



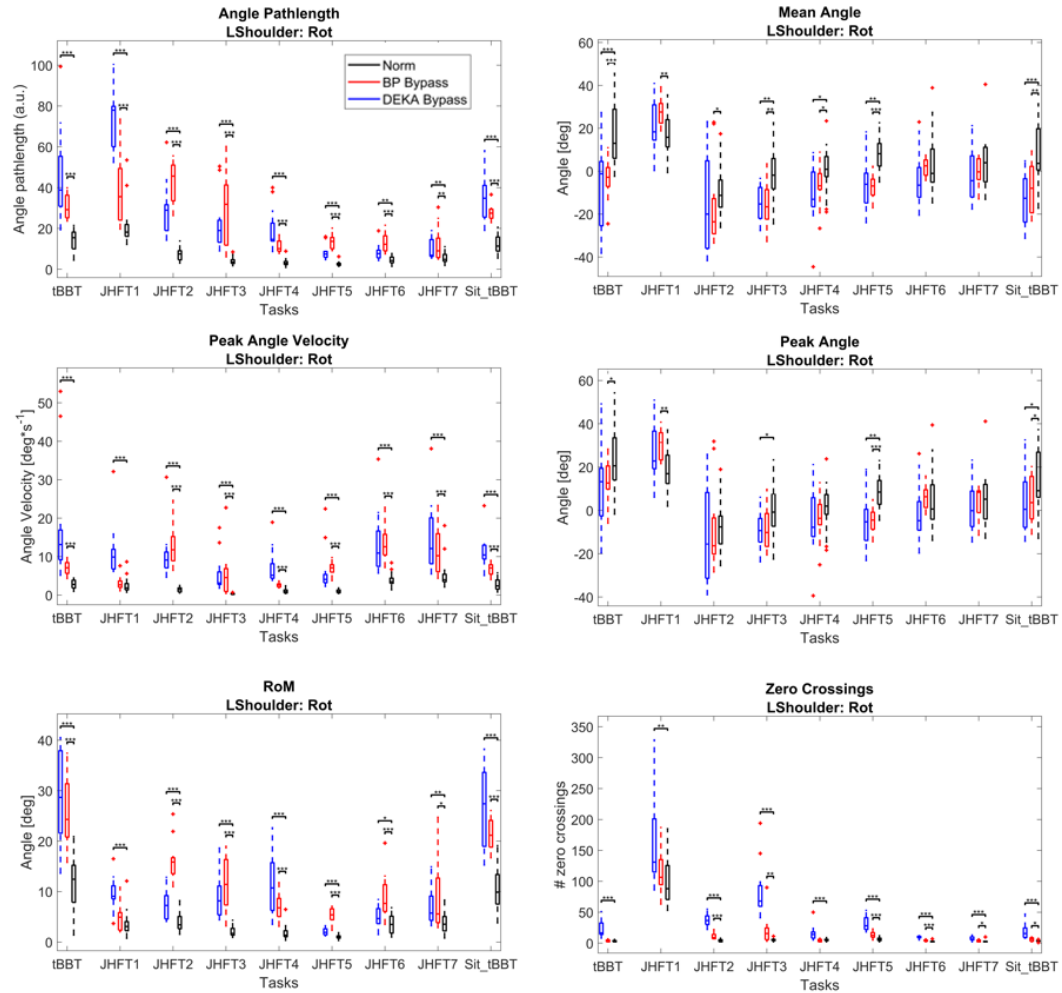
Supplemental Figure 10 Distributions of features for DEKA Bypass (blue), BP Bypass (red), and Norm (black) conditions for neck rotation. Tasks JHFT1 - Writing, JHFT2 - Page Turning, JHFT3 - Picking Up Small Objects, JHFT4 - Simulated Feeding, JHFT5 - Stacking Checkers, JHFT6 - Moving Large Light Objects and JHFT7 - Moving Large Heavy. Stars denote statistical significance of Wilcoxon ranksum test between each bypass condition data and the Norm condition data. \* $p < 0.05$ , \*\* $p < 0.01$ , \*\*\* $p < 0.001$ . (From Wang et al., 2021[93])



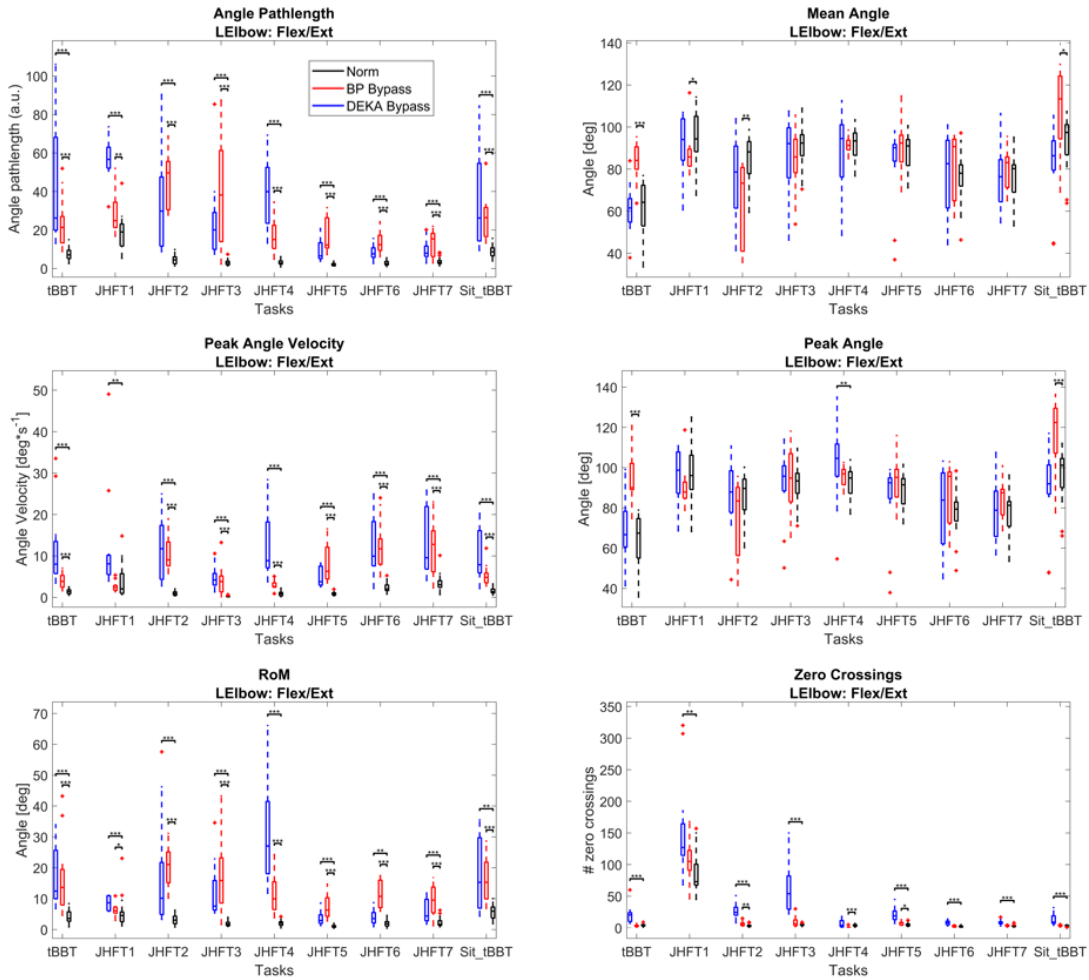
Supplemental Figure 11 Distributions of features for DEKA Bypass (blue), BP Bypass (red), and Norm (black) conditions for left shoulder flexion/extension. Tasks JHFT1 - Writing, JHFT2 - Page Turning, JHFT3 - Picking Up Small Objects, JHFT4 - Simulated Feeding, JHFT5 - Stacking Checkers, JHFT6 - Moving Large Light Objects and JHFT7 - Moving Large Heavy. Stars denote statistical significance of Wilcoxon ranksum test between each bypass condition data and the Norm condition data. \* $p < 0.05$ , \*\* $p < 0.01$ , \*\*\* $p < 0.001$ . (From Wang et al., 2021[93])



Supplemental Figure 12 Distributions of features for DEKA Bypass (blue), BP Bypass (red), and Norm (black) conditions for left shoulder abduction/adduction. Tasks JHFT1 - Writing, JHFT2 - Page Turning, JHFT3 - Picking Up Small Objects, JHFT4 - Simulated Feeding, JHFT5 - Stacking Checkers, JHFT6 - Moving Large Light Objects and JHFT7 - Moving Large Heavy. Stars denote statistical significance of Wilcoxon ranksum test between each bypass condition data and the Norm condition data. \* $p < 0.05$ , \*\* $p < 0.01$ , \*\*\* $p < 0.001$ . (From Wang et al., 2021[93])



Supplemental Figure 13 Distributions of features for DEKA Bypass (blue), BP Bypass (red), and Norm (black) conditions for left shoulder rotation. Tasks JHFT1 - Writing, JHFT2 - Page Turning, JHFT3 - Picking Up Small Objects, JHFT4 - Simulated Feeding, JHFT5 - Stacking Checkers, JHFT6 - Moving Large Light Objects and JHFT7 - Moving Large Heavy. Stars denote statistical significance of Wilcoxon ranksum test between each bypass condition data and the Norm condition data. \* $p < 0.05$ , \*\* $p < 0.01$ , \*\*\* $p < 0.001$ . (From Wang et al., 2021[93])



Supplemental Figure 14 Distributions of features for DEKA Bypass (blue), BP Bypass (red), and Norm (black) conditions for left elbow flexion/extension. Tasks JHFT1 - Writing, JHFT2 - Page Turning, JHFT3 - Picking Up Small Objects, JHFT4 - Simulated Feeding, JHFT5 - Stacking Checkers, JHFT6 - Moving Large Light Objects and JHFT7 - Moving Large Heavy. Stars denote statistical significance of Wilcoxon ranksum test between each bypass condition data and the Norm condition data. \* $p < 0.05$ , \*\* $p < 0.01$ , \*\*\* $p < 0.001$ . (From Wang et al., 2021[93])

## Bibliography

1. Ziegler-Graham, K., et al., *Estimating the prevalence of limb loss in the United States: 2005 to 2050*. Arch Phys Med Rehabil, 2008. **89**(3): p. 422-9.
2. Cordella, F., et al., *Literature Review on Needs of Upper Limb Prosthesis Users*. Front Neurosci, 2016. **10**: p. 209.
3. Biddiss, E.A. and T.T. Chau, *Upper limb prosthesis use and abandonment: a survey of the last 25 years*. Prosthet Orthot Int, 2007. **31**(3): p. 236-57.
4. Millstein, S., H. Heger, and G. Hunter, *A Review of the Failures in Use of the Below Elbow Myoelectric Prosthesis*. Orthotics and Prosthetics, 1982. **36**(2): p. 29-34.
5. Gambrell, C.R., *Overuse Syndrome and the Unilateral Upper Limb Amputee: Consequences and Prevention*. JPO Journal of Prosthetics and Orthotics, 2008. **20**(3): p. 126-132.
6. Ostlie, K., et al., *Musculoskeletal pain and overuse syndromes in adult acquired major upper-limb amputees*. Arch Phys Med Rehabil, 2011. **92**(12): p. 1967-1973 e1.
7. Metzger, A.J., et al., *Characterization of compensatory trunk movements during prosthetic upper limb reaching tasks*. Arch Phys Med Rehabil, 2012. **93**(11): p. 2029-34.
8. Huinink, L.H., et al., *Learning to use a body-powered prosthesis: changes in functionality and kinematics*. J Neuroeng Rehabil, 2016. **13**(1): p. 90.
9. Bouma, S.E., et al., *Musculoskeletal complaints in individuals with finger or partial hand amputations in the Netherlands: a cross-sectional study*. Disabil Rehabil, 2018. **40**(10): p. 1146-1153.
10. Marshall, M., E. Helmes, and A.B. Deathe, *A comparison of psychosocial functioning and personality in amputee and chronic pain populations*. Clin J Pain, 1992. **8**(4): p. 351-7.
11. Postema, S.G., et al., *Musculoskeletal Complaints in Transverse Upper Limb Reduction Deficiency and Amputation in The Netherlands: Prevalence, Predictors, and Effect on Health*. Arch Phys Med Rehabil, 2016. **97**(7): p. 1137-45.
12. Wang, S., et al., *Evaluation of Performance-Based Outcome Measures for the Upper Limb: A Comprehensive Narrative Review*. PM R, 2018. **10**(9): p. 951-962 e3.
13. Carey, S.L., et al., *Compensatory movements of transradial prosthesis users during common tasks*. Clin Biomech (Bristol, Avon), 2008. **23**(9): p. 1128-35.
14. Hussaini, A., A. Zinck, and P. Kyberd, *Categorization of compensatory motions in transradial myoelectric prosthesis users*. Prosthet Orthot Int, 2017. **41**(3): p. 286-293.
15. Major, M.J., et al., *Comparison of range-of-motion and variability in upper body movements between transradial prosthesis users and able-bodied controls when executing goal-oriented tasks*. J Neuroeng Rehabil, 2014. **11**: p. 132.

16. Ehara, Y., et al., *Comparison of the performance of 3D camera systems*. Gait & Posture, 1995. **3**(3): p. 166-169.
17. Guerra-Filho, G.B., *Optical Motion Capture: Theory and Implementation*. Journal of Theoretical and Applied Informatics, 1995. **12**(2): p. 61-90.
18. Cappozzo, A., et al., *Position and orientation in space of bones during movement: experimental artefacts*. Clinical Biomechanics, 1996. **11**(2): p. 90-100.
19. Ramos, E., et al., *Quantification of upper extremity function using kinematic analysis*. Archives of Physical Medicine and Rehabilitation, 1997. **78**(5): p. 491-496.
20. Lucchetti, L., et al., *Skin movement artefact assessment and compensation in the estimation of knee-joint kinematics*. Journal of Biomechanics, 1998. **31**(11): p. 977-984.
21. Aggarwal, J.K. and Q. Cai, *Human Motion Analysis: A Review*. Computer Vision and Image Understanding, 1999. **73**(3): p. 428-440.
22. Richards, J.G., *The measurement of human motion: A comparison of commercially available systems*. Human Movement Science, 1999. **18**(5): p. 589-602.
23. Maletsky, L.P., J. Sun, and N.A. Morton, *Accuracy of an optical active-marker system to track the relative motion of rigid bodies*. J Biomech, 2007. **40**(3): p. 682-5.
24. Matsen, F.A., 3rd, et al., *Measurement of active shoulder motion using the Kinect, a commercially available infrared position detection system*. J Shoulder Elbow Surg, 2016. **25**(2): p. 216-23.
25. Patrizi, A., E. Pennestri, and P.P. Valentini, *Comparison between low-cost marker-less and high-end marker-based motion capture systems for the computer-aided assessment of working ergonomics*. Ergonomics, 2016. **59**(1): p. 155-62.
26. Chang, C.-Y., et al., *Towards Pervasive Physical Rehabilitation Using Microsoft Kinect*. 2012.
27. Clark, R.A., et al., *Validity of the Microsoft Kinect for assessment of postural control*. Gait Posture, 2012. **36**(3): p. 372-7.
28. Fern'ndez-Baena, A., A. Susin, and X. Lligadas, *Biomechanical Validation of Upper-Body and Lower-Body Joint Movements of Kinect Motion Capture Data for Rehabilitation Treatments*. 2012: p. 656-661.
29. Metcalf, C.D., et al., *Markerless motion capture and measurement of hand kinematics: validation and application to home-based upper limb rehabilitation*. IEEE Trans Biomed Eng, 2013. **60**(8): p. 2184-92.
30. Galna, B., et al., *Accuracy of the Microsoft Kinect sensor for measuring movement in people with Parkinson's disease*. Gait Posture, 2014. **39**(4): p. 1062-8.
31. Mousavi Hondori, H. and M. Khademi, *A Review on Technical and Clinical Impact of Microsoft Kinect on Physical Therapy and Rehabilitation*. J Med Eng, 2014. **2014**: p. 846514.

32. Brodie, M.A., A. Walmsley, and W. Page, *The static accuracy and calibration of inertial measurement units for 3D orientation*. Comput Methods Biomech Biomed Engin, 2008. **11**(6): p. 641-8.
33. Saber-Sheikh, K., et al., *Feasibility of using inertial sensors to assess human movement*. Man Ther, 2010. **15**(1): p. 122-5.
34. Zhang, J.T., et al., *Concurrent validation of Xsens MVN measurement of lower limb joint angular kinematics*. Physiol Meas, 2013. **34**(8): p. N63-9.
35. Pfau, T. and R. Weller, *Comparison of a standalone consumer grade smartphone with a specialist inertial measurement unit for quantification of movement symmetry in the trotting horse*. Equine Vet J, 2017. **49**(1): p. 124-129.
36. Poitras, I., et al., *Validity of Wearable Sensors at the Shoulder Joint: Combining Wireless Electromyography Sensors and Inertial Measurement Units to Perform Physical Workplace Assessments*. Sensors (Basel), 2019. **19**(8).
37. Cuesta-Vargas, A.I. and C. Roldan-Jimenez, *Validity and reliability of arm abduction angle measured on smartphone: a cross-sectional study*. BMC Musculoskelet Disord, 2016. **17**: p. 93.
38. Mourcou, Q., et al., *Performance Evaluation of Smartphone Inertial Sensors Measurement for Range of Motion*. Sensors (Basel), 2015. **15**(9): p. 23168-87.
39. Srinivasan, D. and S.E. Mathiassen, *Motor variability in occupational health and performance*. Clin Biomech (Bristol, Avon), 2012. **27**(10): p. 979-93.
40. Santisteban, L., et al., *Upper Limb Outcome Measures Used in Stroke Rehabilitation Studies: A Systematic Literature Review*. PLoS One, 2016. **11**(5): p. e0154792.
41. Cowley, J., et al., *Movement quality of conventional prostheses and the DEKA Arm during everyday tasks*. Prosthet Orthot Int, 2017. **41**(1): p. 33-40.
42. Hebert, J.S., et al., *Quantitative Eye Gaze and Movement Differences in Visuomotor Adaptations to Varying Task Demands Among Upper-Extremity Prosthesis Users*. JAMA Netw Open, 2019. **2**(9): p. e1911197.
43. Carey, S.L., et al., *Kinematic comparison of myoelectric and body powered prostheses while performing common activities*. Prosthet Orthot Int, 2009. **33**(2): p. 179-86.
44. Kearns, N.T., et al., *Development and Psychometric Validation of Capacity Assessment of Prosthetic Performance for the Upper Limb (CAPPFUL)*. Arch Phys Med Rehabil, 2018. **99**(9): p. 1789-1797.
45. Resnik, L., et al., *Development and evaluation of the activities measure for upper limb amputees*. Arch Phys Med Rehabil, 2013. **94**(3): p. 488-494 e4.
46. Abd Razak, N.A., N.A. Abu Osman, and W.A. Wan Abas, *Kinematic comparison of the wrist movements that are possible with a biomechatronics wrist prosthesis and a body-powered prosthesis: a preliminary study*. Disabil Rehabil Assist Technol, 2013. **8**(3): p. 255-60.
47. de los Reyes-Guzman, A., et al., *Quantitative assessment based on kinematic measures of functional impairments during upper extremity movements: A review*. Clin Biomech (Bristol, Avon), 2014. **29**(7): p. 719-27.

48. Resnik, L., S.L. Klinger, and K. Etter, *The DEKA Arm: its features, functionality, and evolution during the Veterans Affairs Study to optimize the DEKA Arm*. *Prosthet Orthot Int*, 2014. **38**(6): p. 492-504.
49. Resnik, L., et al., *Controlling a multi-degree of freedom upper limb prosthesis using foot controls: user experience*. *Disabil Rehabil Assist Technol*, 2014. **9**(4): p. 318-29.
50. Resnik, L., et al., *Do users want to receive a DEKA Arm and why? Overall findings from the Veterans Affairs Study to optimize the DEKA Arm*. *Prosthet Orthot Int*, 2014. **38**(6): p. 456-66.
51. Resnik, L.J., F. Acluche, and S. Lieberman Klinger, *User experience of controlling the DEKA Arm with EMG pattern recognition*. *PLoS One*, 2018. **13**(9): p. e0203987.
52. Bloomer, C. and K.L. Kontson, *Comparison of DEKA Arm and body-powered upper limb prosthesis joint kinematics*. *Archives of Rehabilitation Research and Clinical Translation*, 2020.
53. Biswas, D., et al., *Recognizing upper limb movements with wrist worn inertial sensors using k-means clustering classification*. *Hum Mov Sci*, 2015. **40**: p. 59-76.
54. McLeod, A., et al., *Using Wearable Sensors and Machine Learning Models to Separate Functional Upper Extremity Use From Walking-Associated Arm Movements*. *Arch Phys Med Rehabil*, 2016. **97**(2): p. 224-31.
55. Pendharkar, G., G.R. Naik, and H.T. Nguyen, *Using Blind Source Separation on accelerometry data to analyze and distinguish the toe walking gait from normal gait in ITW children*. *Biomedical Signal Processing and Control*, 2014. **13**: p. 41-49.
56. Kapsouras, I. and N. Nikolaidis, *Action recognition on motion capture data using a dynemes and forward differences representation*. *Journal of Visual Communication and Image Representation*, 2014. **25**(6): p. 1432-1445.
57. Rozumalski, A. and M.H. Schwartz, *Crouch gait patterns defined using k-means cluster analysis are related to underlying clinical pathology*. *Gait Posture*, 2009. **30**(2): p. 155-60.
58. White, S.G. and P.J. McNair, *Abdominal and erector spinae muscle activity during gait: the use of cluster analysis to identify patterns of activity*. *Clin Biomech (Bristol, Avon)*, 2002. **17**(3): p. 177-84.
59. Moeslund, T.B., A. Hilton, and V. Krüger, *A survey of advances in vision-based human motion capture and analysis*. *Computer Vision and Image Understanding*, 2006. **104**(2-3): p. 90-126.
60. Mundermann, L., S. Corazza, and T.P. Andriacchi, *The evolution of methods for the capture of human movement leading to markerless motion capture for biomechanical applications*. *J Neuroeng Rehabil*, 2006. **3**: p. 6.
61. Duc, C., et al., *A wearable inertial system to assess the cervical spine mobility: comparison with an optoelectronic-based motion capture evaluation*. *Med Eng Phys*, 2014. **36**(1): p. 49-56.
62. Bouvier, B., et al., *Upper Limb Kinematics Using Inertial and Magnetic Sensors: Comparison of Sensor-to-Segment Calibrations*. *Sensors (Basel)*, 2015. **15**(8): p. 18813-33.

63. Schlagenhauf F, P.S.P.a.S.W., *A Comparison of Dual-Kinect and Vicon Tracking of Human Motion for Use in Robotic Motion Programming*. Robotics & Automation Engineering Journal, 2017. **1**(2).
64. Windolf, M., N. Gotzen, and M. Morlock, *Systematic accuracy and precision analysis of video motion capturing systems--exemplified on the Vicon-460 system*. J Biomech, 2008. **41**(12): p. 2776-80.
65. Mjosund, H.L., et al., *Clinically acceptable agreement between the ViMove wireless motion sensor system and the Vicon motion capture system when measuring lumbar region inclination motion in the sagittal and coronal planes*. BMC Musculoskelet Disord, 2017. **18**(1): p. 124.
66. Yeung, L.F., et al., *Evaluation of the Microsoft Kinect as a clinical assessment tool of body sway*. Gait Posture, 2014. **40**(4): p. 532-8.
67. Richter, C., et al., *Agreement between An Inertia and Optical Based Motion Capture during the VU-Return-to-Play- Field-Test*. Sensors (Basel), 2020. **20**(3).
68. van der Straaten, R., et al., *Reliability and Agreement of 3D Trunk and Lower Extremity Movement Analysis by Means of Inertial Sensor Technology for Unipodal and Bipodal Tasks*. Sensors (Basel), 2019. **19**(1).
69. Dogan, M., et al., *Functional range of motion in the upper extremity and trunk joints: Nine functional everyday tasks with inertial sensors*. Gait Posture, 2019. **70**: p. 141-147.
70. Moon, Y., et al., *Monitoring gait in multiple sclerosis with novel wearable motion sensors*. PLoS One, 2017. **12**(2): p. e0171346.
71. Weenk, D., et al., *Automatic identification of inertial sensor placement on human body segments during walking*. J Neuroeng Rehabil, 2013. **10**: p. 31.
72. Muller, B., et al., *Validation of enhanced kinect sensor based motion capturing for gait assessment*. PLoS One, 2017. **12**(4): p. e0175813.
73. Pfister, A., et al., *Comparative abilities of Microsoft Kinect and Vicon 3D motion capture for gait analysis*. J Med Eng Technol, 2014. **38**(5): p. 274-80.
74. Pagliari, D. and L. Pinto, *Calibration of Kinect for Xbox One and Comparison between the Two Generations of Microsoft Sensors*. Sensors (Basel), 2015. **15**(11): p. 27569-89.
75. Schmitz, A., et al., *Accuracy and repeatability of joint angles measured using a single camera markerless motion capture system*. J Biomech, 2014. **47**(2): p. 587-91.
76. Elliott, B.C., J.A. Alderson, and E.R. Denver, *System and modelling errors in motion analysis: implications for the measurement of the elbow angle in cricket bowling*. J Biomech, 2007. **40**(12): p. 2679-85.
77. van Andel, C.J., et al., *Complete 3D kinematics of upper extremity functional tasks*. Gait Posture, 2008. **27**(1): p. 120-7.
78. Jaspers, E., et al., *The reliability of upper limb kinematics in children with hemiplegic cerebral palsy*. Gait Posture, 2011. **33**(4): p. 568-75.
79. Jaspers, E., et al., *Upper limb kinematics: development and reliability of a clinical protocol for children*. Gait Posture, 2011. **33**(2): p. 279-85.

80. Kim, K., et al., *Kinematic analysis of upper extremity movement during drinking in hemiplegic subjects*. Clin Biomech (Bristol, Avon), 2014. **29**(3): p. 248-56.
81. Pianta, L., et al., *Quantitative evaluation of the upper limb kinematics in post-stroke patients undergoing rehabilitation: Integrated vs. traditional rehabilitation treatment*. Gait & Posture, 2015. **42**: p. S56-S57.
82. Bloomer, C., S. Wang, and K. Kontson, *Creating a standardized, quantitative training protocol for upper limb bypass prostheses*. Phys Med Rehabil Res, 2018. **3**(6): p. 1-8.
83. Kontson, K.L., et al., *Assessing kinematic variability during performance of Jebsen-Taylor Hand Function Test*. J Hand Ther, 2019.
84. Kontson, K., et al., *Targeted box and blocks test: Normative data and comparison to standard tests*. PLoS One, 2017. **12**(5): p. e0177965.
85. Resnik, L., et al., *Self-reported and performance-based outcomes using DEKA Arm*. J Rehabil Res Dev, 2014. **51**(3): p. 351-62.
86. Lindner, H.Y., A. Langius-Eklöf, and L.M. Hermansson, *Test-retest reliability and rater agreements of assessment of capacity for myoelectric control version 2.0*. J Rehabil Res Dev, 2014. **51**(4): p. 635-44.
87. Boyle, A., et al., *Capacity Assessment of Prosthetic Performance for the Upper Limb (CAPPFUL): Characterization of Normative Kinematics and Performance*. PM R, 2019.
88. Kontson, K.L., et al., *An Integrated Movement Analysis Framework to Study Upper Limb Function: A Pilot Study*. IEEE Trans Neural Syst Rehabil Eng, 2017. **25**(10): p. 1874-1883.
89. Bouwsema, H., C.K. van der Sluis, and R.M. Bongers, *Changes in performance over time while learning to use a myoelectric prosthesis*. J Neuroeng Rehabil, 2014. **11**: p. 16.
90. Berning, K., et al., *Comparison of body-powered voluntary opening and voluntary closing prehensor for activities of daily life*. J Rehabil Res Dev, 2014. **51**(2): p. 253-61.
91. Haverkate, L., G. Smit, and D.H. Plettenburg, *Assessment of body-powered upper limb prostheses by able-bodied subjects, using the Box and Blocks Test and the Nine-Hole Peg Test*. Prosthet Orthot Int, 2016. **40**(1): p. 109-16.
92. Weeks, D.L., S.A. Wallace, and D.I. Anderson, *Training with an upper-limb prosthetic simulator to enhance transfer of skill across limbs*. Arch Phys Med Rehabil, 2003. **84**(3): p. 437-43.
93. Wang, S.L., et al., *Application of machine learning to the identification of joint degrees of freedom involved in abnormal movement during upper limb prosthesis use*. PLoS One, 2021. **16**(2): p. e0246795.
94. Oldfield, R.C., *The assessment and analysis of handedness: The Edinburgh inventory*. Neuropsychologia, 1971. **9**(1): p. 97-113.
95. Wang, S.L., et al., *Comparison of Motion Analysis Systems in Tracking Upper Body Movement of Myoelectric Bypass Prosthesis Users*. Sensors (Basel), 2022. **22**(8).

96. Bloomer, C., S. Wang, and K. Kontson, *Kinematic analysis of motor learning in upper limb body-powered bypass prosthesis training*. PLoS One, 2020. **15**(1): p. e0226563.
97. Atkins, D., *Adult Upper Limb Prosthetic Training*, in *Atlas of Limb Prosthetics: Surgical, Prosthetic, and Rehabilitation Principles*. 1992, American Academy of Orthopedic Surgeons: Rosemont, IL.
98. Dakpa, R. and H. Heger, *Prosthetic management and training of adult upper limb amputees*. Current Orthopaedics, 1997. **11**(3): p. 193-202.
99. Wang, S., et al., *Evaluation of Performance-Based Outcome Measures for the Upper Limb: A Systematic Review*. PM R, 2018.
100. Choi, A., et al., *Kinematic evaluation of movement smoothness in golf: relationship between the normalized jerk cost of body joints and the clubhead*. Biomed Eng Online, 2014. **13**(1): p. 20.
101. Murphy, M.A.H., C.K., *Kinematic analysis of the upper extremity after stroke - how far have we reached and what have we grasped?* Physical Therapy Reviews, 2015. **20**(3).
102. Fitoussi, F., et al., *Upper extremity kinematics analysis in obstetrical brachial plexus palsy*. Orthop Traumatol Surg Res, 2009. **95**(5): p. 336-42.
103. Valevicius, A.M., et al., *Characterization of normative angular joint kinematics during two functional upper limb tasks*. Gait Posture, 2019. **69**: p. 176-186.
104. Sanchez-Margallo, J.A., et al., *Objective assessment based on motion-related metrics and technical performance in laparoscopic suturing*. Int J Comput Assist Radiol Surg, 2017. **12**(2): p. 307-314.
105. Xiao, X., et al., *Comparison of dominant hand to non-dominant hand in conduction of reaching task from 3D kinematic data: Trade-off between successful rate and movement efficiency*. Math Biosci Eng, 2019. **16**(3): p. 1611-1624.
106. !!! INVALID CITATION !!! {}.
107. Anand, N. and P. Vikram, *Comprehensive Analysis & Performance Comparison of Clustering Algorithms for Big Data*. Review of Computer Engineering Research, 2017. **4**(2): p. 54-80.
108. Semasinghe, C.L., et al., *Transradial prostheses: Trends in development of hardware and control systems*. Int J Med Robot, 2019. **15**(1): p. e1960.
109. Jebsen, R.H., et al., *An objective and standardized test of hand function*. Arch Phys Med Rehabil, 1969. **50**(6): p. 311-9.
110. Gastaldi, L., G. Lisco, and S. Pastorelli, *Evaluation of functional methods for human movement modelling*. Acta Bioeng Biomech, 2015. **17**(4): p. 32-8.
111. Abd Razak, N.A., et al., *Development and performance of a new prosthesis system using ultrasonic sensor for wrist movements: a preliminary study*. Biomed Eng Online, 2014. **13**: p. 49.
112. Hingtgen, B., et al., *An upper extremity kinematic model for evaluation of hemiparetic stroke*. J Biomech, 2006. **39**(4): p. 681-8.
113. Wouda, F.J., et al., *Estimation of Full-Body Poses Using Only Five Inertial Sensors: An Eager or Lazy Learning Approach?* Sensors (Basel), 2016. **16**(12).

114. Luinge, H.J., P.H. Veltink, and C.T. Baten, *Ambulatory measurement of arm orientation*. J Biomech, 2007. **40**(1): p. 78-85.
115. Al-Amri, M., et al., *Inertial Measurement Units for Clinical Movement Analysis: Reliability and Concurrent Validity*. Sensors (Basel), 2018. **18**(3).
116. Gao, Z., et al., *Leveraging Two Kinect Sensors for Accurate Full-Body Motion Capture*. Sensors (Basel), 2015. **15**(9): p. 24297-317.
117. Pohlmann, S.T., et al., *Evaluation of Kinect 3D Sensor for Healthcare Imaging*. J Med Biol Eng, 2016. **36**(6): p. 857-870.
118. iPiSoft. *User Guide for Multiple Depth Sensors Configuration*. 2019 [cited 2019 Feb ]; Available from:  
[http://docs.ipisoft.com/index.php?title=User\\_Guide\\_for\\_Multiple\\_Depth\\_Sensors\\_Configuration&oldid=2024](http://docs.ipisoft.com/index.php?title=User_Guide_for_Multiple_Depth_Sensors_Configuration&oldid=2024).
119. Shrout, P.E. and J.L. Fleiss, *Intraclass correlations: uses in assessing rater reliability*. Psychol Bull, 1979. **86**(2): p. 420-8.
120. Robert-Lachaine, X., et al., *Validation of inertial measurement units with an optoelectronic system for whole-body motion analysis*. Med Biol Eng Comput, 2017. **55**(4): p. 609-619.